Design and Development of a Squeeze-Mode Rheometer for Evaluating Magneto-Rheological Fluids

By

Ryan Hale Cavey

Thesis submitted to the Faculty of the

Virginia Polytechnic Institute and State University

in partial fulfillment of the requirements for the degree of

Master of Science

in

Mechanical Engineering

Approved:

Dr. Mehdi Ahmadian, Chairman

Dr. Corina Sandu

Dr. Robert L. West

September 9, 2008
Blacksburg, Virginia

Keywords: MR fluid, Magneto-rheological, Squeeze mode, Rheometer, MR Rheometer, Squeeze flow

Design and Development of a Squeeze-Mode Rheometer for Evaluating Magneto-Rheological Fluids

by

Ryan H. Cavey

Abstract

This study aims to better understand the behavior of magnetorheological (MR) fluids operated in the non-conventional squeeze mode through the use of a custom designed rheometer. Squeeze mode is the least understood of the three operational modes of MR fluid and thus its potential has yet to be realized in practical applications. By identifying the behavior of MR fluid in this mode, the foundation for future development of MR technology will be laid.

Using the limited amount of literature available on squeeze-mode operation in conjunction with conventional principles associated with MR technology, a custom rheometer was designed and fabricated. A detailed account of the design considerations and background information on the fundamentals incorporated into the design are provided. The squeeze-mode rheometer was used to evaluate a variety of MR fluids to observe trends that may exist across fluids. Specifically, fluids of different ferrous particle volume fractions were considered.

Through testing, common trends in fluid stiffness were observed for multiple fluids tested with the squeeze-mode rheometer. When operated in squeeze mode, activated MR fluid has shown to provide substantial resistance to compressive loading, possibly making it attractive for low-displacement high-load systems. The primary observation from the tests is that the activated fluid's stiffness progressively increases over the duration of fluid operation. This phenomenon is due to severe carrier-fluid separation coupled with the formation of ferrous particle aggregate clumps in the fluid. This effect is further explored in this research.

Acknowledgments

I would like to thank my advisor Dr. Mehdi Ahmadian, who has provided me with countless opportunities and excellent guidance throughout my time in graduate school at Virginia Tech. He has been supportive, patient, and understanding during my tenure at CVeSS and has become a valuable mentor both in the area of research and for life in general. I also wish to thank the members of my committee, Dr. Robert West and Dr. Corina Sandu, for their support in this endeavor. For financial support during my graduate studies at Virginia Tech, I am grateful to the Department of Mechanical Engineering and Dr. Mehdi Ahmadian, who together, provided me with the most rewarding job I can imagine having as a graduate student. I would like to thank the Formula SAE team of Virginia Tech for their support, friendship, and guidance throughout my college career.

I would like to thank all of my colleagues at CVeSS for the support. Specifically, I want to thank my lab partner Alireza Farjoud, who always had a smile on his face and showed me infinite patience throughout this project. I would also like to thank Eric Steinburg for his contributions and support. I also wish to thank Brian Southern for sharing his wisdom, experience, and resources during this effort.

I would like to express my deepest gratitude to my parents, Warren and Susan Cavey, for their encouragement, love, and support. They have gone above and beyond to provide for me and I am grateful for the opportunities they have made possible. I would also like to thank my brother Shaun Cavey for being a constant source of enthusiasm and support.

Most importantly, I want to thank my unbelievable wife Virginia Cavey. Words cannot express how grateful I am for her never-ending support, understanding, and patience. It is thanks to her continual encouragement that this endeavor has been possible for me.

Contents

List of Figures

List of Tables

1. Introduction

This chapter presents an overview of vibration control systems as well as an introduction to magnetorheological (MR) applications. A motivation section presents the possible benefits that are driving this research. The discussion then leads to an objectives section that lays out the primary goals of the research. The following section provides the approach taken to accomplish the previously mentioned goals. The next section outlines the organization of the research and this document. Finally, the last section briefly presents the contributions from this research.

1.1 Overview

There are many applications in the world today that use some sort of vibration control. These applications can range from vehicle suspension systems to vibration isolators on large scale manufacturing machinery. Most systems vibration control systems found in the world today are passive in nature, meaning that their spring and damping characteristics are preset and do not change with input to the system. This method can be very effective for certain systems, for example, one that is influenced by an oscillatory force of a known constant frequency. In this example, it is possible to design a passive vibration isolator with a stiffness that will cancel out the oscillatory force completely. Unfortunately, this ideal case rarely occurs in the real world. Even when this case does occur, such as when a piece of machinery operates at a constant RPM, there are often situations that will require deviation from the optimal design range, such as machinery startup and shutdown during maintenance periods. Passive vibration control systems are limited to a narrow window of operation. Outside of this window, performance compromises are realized.

Another form of vibration control employs the use of a “semi-active” system. In this configuration, the stiffness and damping characteristics of the system may be adjustable. This allows for a wider range of operation. It is common to see the application of semi-active systems on vehicle suspensions. In this application, the damper is commonly adjustable via the magnetorheological (MR) fluid inside the shock absorber. This system has tremendous performance benefits over the traditional passive suspension system. It is,

however, not without its drawbacks. Among them are increased cost and significant increase in weight. Both drawbacks are due to the inherent nature of the MR fluid used in these systems. Currently, the MR fluid used in vehicle suspension systems is operated in a similar manner to the oil in a conventional damper. This operation is generally called "valve mode" and will be discussed later in this document. This form of operation requires a significant volume of the working fluid in order to obtain an acceptable operating range for the damper in terms of force and stroke. This requirement for large amounts of the MR fluid in the semi-active system directly leads to its two main drawbacks . . . cost and weight.

Currently, there is research in place to investigate different forms of operation for the MR fluid with an end goal of reducing the volume of fluid needed for a damper. The method being investigated is called "squeeze-mode" and will also be discussed later in this document. At the time that this is being written, there is a wealth of information available on the behavior of MR fluids in operated in the conventional ways of valve and shear mode. There is, however, very little information available on the behavior of MR fluids in squeeze mode. The ultimate purpose of this project is to construct a piece of test equipment that will lead to a better understanding of MR fluid behavior under squeeze mode. This will allow for a new wave of technology in semi-active systems that may produce lighter and less expensive solutions for today's applications.

1.2 Motivation

The motivation for this research is to design and implement an instrument that will aid in the understanding of MR fluid behavior in "squeeze mode". Further understanding of MR fluid behavior in this mode would lead to new technologies that can be implemented in the immediate future to complement the other modes in which MR fluid is used. As previously mentioned, the automotive damper is one area that will directly benefit from this research leading to lighter more cost effective solutions. Vibration isolation devices may also benefit from this project as well. In particular, the MR fluid-filled elastomer vibration isolators developed at the Center for Vehicle Systems and Safety (CVeSS) at Virginia Tech, which operate in a similar manner to the squeeze mode rheometer, may see further refinement and allow for a better understanding of the operation of this type of

isolator. This instrument will directly benefit some of the current technologies in the MR field, but the real hope is that this research will open the door for a new wave of technology development in the field of semi-active vibration control.

1.3 Objectives

The primary objectives of this research are to:

1. provide guidelines for the design and fabrication of a "squeeze mode" rheometer,
2. provide a preliminary evaluation and analysis of magnetorheological (MR) fluids operated in "squeeze mode", and
3. investigate the factors that govern squeeze mode performance.

1.4 Approach

The approach that was adopted for reaching the objectives above was an evolutionary process. Specifically, the following tasks were performed:

- Initial design of the rheometer chamber and magnetic circuit
- Fabrication of the rheometer and coil magnet
- Setup of hydraulic test stand along with load cell and data acquisition system
- Initial testing with multiple MR fluids
- Rheometer piston redesign and fabrication
- Re-testing with new piston design

1.5 Outline

Chapter 2 provides background information on magnetorheological (MR) systems and conventional rheometer design. The different operational modes of MR fluid, including "squeeze mode", is discussed in Chapter 3. Chapter 4 presents the design, fabrication techniques, and assembly of the "squeeze-mode" rheometer. The test setup, test procedures, and results are included in Chapter 5 along with a discussion of the redesigned rheometer piston. Finally, Chapter 6 provides a conclusion of the work and also presents suggestions for future research.

1.6 Contributions

This research has identified the behavior of MR fluid in an, as yet, uncharacterized operational mode. This research also provides a foundation for designing a rheometer for the purpose of characterizing MR fluids in squeeze mode. The squeeze-mode behavior of the fluid was identified for multiple volume fractions and was tested with varying magnetic field intensities. Under the conditions of squeeze-mode operation, the behavior of the fluid has been shown to depart from the commonly accepted behavior. The current study may serve as a platform for future studies in the squeeze-mode operation of MR fluid, and has identified practical potential for MR devices utilizing the squeeze mode.

Specific contributions can be summarized as follows:

- Design considerations and fabrication techniques for the squeeze-mode rheometer have been thoroughly discussed and documented.
- The squeeze-mode behavior of multiple MR fluids with varying volume fractions has been identified. Each of these fluids was investigated with a range of magnetic field intensities. The activated fluid has been shown to provide substantial resistance to compressive loading.
- Practical limitations of MR fluids in squeeze-mode operation have been identified. Separation of the carrier fluid in conjunction with the formation of aggregate clumps in fluid lead to a progressive increase in stiffness during operation.
- The outcome of the current study may serve as a foundation for future studies in squeeze-mode applications of MR fluid and MR fluid devices.

2. Background

This chapter starts by presenting a brief overview of magnetorheological (MR) fluid characteristics and some of its history. A section is then devoted to the discussion of MR devices and applications. Next, the design and operation of a conventional shear mode rheometer is discussed. Finally, each key point of the chapter is briefly reviewed in a summary section.

2.1 MR Fluid History and Devices: Literature Review

Magnetorheological fluids belong to a class of fluids that exhibit variable yield stress [1]. The fluid was discovered by Jacob Rabinow at the US National Bureau of Standards in 1948 [2]. MR fluid has the unique ability to change from a fluid state to a semi-solid or plastic state instantaneously upon the application of a magnetic field [1,3]. The ability of the fluid to make this unique change is due to the composition of the fluid. MR fluid is composed of micron-sized ferrous particles suspended in a base fluid of oil. In the absence of a magnetic field, the fluid is free-flowing with a consistency similar to motor oil [1]. As a magnetic field is introduced into the fluid, the ferrous particles begin to form chains through the fluid and thus change its rheology. When the MR fluid is in this "energized" state, it has the consistency of toothpaste as modeled with Bingham plastic flow [4]. In order to maintain a free-flowing consistency in its relaxed state, the percentage of ferrous particles in an MR fluid is typically limited to 20-40% [3]. Figure 2-1 illustrates the process of energizing MR fluid. The fluid begins in its free-flowing state with no magnetic field present and the ferrous particles arranged in an amorphous pattern, shown in Figure 2-1a. When a magnetic field is applied, the particles begin to align themselves with the flux lines of the applied field, shown in Figure 2-1b. Figure 2-1c shows the MR fluid in its fully energized state with the ferrous particles forming well-defined chains along the flux lines of the magnetic field.

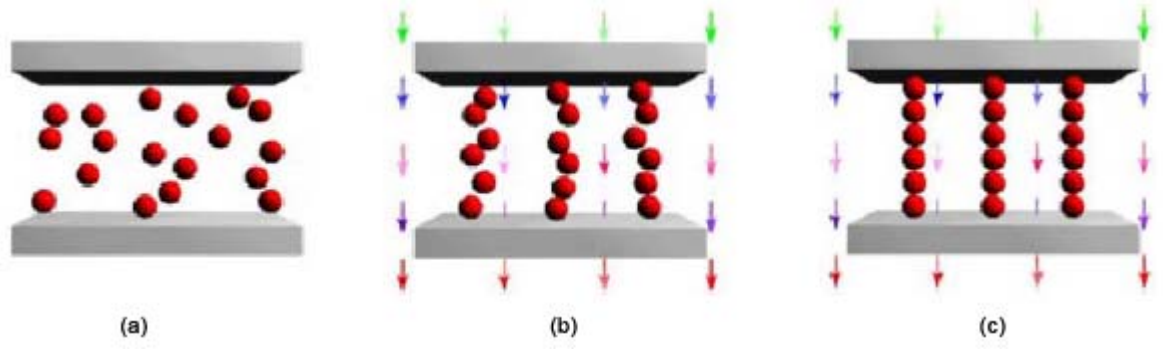

Figure 2-1. Activation of MR fluid: (a) no magnetic field applied; (b) magnetic field applied; (c) ferrous particle chains have formed [1, 5] (image adapted from [1])

While this process is shown in three separate parts here, the actual process occurs in a matter of milliseconds [6, 7]. The formation of ferrous particle chains alters the yield stress of the MR fluid and thus the apparent viscosity [3]. The particles found in these chains may be from 1-20 microns in size [8]. The degree to which the yield stress and apparent viscosity is altered is proportional to the intensity of the magnetic field applied to the fluid. The nearly instantaneous response of the fluid, as well as its ability to completely reverse rheological changes, makes it an attractive material for many applications.

2.1.1 MR Fluid and Devices

MR fluid has proven useful in a variety of different applications since its discovery in the 1940's. Examples of these applications include linear dampers, fluid-filled vibration mounts, and rotary clutches and brakes. MR fluid-filled dampers, dubbed "MR dampers", are among the most widespread applications of the fluid. The fluid is particularly well-suited for use in conventional linear dampers, such as those found on production automobiles. Conventional dampers dissipate energy based on the viscosity of the working fluid and geometry of its piston assembly [3]. With the ability to instantaneously change the apparent viscosity of the working fluid, the performance characteristics of the damper and be instantly changed to better accommodate the demands of a system.

When used in the primary suspension of an automobile, the shock absorber (damper) can be adjusted to a "soft" setting to facilitate a smooth ride and then instantaneously

changed to a harder setting for better vehicle response and handling [9]. This idea has been embraced by major automotive manufacturers, such as General Motors and Audi who employs this technology on the Corvette and TT models respectively [10]. While the Corvette does offer a user selectable button that allows for the choice of a comfortable ride or more responsive handling, the real advantage of the MR system is that it can be combined with a controller that will continuously adjust damping based on the demands of road conditions and driver input. Figure 2-2 illustrates the performance benefits of the Magnetic Selective Ride Control system employed on the Corvette [1]. A 60 mph pass over the Ride and Handling Loop at the Milford Proving Grounds demonstrates the superior control of the MR suspension [1,11].

Figure 2-2. Base C5 Corvette and 50th anniversary Corvette with Magnetic Selective Ride Control Suspension [1] (image adapted from [11])

The control policies used in conjunction with semi-active suspension systems has become a specialty field in itself. Some of the common control strategies currently employed in this application include skyhook, groundhook, and hybrid control. Hybrid control, which combines both skyhook and groundhook control, has been studied in detail to understand transient performance in suspension applications [12].

In addition to semi-active suspension systems, MR fluid has also found a use in rotary clutches as well as drum brake systems [13, 14]. In these applications, the fluid is operated in a direct shear mode. Standard friction-based clutches and brake systems are generally considered “high-wear” items, which often have short service lives. This is particularly true for clutch systems that undergo heavy slip conditions. The use of an MR clutch is especially attractive in this situation because gradual slipping does not increase

the wear on the MR system thus allowing for a longer service life over a conventional system.

2.2 Shear Mode Rheometer

Rheology is defined as the study of the flow and deformation of materials [15]. The relationship between stress and deformation is a property of the material. Rheology can therefore also be described as the study of stress-deformation relationships [16]. A rheometer is an instrument used to characterize the rheology of a material. In the MR fluid world this generally means finding the yield-stress of a fluid under varying magnetic fields.

The most common type of rheometer used to characterize MR fluids is called a shear mode rheometer or rotary rheometer. In this configuration, a sample is placed between two plates that will rotate in relation to one another. Typically, one plate will rotate via electric motor while the other plate serves as a torque transducer. The fluid is placed into a shear mode operation by the rotating plates while the torque transferred across the fluid is measured and later used to characterize the rheology of the fluid. Shear mode rheometers are used to characterize a variety of materials with a wide range of viscosities. Different head geometries may be used in a shear mode rheometer to better accommodate the material being tested. A few common head geometries are shown in Figure 2-3. The concentric cylinder, also called a Couette, shown in Figure 2-3a, is commonly used for very low viscosity samples. This geometry is favorable because of its increased surface area over other available options. The cone and plate configuration, see Figure 2-3b, is the most common geometry used in rotary rheometers. This geometry provides the most consistent results and a convenient method for obtaining true viscosity [18]. When considering MR fluid, the cone and plate geometry presents one major drawback. It is extremely difficult to achieve a uniform magnetic flux across a fluid gap that varies in thickness, as it does with this geometry. It is for this reason that rotary rheometers used to test MR fluid samples use the parallel plate configuration shown in Figure 2-3c. This geometry lends itself well to the adaptation of a magnetic circuit capable of producing a uniform magnetic flux across the fluid, and thus producing a uniform behavior across the fluid.

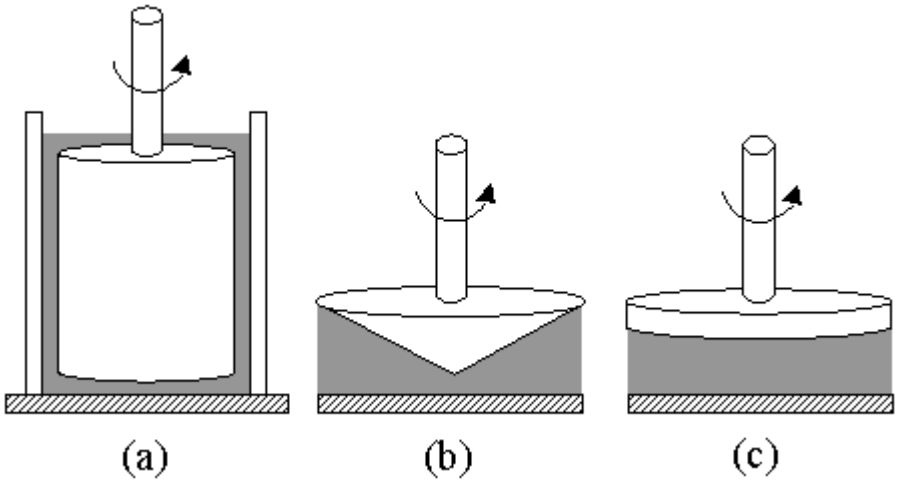

Figure 2-3. Schematic diagram of basic tool geometries for the rotational rheometer: (a) concentric cylinder, (b) cone and plate, (c) parallel plate (adapted from [17])

While there are commercially available rheometers capable of activating and testing MR fluids, it is also quite common to find conventional rheometers that have been modified to accept a magnetic circuit that will activate the fluid [19]. An example of a modified rotary rheometer is shown in Figure 2-4. In this design, a coil magnet is placed around the test section with a steel casing serving as a controlled pathway for the magnetic flux lines. The magnetic flux lines jump across the fluid gap in a uniform manner and thus activating the fluid uniformly. The yield stress of the fluid is obtained by the rheometer typically at varying magnetic field intensities.

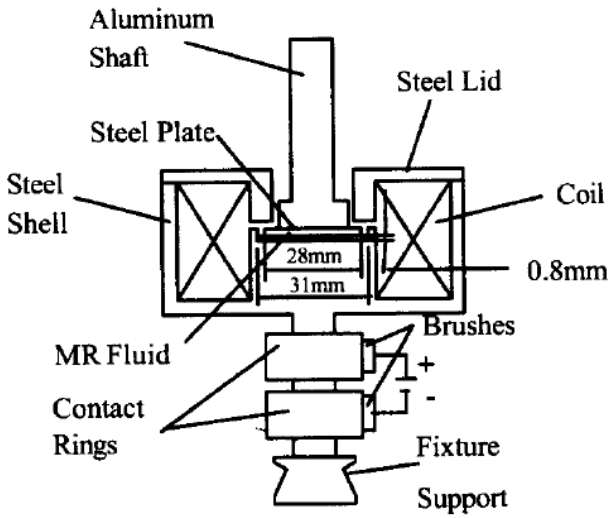

Figure 2-4. Custom designed rheometric cell allows for the activation of MR fluids (adapted from [19])

2.3 Summary of Literature Review

MR fluids have a unique ability to change rheology in response to an applied magnetic field. The degree of the change is dependent of the percentage of ferrous particles suspended in the fluid and the intensity of the applied magnetic field. Many applications have made use of MR technology. The automotive industry in particular has embraced the concept for use in suspension systems. MR dampers have many advantages over their conventional counterparts in this application. The nearly instantaneous response time of the fluid allows for dynamic control systems that continuously adjust damper characteristics to meet the needs of changing road conditions and driver input. MR technology has also proven effective in the area of power transmission. MR clutch and brake devices provide increased service lifetime over conventional friction-based systems. MR fluids are characterized by their yield-stress in comparison to the strength of an applied magnetic field. The instrument used to characterize MR fluids is called a rheometer. For MR fluids, a rotary or shear mode rheometer is commonly used. While shear mode rheometers are generally adequate for providing the necessary fluid characteristics, new areas of research are increasingly using squeeze mode operation. This new demand has necessitated the implementation of an instrument that can characterize MR fluids in squeeze mode.

3. MR Fluid Behavior

This chapter provides information on the operational modes of MR fluid. The chapter begins with a brief introduction to the three modes of operation. The next section presents a discussion of valve mode operation and its applications. Following this, a section is devoted to shear mode operation as well as some of its uses. The next section will cover the final mode of operation, squeeze mode. Finally, a summary is provided to highlight the key points of the chapter.

3.1 Introduction

MR fluids may be operated in a variety of different ways depending on the particular needs of an application. The three common operational modes include valve mode, shear mode, and squeeze mode, all shown in Figure 3-1.

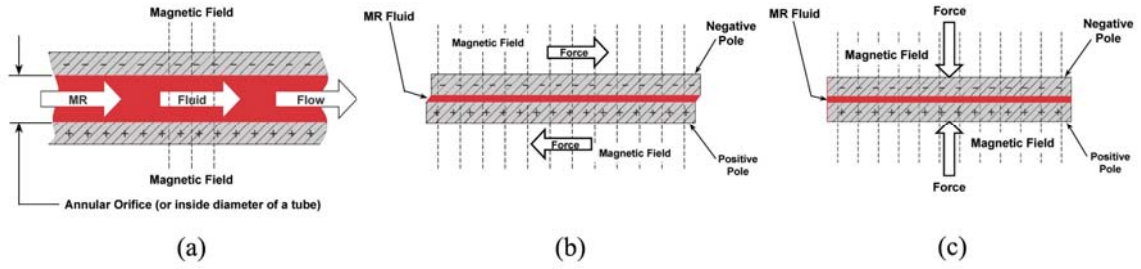

Figure 3-1. MR fluid modes: (a) valve mode; (b) shear mode; (c) squeeze mode (adapted from [25])

Most devices that use controllable fluids can be classified as having either fixed poles (valve mode) or relatively moveable poles (direct-shear mode) [20, 21]. Examples of valve mode devices include servo-valves, dampers, and shock absorbers [21]. Examples of shear mode devices include clutches, brakes, chucking and locking devices [22]. The last mode of operation, squeeze mode, is much less common with the current state of MR technology. Thus far squeeze mode applications have been limited to low displacement devices such as vibration isolation mounts.

3.2 Valve Mode

In valve mode, MR fluid flows between fixed magnetic poles. This means that it flows perpendicular to the magnetic flux lines and thus perpendicular to the ferrous particle chains as well, shown in Figure 3-2. The flow of MR fluid in valve mode is also referred to as pressure driven flow mode as described by Lord Materials Division [23].

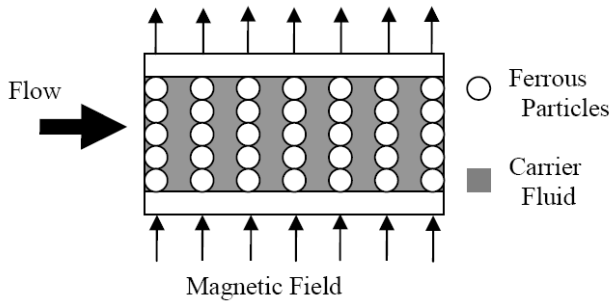

Figure 3-2. MR fluid in valve mode with an applied magnetic field (adapted from [20])

In valve mode operation, a magnetic field is applied across a fluid gap forming ferrous particle chains in the fluid. As the fluid flows through this device, it continuously breaks and then nearly instantaneously reforms the ferrous particle chains. Varying the intensity of the applied magnetic field changes the strength of these chains and in turn the apparent viscosity of the MR fluid. In valve mode, there is a pressure drop across the fluid as it flows through the device. This pressure drop is essentially what is used in a device, such as a shock absorber, to resist an input force

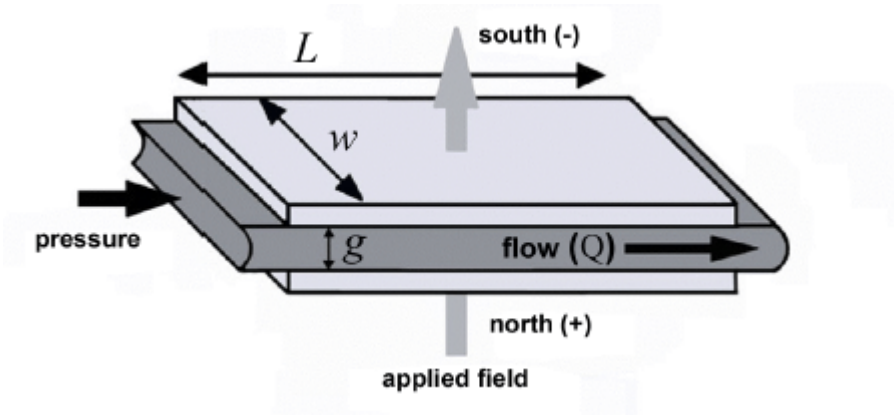

Figure 3-3. Valve mode operation (adapted from [21])

The pressure drop developed in a valve mode device can be divided into a field independent viscous (pure rheological) component ΔP_η and a magnetic field dependent (magneto-rheological) component ΔP_{mr} [21]. The value of this pressure drop may be approximated by

$$\Delta P = \Delta P_\eta + \Delta P_{\text{mr}} = \frac{12\eta Q L}{g^3 w} + \frac{c\,\tau_{\text{mr}} L}{g} \tag{3.1}$$

where η (Pa-s) represents the dynamic viscosity, Q (m^3-s) is the volumetric flow rate of the fluid, and L, g, and w (m) represent the length, fluid gap, and the width of the flow orifice that exists between the fixed magnetic poles, as can be seen in Figure 3-3 [24]. In the magnetic field dependent component of the equation, τ_{mr} (N/mm^2) represents the yield stress developed in response to an applied magnetic field while L and g (m) are the same geometric data found in the rheological component of the equation. The other factor c (no unit) is an empirical factor determined experimentally. This factor is dependent on the ratio of the pressure drop related to the magneto-rheological response compared to the pressure drop related to the inherent viscoelastic properties of the fluid. This constant c varies from a minimum of 2 to a maximum of 3 depending on what $\Delta P_{\text{mr}}/\Delta P_\eta$ ratio, also called the control ratio, is present in the device being considered. For $\Delta P_{\text{mr}}/\Delta P_\eta$ ratios of approximately 1 or less, the value of c is chosen to be 2. For $\Delta P_{\text{mr}}/\Delta P_\eta$ ratios of approximately 100 or larger, the value of c is chosen to be 3 [25]. Equation (3.1) is

commonly used for the design of MR fluid applications in valve mode [26]. Rearranging this equation, the minimum volume of active fluid is established as

$$V = L \cdot w \cdot g = \left[\frac{12}{c^2}\right]\frac{\eta}{\tau^2}\left[\frac{\Delta P_{\text{mr}}}{\Delta P_{\eta}}\right] Q \cdot \Delta P_{\text{mr}} \tag{3.2}$$

where all variables remain as defined in Equation (3.1). This represents the minimum volume of activated fluid required to achieve a desired MR effect (represented by the control ratio in the equation) at a given flow rate Q with the specified pressure drop.

Valve mode is the most common of the three operational modes for MR fluid and serves as the primary method used in MR dampers. Among MR devices, MR dampers have been most widely studied and developed for commercial applications [25]. One example of a successfully commercialized MR damper can be found in the Rheonetic RD-1005-3 manufactured by the Lord Corporation [27]. Much of the success attributed to this MR damper is due its implementation in semi-active seat suspension systems for large on and off road vehicles [21]. This particular damper is used in a seat suspension system available from the Lord Corporation called the MotionMaster™ Ride Management System, which consists of the damper and a control unit as shown in Figure 3-4 [1]. The damper used in this system is of a monotube construction with an extended and compressed length of 8.2 and 6.1 inches respectively. What makes MR dampers so appealing is their wide range of performance adjustability. The Lord Rheonetic RD-1005-3 damper is a perfect example this exhibiting a damping force of more than 500 lbs at velocities larger than 2 in/sec with 1 amp of current and an off-state (i.e. zero current) damping force of less than 150 lbs at 8 in/sec [25].

Figure 3-4. Lord MotionMaster™ Ride Management System (image from adapted from [5])

This damper has also been found in other applications as well, including an innovative prosthetic leg design by Biedermann Motech GmbH [28]. The device, shown in Figure 3-5, dramatically improves the mobility of leg amputees by mimicking a natural gait. Coupled with a combination of sensors and controllers, the device can adapt to varying movements, ranging from uphill and downhill motion to stairs, and even bicycling [1, 29].

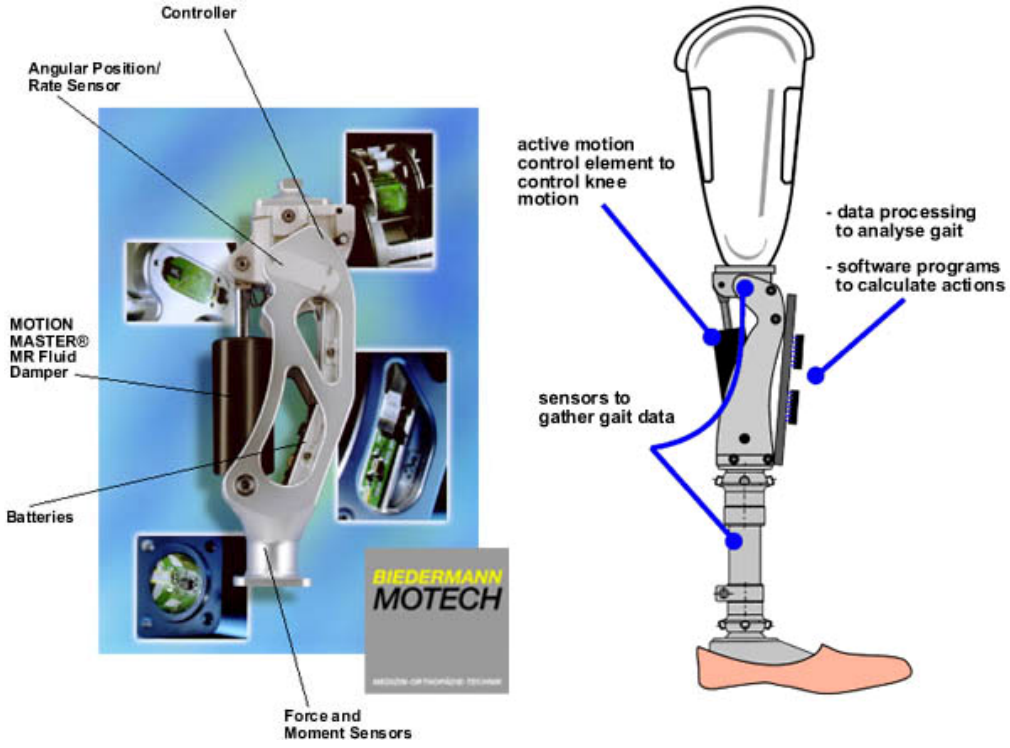

Figure 3-5. Biedermann Motech prosthetic leg (image from adapted from [5])

3.3 Shear Mode

In shear mode, also referred to as direct shear mode, the MR fluid experiences a relative shearing force from one of the plates enclosing the fluid gap. Ferrous particle chains, shown in Figure 3-6, are formed along the flux path of the magnetic field, which runs perpendicular to the pole plates just as in the valve mode configuration. What separates shear mode from valve mode is that the pole plates are not stationary. One of the pole

plates moves parallel to the other causing a shearing force to develop across the fluid gap. Just as in valve mode operation, ferrous particle chains form a mechanical resistance to fluid flow in response to an applied magnetic field. The intensity of the applied magnetic field determines the apparent viscosity of the MR fluid and thus the force transmitted between the pole plates.

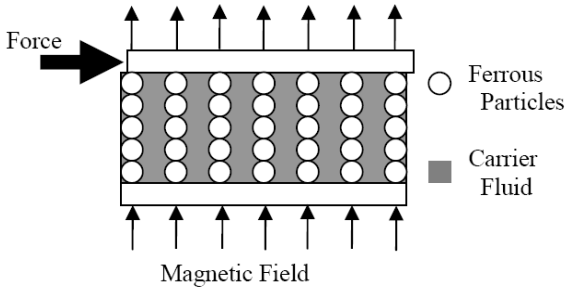

Figure 3-6. MR fluid in shear mode with an applied magnetic field (adapted from [20])

The total force in shear mode can be separated into a viscous (pure rheological) component F_η and a magnetic field dependent (magneto-rheological) component F_{mr} [26]. The total shear force sustained by the fluid is approximated as

$$F = F_\eta + F_{\text{mr}} = \frac{[\eta\ S\ A]}{g} + \tau_{\text{mr}}\ A \qquad \textit{where} \quad A = L \cdot w \tag{3.3}$$

where η (Pa-s) is the dynamic viscosity, S (m/s) is the relative speed of the pole plates. As illustrated in Figure 3-7, *L*, *w*, and *g* (m) represent the length, width, and gap size of the flow channel respectively, while A (m^2) defines the working interface area of the activated fluid. The last variable τ_{mr} represents the yield stress developed in response to an applied magnetic field.

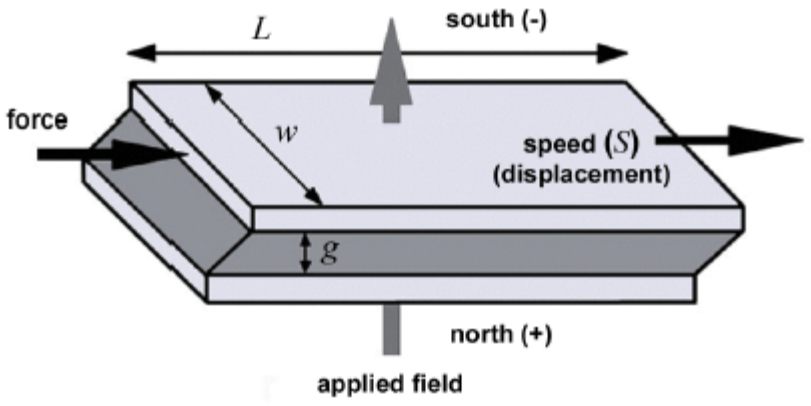

Figure 3-7. Direct shear mode operation (adapted from [21])

When designing an MR device using shear mode operation, the level of force generated by the magneto-rheological effect in comparison to the base rheology of the fluid is generally of great interest. The proportion F_{mr}/F_{η}, called the control ratio, is an indication of the range of force adjustability inherent in the device [26]. A larger ratio would imply that the device is capable of substantial force variation from off-state (zero field) to an energized state (applied field). By manipulating Equation (3.3), a minimum volume of activated fluid can be calculated using

$$V = L \cdot w \cdot g = \left[\frac{\eta}{\tau^2}\right] \cdot \left[\frac{F_{\text{mr}}}{F_{\eta}}\right] \cdot F_{\text{mr}} \cdot S \tag{3.4}$$

where all variables remain as defined for Equation (3.3). This equation represents the minimum volume of MR fluid that must be acted upon to maintain a given control ratio, relative plate speed, and controlled force [21].

Behind valve mode, direct shear mode is the next most common form of MR fluid operation and is widely used in applications such as rotary clutches or brakes. Shear mode operation lends itself particularly well to rotational power transfer devices. When the fluid is in its relaxed state (i.e. the absence of a magnetic field) the shear force generated by the fluid is negligible, as it behaves as a fluid similar to motor oil. In this state, the parallel magnetic pole plates are left uncoupled with virtually no force being transmitted across the fluid. With the application of a magnetic field the MR fluid is able

to generate considerable shear forces, which can be used to transmit power from one plate to another.

One example of this technology can be found in the MR rotary brake system produced by the Lord Corporation, shown in Figure 3-8. This system can be used for a variety of application including exercise equipment, pneumatic actuators, steer-by-wire systems, and other similar torque transfer applications [30]. This device offers high controllability, fast response time (10 to 30 milliseconds), high torque transfer at low speed, and requires very low power. Other benefits of this device include ease of integration, programmable functionality, rugged construction, and long service life [21].

Figure 3-8. Lord Corporation MR rotary brake (image from adapted from [5])

Functionally, this rotary brake consists of a steel disk that rotates in a bath of MR fluid, as shown in Figure 3-9. The MR fluid is activated in shear mode, shown in red above, by an electromagnetic coil that surrounds the periphery of the device [25]. Torque is transferred from the stationary housing to the rotating inner rotor via the activated MR fluid around the circumference of the device. This is a typical design for a shear mode MR device and is representative of the current technology in the marketplace.

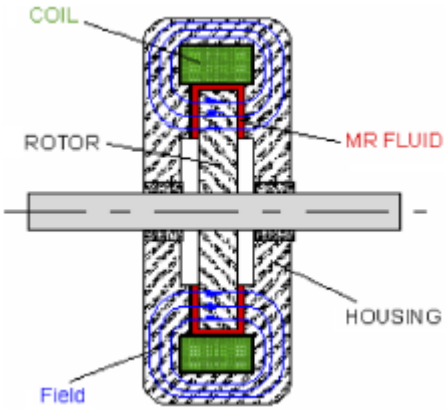

Figure 3-9. Functional principle of an MR fluid brake [26, 31]

3.4 Squeeze Mode

The final mode of operation is the least common and perhaps the least understood. Squeeze mode, shown in Figure 3-10, places the acting force in line with the magnetic flux lines and the particle chains [20, 32].

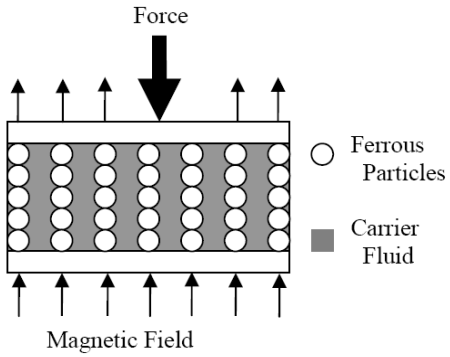

Figure 3-10. MR fluid in squeeze mode setup prior to axial force with an applied magnetic field (adapted from [20])

It is thought that this mode effectively places the ferrous particle chains in a situation similar to columnar buckling [20]. As with the other modes of operation, the strength of the ferrous particle chains is dependent on the intensity of the applied magnetic field. However, unlike the other modes, the usable force generated from squeeze mode is not due to an increase in apparent viscosity. Typically, in squeeze mode devices there is little

or no flow of MR fluid. The force supported in this mode is a mechanical property of the ferrous particles chains rather than the apparent viscosity change of the fluid. Unlike the previous two modes, squeeze mode operation has been developed very little to date and there is no uniformly accepted fluid behavior model to draw from. While less understood than the other modes, squeeze mode has been explored for use in small amplitude vibration control, impact dampers, and MR fluid-elastomer vibration isolators [33, 34].

Much of the work performed to date has focused on vibration controllers for rotor systems [32]. Forte *et al* [35], Ahn *et al* [36], and Carmignani *et al* [37] have developed an MR squeeze film damper system for rotor applications. Wang *et al* [38] investigated the dynamic performance of this system and subsequently went on to analyze the mechanical properties of the film and the unbalanced response characteristics of the MR squeeze film in the damper-rigid rotor system [39]. These studies center around thin film squeeze mode where the typical initial fluid gap is no more than 0.075" thick and low displacements on the order of 0.010" or less [36]. However, a thorough study of the stress-strain characteristics in compression of MR fluids in squeeze mode is still not complete [32].

Another application that has adopted the use of squeeze mode operation is fluid-filled elastomer vibration mounts. In this device, shown in Figure 3-11, a hollow elastomer puck is filled with MR fluid to provide a means of adjusting the stiffness of the device [3]. In some designs the elastomer puck is capped by ferrous pole plates on the top and bottom to promote the magnetic flux path through the MR fluid gap. The various parts that make up a typical MR fluid-elastomer isolator can be seen in Figure 3-12.

Figure 3-11. Photograph of MR fluid-elastomer vibration isolator specimens (adapted from [3])

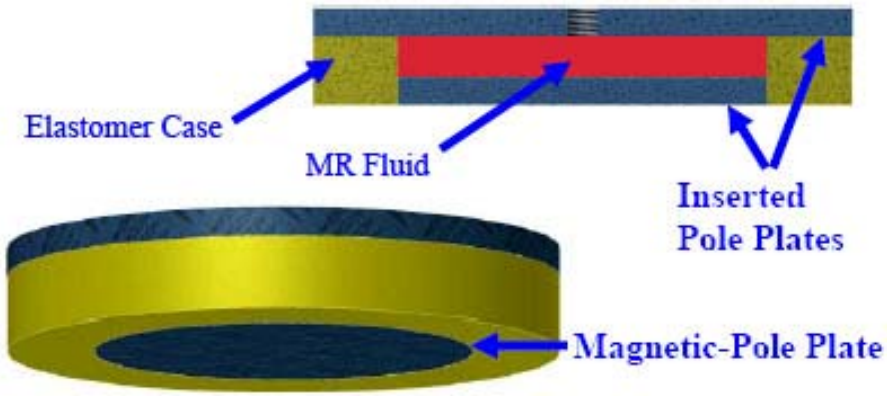

Figure 3-12. Section view of an MR fluid-elastomer vibration isolator (adapted from [3])

Typically, a vibration isolator such as this would be found in a mechanical system with a known operating frequency, such as an engine turning at a constant RPM. In a case such as this, it is possible to design a simple non-adjustable mount with a stiffness that is matched to the system's mass and input frequency in a way that will cancel much of the transmitted vibration. The need for a mount with adjustable stiffness arises when the operating parameters of the system vary such that it may pass through a resonance zone with the mount, which has the potential to create forces far beyond normal conditions and potentially damage equipment. This can commonly occur during the startup or shut down of large-scale steam turbines used in power generation. A mount with adjustable stiffness can be continuously matched to changing operating conditions to provide the optimum vibration cancellation characteristics. These devices are still in their infancy and have yet to be implemented on a commercial scale, but the work by Southern *et al* [3, 40] shows promising potential for this application.

Larger displacement applications of squeeze mode have yet to be investigated, but some innovative damper designs are currently underway to explore this concept. During the limited investigations of squeeze mode operation it has been discovered that squeeze mode is capable of producing compression and tensile stresses which are much higher than the other operational modes [32]. In particular, the compressive stress supported by activated MR fluid has proved to be quite impressive. When a magnetic field is applied to a device operating in squeeze mode, the ferrous particle chains form through the MR fluid

aligning themselves with the flux path of the magnetic field. In squeeze mode, the flux path happens to parallel the direction of the external force, as shown in Figure 3-13. This places the particle chains in a position where they are thought to act as columnar structures supporting the pole plates [32].

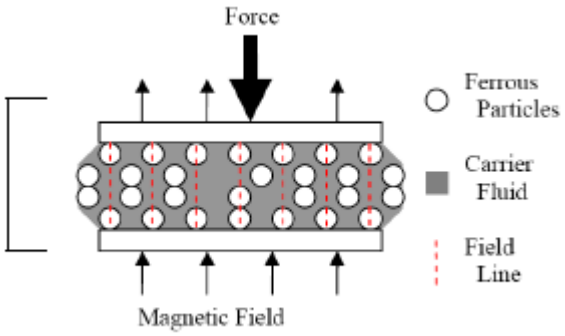

Figure 3-13. MR fluid in squeeze mode operation with axial force and applied magnetic field (adapted from [3])

When an external force is applied with the columnar structures in place from an applied magnetic field, the fluid must push laterally through these columns in response to the changing gap height between the plates [3]. This motion tends to place the columnar structures in a buckling condition which is resisted only by the axial compressive strength of particle chains, which are in turn dependent on the intensity of the applied magnetic field. Because the fluid is assumed incompressible, an elastic deformation at the boundary must occur to account for displaced fluid as the gap height decreases, shown in Figure 3-13 [3]. Typically, this is achieved with an elastic container or expandable diaphragm designed to encapsulate the fluid.

As fluid is squeezed, the ferrous iron particles tend to aggregate as discussed by Goncalves *et al* [3, 41]. An example of this particle aggregation is shown in Figure 3-14. Aggregation occurs in squeeze mode applications more commonly than in the other operational modes partly because the fluid has no device to mix the fluid while in use. In the case of valve or shear mode, the iron particles are continuously remixed with the carrier fluid simply due to the nature of the fluid flow in those modes. This particle aggregation tends to add to the compressive strengthening effect of the MR fluid,

however, it does not have the same strengthening effect when the fluid is unloaded and placed in a tensile stress condition. Therefore, squeeze mode operation may increase the hysteresis between loading and unloading the fluid or the dynamic damping element when placed in an elastomer, as seen in the work by York *et al* [3, 42].

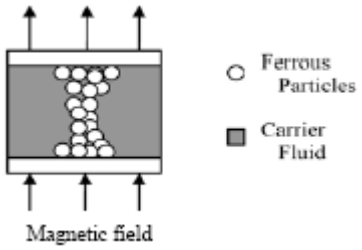

Figure 3-14. Ferrous particle aggregation in squeeze mode operation after experiencing compressive load (adapted from [3, 41])

3.5 Summary

MR fluid may be operated in three distinct modes: valve mode, direct-shear mode, and squeeze mode. Valve mode is the most common of the operational modes and is also perhaps the best understood at present. Valve mode is defined by the use of stationary pole plates with pressure driven MR fluid flow through the gap between plates. Valve mode is the principle device used in MR dampers, which is the most widely-used application of MR technology. Shear mode, like valve mode, is also widely studied and understood. It is primarily used in devices such as rotary brakes, clutches, or other similar torque transfer devices. Shear mode is characterized by the use of pole plates that slide parallel to one another, while the MR fluid between them resists said motion. The last and least understood operational mode is called squeeze mode. This form of operation is still in its infancy and has seen limited application as of yet. Squeeze mode offers increased compressive strength over other modes of operation, but is limited to relatively low displacement applications in the current state of the technology. Applications that have been investigated with this mode include squeeze film damper systems for rotor applications and MR fluid-elastomer vibration isolator mounts. Particle aggregation is a phenomenon that arises in squeeze mode more commonly than in other modes due to the lack of continuous fluid mixing that naturally occurs in valve and shear mode.

4. Squeeze Mode Rheometer

This chapter provides information on the squeeze mode rheometer developed for this research. The chapter begins with a brief overview of rheometers and their uses. The following section includes a top level discussion of what should be included in a squeeze mode rheometer. The next section is dedicated to the design of the squeeze mode rheometer. Following this, a discussion on the fabrication and assembly of the rheometer is provided. The chapter concludes with a section summarizing the key points presented in this portion of the document.

4.1 Introduction to Rheometers

A rheometer is a device used to characterize the viscous properties of fluids, as well as reading their elastic responses. As stated previously, the rheology of a fluid refers to the properties of its flow and deformation. Rheology may also be described as the study of the stress-deformation relationship in a material [16]. Rheometers quantify the properties of fluids through creep testing including dynamic tests (oscillation method), normal force measurement (squeeze testing), shear, stress jumps, or a combination of the above [43].

The rheology of materials is of great interest for a variety of industries including the pharmaceutical, food, oil, and construction industries [17, 43, 44]. The types of fluids measured with rheometers vary as widely as the industries they serve. Some examples of fluids commonly studied using rheometers include pharmaceutical pastes, wet concrete samples, plastic melts, greases, oils, and a variety of edible slurries and liquids found in the food industry. For many of these applications, the knowledge of fluid rheology is used to design optimized pumping equipment or for improved mold and die designs.

Rheometers use a number of different technologies to measure the properties of fluids. Common among these technologies are rotational rheometry, capillary rheometry, and falling ball testing. As previously discussed, in rotational rheometry a torque is required to rotate a spindle at a constant speed while immersed in the sample fluid. The torque is proportional to the viscous drag on the immersed spindle, and thus to the viscosity of the fluid [43]. An example of rotational rheometer is shown in Figure 4-1.

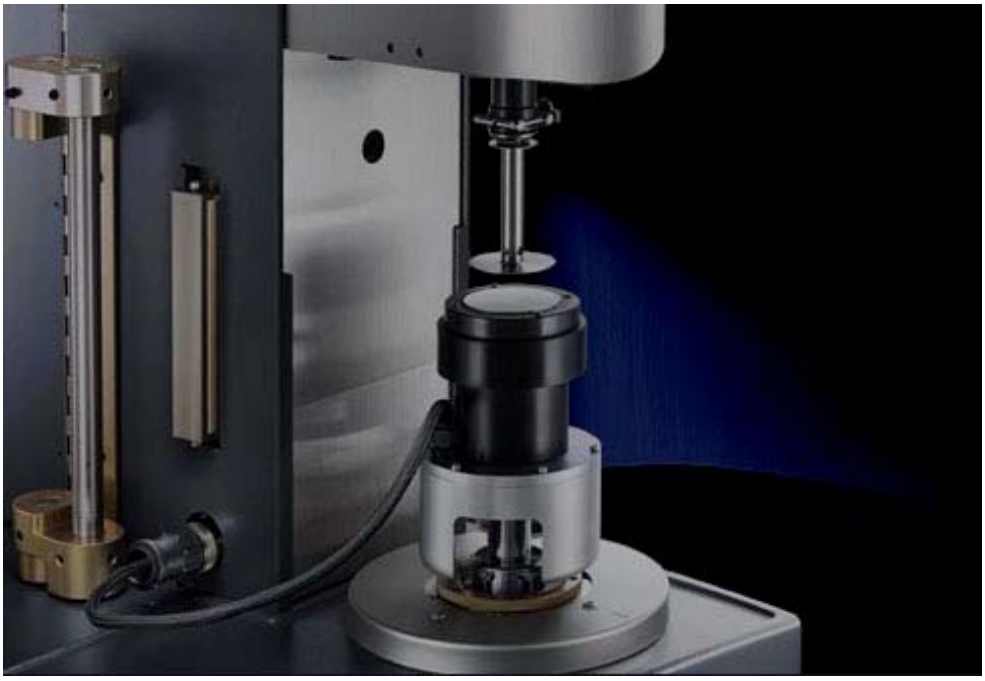

Figure 4-1. A typical rotational shear-type rheometer from TA Instruments (image adapted from [45])

Capillary rheometers measure the flow rate of a fixed volume of fluid through a small orifice at a controlled temperature, as seen in Figure 4-2. In a typical capillary rheometer the rate of shear can be varied from near 0 to over 100 (s^{-1}) by changing capillary diameter and applied pressure. The elapsed time for a specific volume of fluid to pass through the orifice is measured and then correlated to the viscosity of the fluid. A capillary rheometer is limited to the measurement of kinematic viscosity, as opposed to the dynamic viscosity [43].

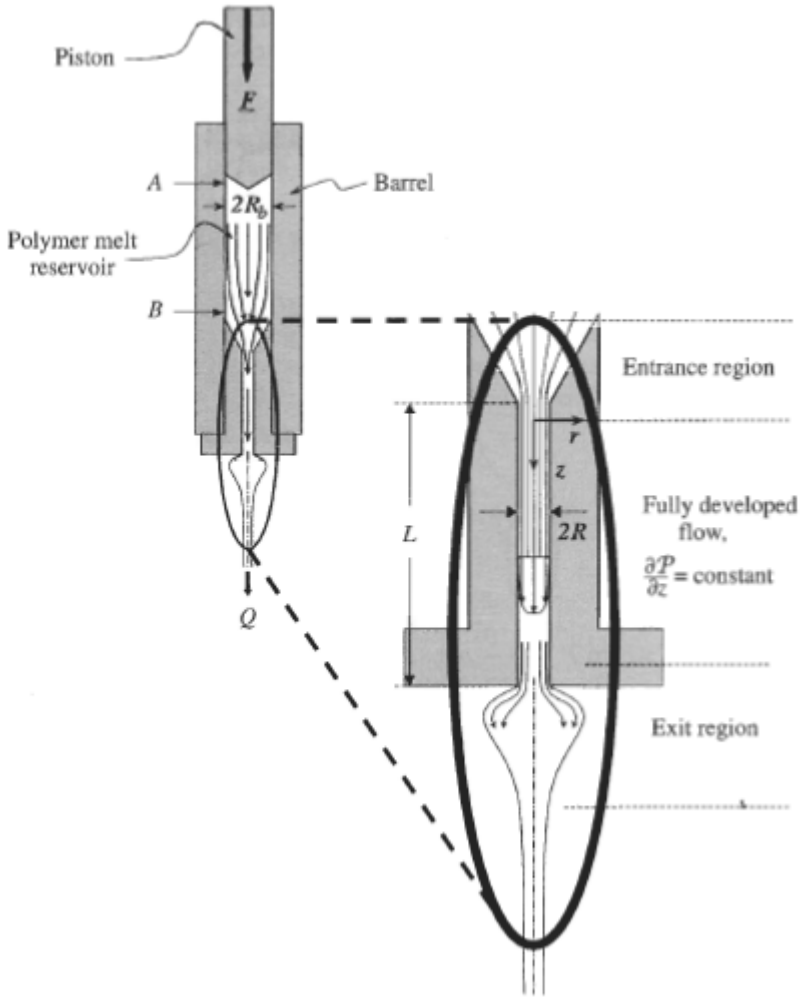

Figure 4-2. Geometry used in a typical commercial capillary rheometer (adapted from [15])

In a falling ball rheometer, as seen in Figure 4-3, the viscosity is proportional to the time required for a ball, which is typically made from steel or a nickel-iron alloy, to fall through the test fluid contained in a precise and temperature controlled glass tube [43, 46].

Squeeze mode rheometers have not been developed until recently for MR fluid applications. A squeeze mode rheometer, shown in Figure 4-4, uses a piston to positively displace MR fluid while a load cell measures the corresponding resistance force generated by the fluid [32].

Figure 4-3. A falling ball rheometer from RheoTec Messtechnik GmbH (image adapted from [46])

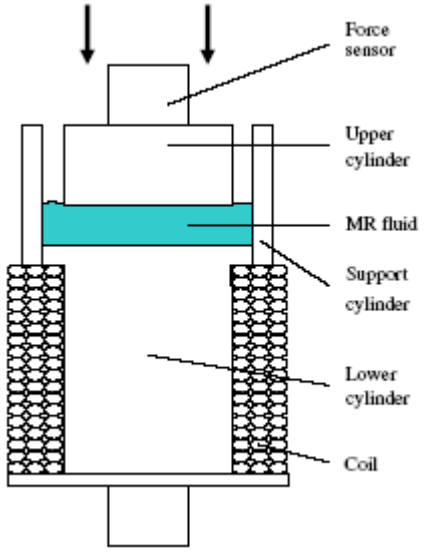

Figure 4-4. Diagram of a squeeze mode rheometer developed by Mazlan *et al* (adapted from [47])

4.2 Squeeze Mode Rheometer Concept

The design of the MR fluid squeeze mode rheometer can be separated into 4 different areas. These areas include fluid actuation, fluid management, data acquisition, and magnetic circuit design. Elements from each of these areas are illustrated in Figure 4-5.

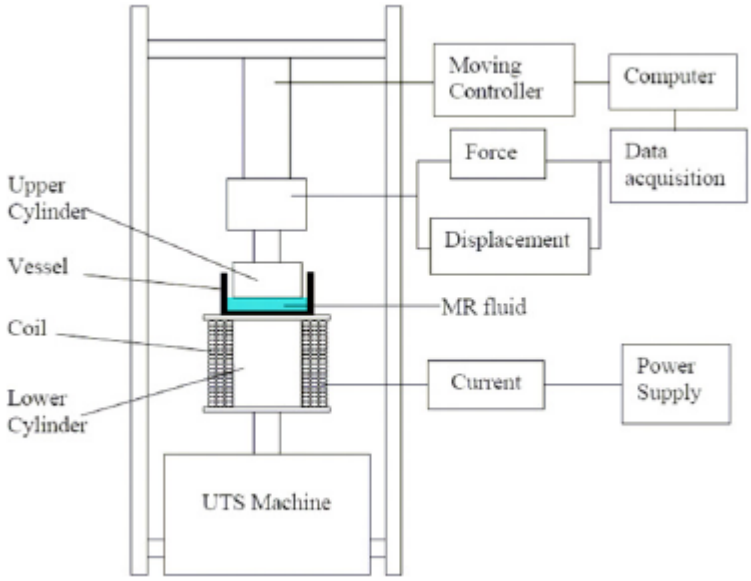

Figure 4-5. Schematic of the squeeze mode rheometer setup used by Mazlan *et al* (adapted from [32])

As mentioned in the previous chapter, MR fluid may be operated in several different ways. The squeeze mode is primarily defined by a force line of action in parallel to the magnetic flux path and ferrous particle chains. This mode requires linear actuation of the fluid in line with the flux path. Pneumatic, hydraulic, or electric linear actuators are all acceptable choices to accomplish this task.

Unlike valve and shear mode, MR fluid actuated in squeeze mode does not lend itself quite as easily to a fully enclosed design. While there are certainly options for having a self-contained unit, they are not the most straightforward and this is not a requirement for the rheometer. As MR fluid is placed into compression by a linear actuator, the fluid gap size is decreased and the available volume for the fluid is reduced from its original state. MR fluid is assumed incompressible and thus the rheometer must allow for a path for excess fluid to be expelled during a compression stroke. Options for accomplishing this

task include using an oversized chamber with an undersized piston, shown in Figure 4-4, which allows the fluid to be expelled through the circumference of the piston. Another way to manage the excess fluid is with the use of a flexible diaphragm that will allow for the volume change, as shown in Figure 4-6.

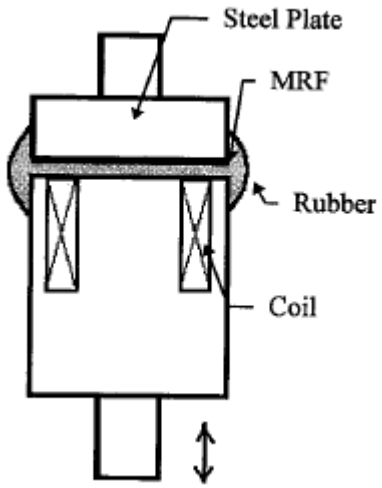

Figure 4-6. This MR device uses a rubber diaphragm around the perimeter to allow for fluid displacement under operation (adapted from [48])

Data acquisition is the next area of concern in the rheometer design. The required measurements for the squeeze mode rheometer include the input force from the linear actuator, the position of the actuator, and the current supplied to the electromagnet. With these measurements, the stress-strain relationship of the fluid may be calculated. The intensity of the magnetic field through the fluid gap may be sufficiently approximated using electrical current, assuming that the physical properties of the coil magnet and device are known. Optional data channels include a direct magnetic flux density measurement via a Gauss-meter.

The last area of interest involves managing the magnetic flux path via a magnetic circuit. A magnetic circuit behaves in much the same way as a simple electrical circuit, but controlling the flow of magnetic flux as opposed to electricity. A simple magnetic circuit starts with the use of a magnetic source, which can be a coil magnet, a permanent magnet, or a combination of the two. The magnetic source is analogous to a battery or

voltage source in an electric circuit. A coil electromagnet, such as the one shown in Figure 4-7, is used to generate a magnetic field using a current supply. The relationship between the supplied current and the magnetic field is defined by the integral equation

$$F = NI = \oint H \cdot dl \tag{4.1}$$

where F represents the magnetomotive force generated by the coil, N is the number of turns of wire in the coil, I is the current supplied, H is the magnetic field strength, and dl represents the closed path of the magnetic field. From Equation (4.1) it is clear that there are two choices for increasing the strength of the magnetic field generated by a coil magnet. These options include increasing the number of turns in the coil and increasing the current supplied to the coil. In many applications, packaging constraints limit the options in wire gauge, and therefore maximum allowable current, and number of turns in the magnet. Fortunately, the packaging constraints of the squeeze mode rheometer are few, thus allowing for design freedom in regards to the coil magnet.

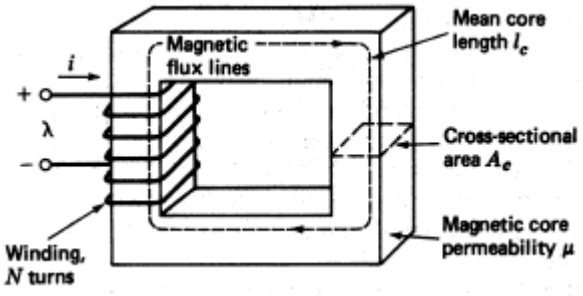

Figure 4-7. A simple magnetic circuit (adapted from [49])

Along with the magnetic field strength H, the magnetic flux density B generated by the coil can be calculated using

$$B = \mu H \tag{4.2}$$

where μ is the permeability of the material. Permeability can be thought of as the magnetic conductivity of a material. A large permeability value, such as those found in iron or steel, indicates that a material will easily pass a magnetic field. Another value of interest is the magnetic flux ϕ at a given point in the magnetic circuit. Total magnetic flux is given by

$$\phi = B \cdot A \tag{4.3}$$

where B is the magnetic flux density at a given point in the circuit and A is the cross-sectional area of the magnet core or flux path at said point. Rearranging Equations (4.1), (4.2), and (4.3), we obtain

$$\phi = \frac{NI}{l/(\mu A)} = \frac{F}{R_m} \tag{4.4}$$

where R_m is the magnetic reluctance of the magnetic circuit and all other values remain as previously defined. The magnetic reluctance is similar to the "resistance" of the circuit and is inversely related to permeability by

$$R_m = \frac{l}{\mu A} \tag{4.5}$$

where l is the length of the magnetic circuit, μ represents the permeability of the material through which magnetic flux travels, and A is the cross-sectional area of the circuit.

With the coil magnet serving as the "power source" for a magnetic circuit, the analogy to a simple electrical circuit becomes clear, as shown in Figure 4-8. An analog of Ohm's law in electrical circuit theory may be applied to magnetic circuits by taking the magnetic flux ϕ as the "current", the magnetomotive force F as the "emf of a voltage source", and the magnetic reluctance R_m as the "resistance" in the magnetic circuit. With this analogy in place, the design of magnetic circuits becomes quite straightforward.

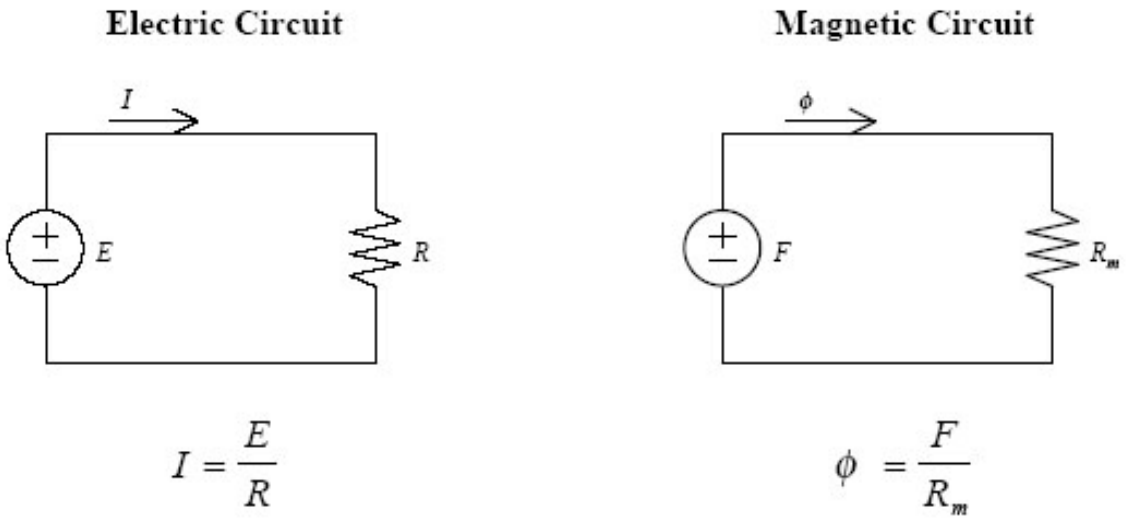

Figure 4-8. A form of Ohm's law can be applied to magnetic circuit in much the same as to a simple electrical circuit (adapted from [49])

4.3 Squeeze Mode Rheometer Design

This section details the design of the squeeze mode rheometer developed for this research. The overall configuration of the rheometer, as shown in Figure 4-9, is of a cylindrical design that incorporates a sliding piston within a shell to apply force to the fluid.

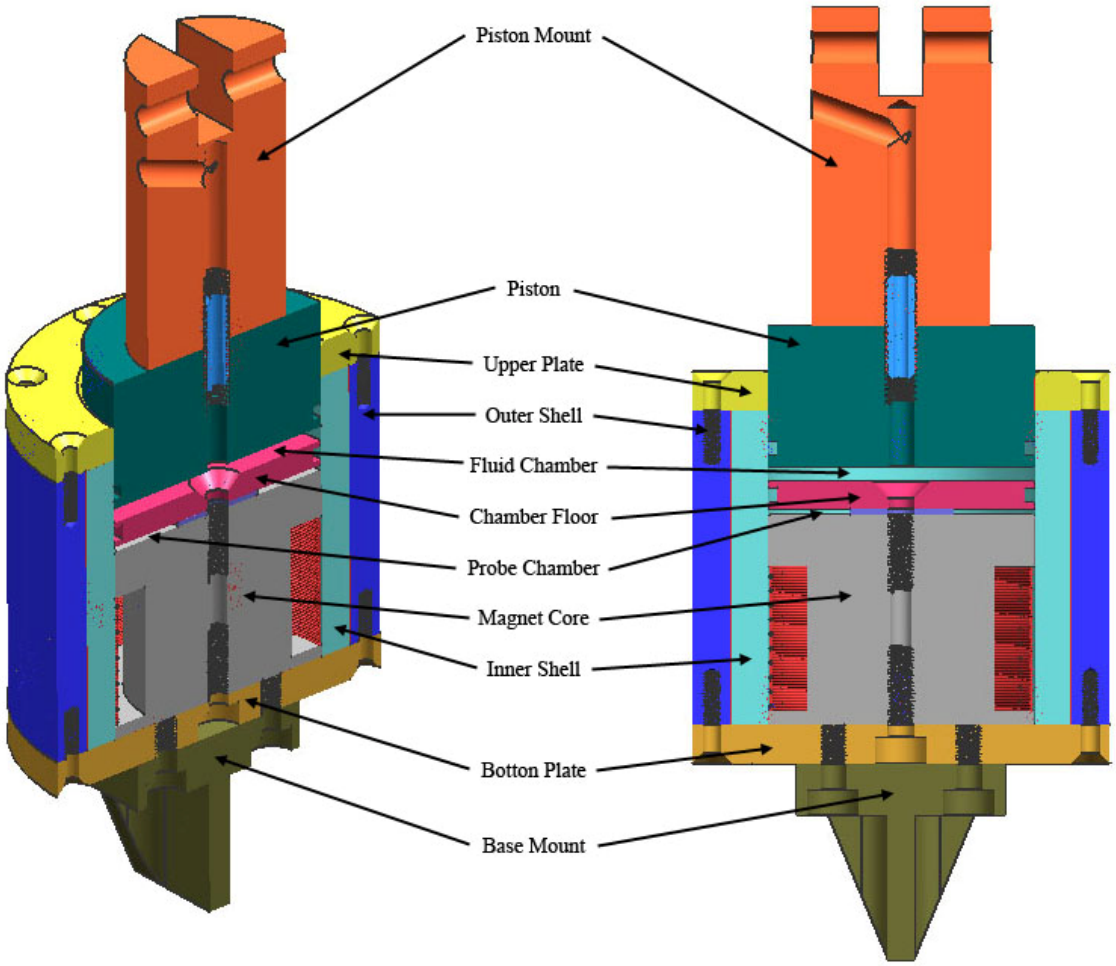

Figure 4-9. A cross-sectional view of the rheometer with major components labeled

In the assembly shown above, only the piston and piston mount are able to move relative to the rest of the rheometer. The MR fluid test chamber is located directly below the piston, which means that the volume of this chamber, and thus the MR fluid within, is dependent on the position of the piston. A steel disk forms the floor of the test chamber. Both the chamber floor disk and piston are sealed to the aluminum inner shell by way of Buna-N o-rings. An air gap of approximately 0.050 in, which is created by a stainless steel (SS) washer, is located between the chamber floor and the top of the magnet core. This air gap provides a location for a Gauss-meter probe that is used to verify the magnetic flux generated by the device. The coil magnet, which uses a 12L14 steel core, is located below the Gauss probe gap and is bolted to the bottom plate. The bottom plate joins the base mount and coil magnet to outer shell. The steel outer shell provides the

return path for the magnetic flux as well as structural rigidity. The aluminum inner shell directs the magnetic flux path through the MR fluid test chamber and also provides a smooth sealing surface for the piston and chamber floor.

The rheometer developed in this research is intended for use predominantly in quasistatic-type testing. This makes the fluid management aspect of the design less of a concern when compared to a rheometer that operates over a wide range of frequencies or velocities. With the intended use in mind, a simple approach is taken in regards to managing excess MR fluid. MR fluid is allowed to escape from the test chamber via a single hole drilled through the center of the circular piston that squeezes the fluid. As shown in Figure 4-10, the passage continues into the center of piston mount where it is plumbed, at an angle, out of the rheometer. A small reservoir is attached to the exit of this passage via ¼ in clear vinyl tubing. Under operation, the reservoir and tubing are filled with a sufficient volume of fluid as to prevent air from being introduced into the test chamber.

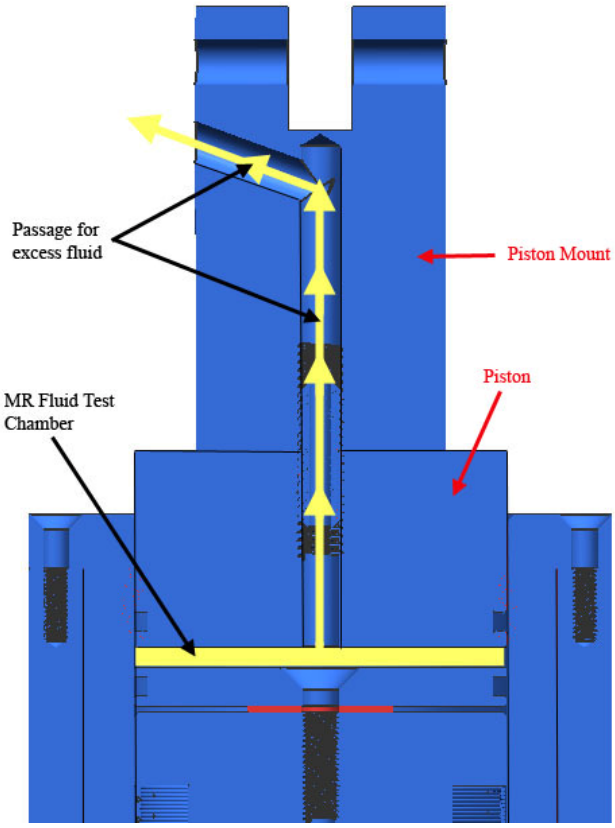

Figure 4-10. MR fluid is allowed in and out of the test chamber through a passage in the piston and piston mount

As discussed in the previous section, one of the areas critical to the design of the rheometer is the management of the magnetic flux path. Much of the design for this rheometer centers around the magnetic circuit. The goal for this design is to be able to generate a sufficient level of magnetic flux to saturate the test fluid with a current supply of 4 Amps. Recalling from Equation (4.4), in order to maximize the magnetic flux with a fixed current supply, the magnetic reluctance must be minimized. As shown in Figure 4-11, the magnetic circuit is formed placing low reluctance materials in strategic locations to form a complete loop for the magnetic flux to follow. The low reluctance materials in these areas are a mix of 1018 mild steel and 12L14 steel, both of which exhibit good magnetic permeability properties and machining characteristics. A high reluctance aluminum shell surrounding the coil magnet is positioned along the length of the rheometer to prevent the magnetic flux path from deviating away from the MR fluid chamber. In this configuration, nearly all of the magnetic flux flows through the MR fluid.

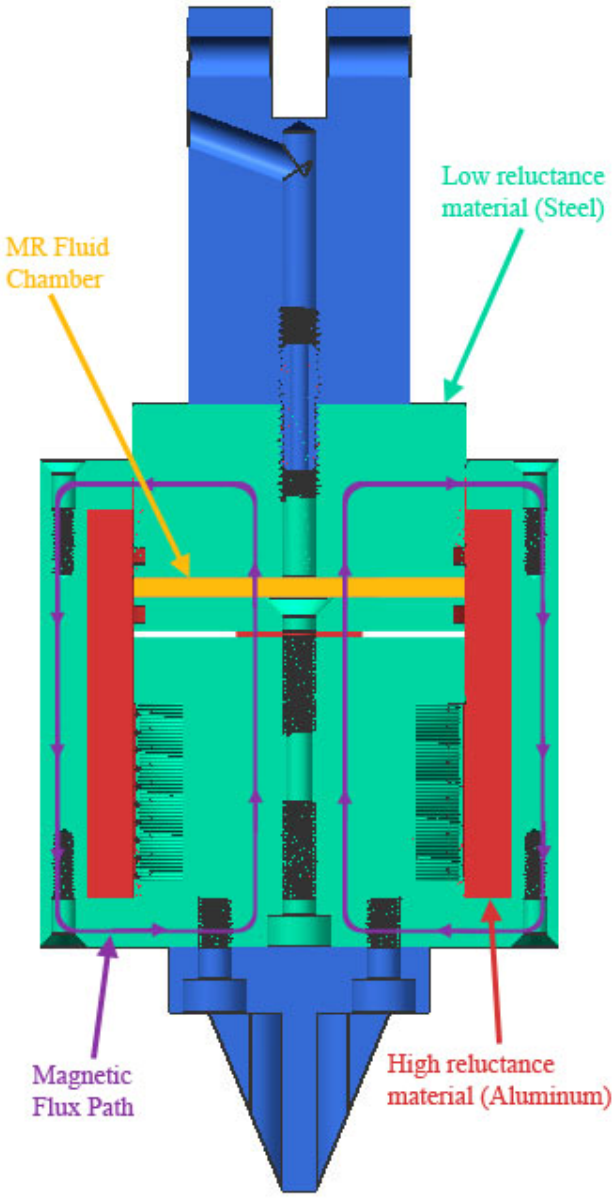

Figure 4-11. The path of magnetic flux is controlled using magnetic conductors and insulators.

Air has a fairly large reluctance value relative to steel; hence, it is generally not desired in the magnetic flux loop. There are two points in the design where an air gap has the opportunity of being introduced. The first is in the interface between the sliding piston and the upper plate. The piston must have enough clearance to slide freely, but a large gap reduces the magnetic flux generated through the circuit. The piston is sized such that its diameter is only 0.001 in smaller than the inner bore of the upper plate and aluminum

shell. With this design, the reluctance contribution from the air gap is assumed negligible. The second area where an air gap is introduced into the magnetic flux path is in the space allocated for the Gauss-meter probe. This air gap is necessary for the probe, but the size of the gap was reduced as much as possible while still allowing enough space for the probe to be easily inserted and positioned. The air gap for the probe is set at 0.050 in by way of a stainless steel washer that sits between the chamber floor and the coil magnet.

A software package called Finite Element Method Magnetics (FEMM) was used throughout the design process of the rheometer [50]. With this software, the magnetic circuit of the rheometer can be quickly analyzed allowing for multiple design iterations before manufacturing. The program is a simple finite element code capable of solving 2-D and axisymmetrical magnetic problems. The magnetic circuit portion of the rheometer design is axisymmetric in nature, thus a more complex 3-D finite element solver is not required. As shown in Figure 4-12, the rheometer design is entered as a series of lines and areas. Each area is assigned a magnetic material property. The leftmost edge of each drawing in Figure 4-12 represents the axis of symmetry. The software assumes that each area drawn to the right of this line is uniformly revolved around the axis of symmetry, thus creating a cylindrical volume. The right-hand picture of Figure 4-12 is color coded by material definitions used in FEMM. The shades of green represent various ferrous materials that readily pass magnetic flux, while the shades of red represent non-ferrous materials that significantly inhibit the magnetic flux path. The area of blue represents the coil magnet, which can be thought of as the “power source” in the magnetic circuit.

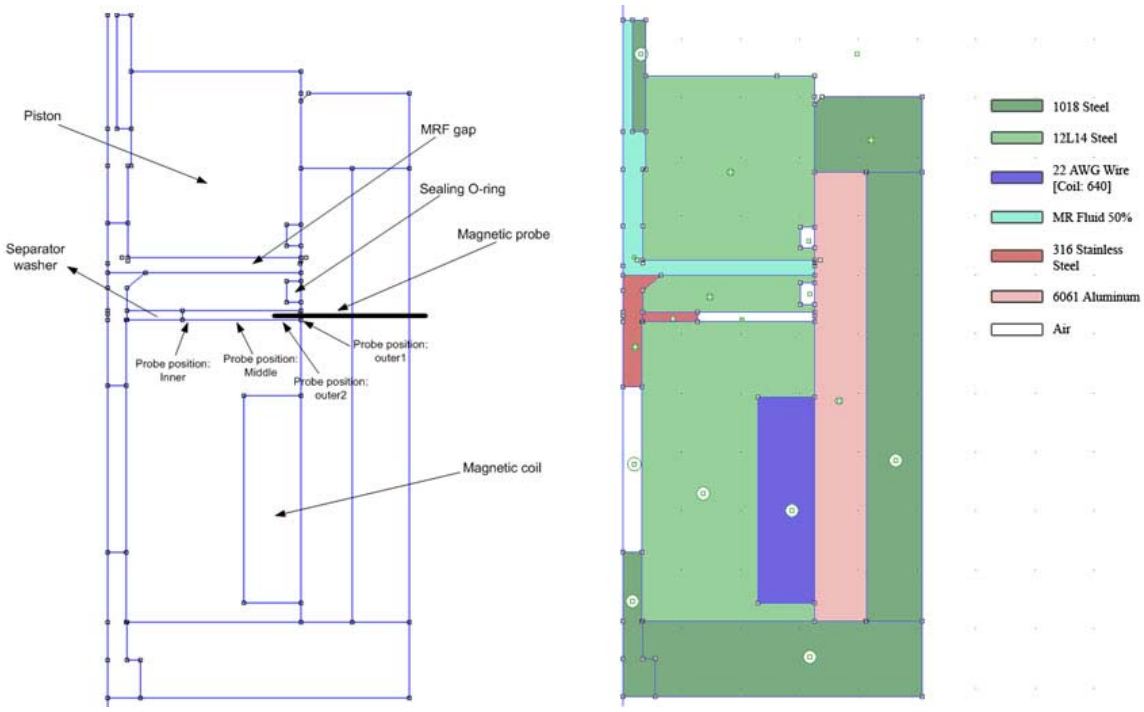

Figure 4-12. The rheometer design as entered in the FEMM program

One feature of the software useful to this research is the analysis of the magnetic flux path and flux density. A contour plot of the magnetic flux path and flux density is shown in Figure 4-13. The flux path is marked by the contour lines, which form a loop through the structure. This plot provides a clear visual of how the ferrous material directs the path of the magnetic flux. The colors in this plot represent the flux density distribution within the rheometer.

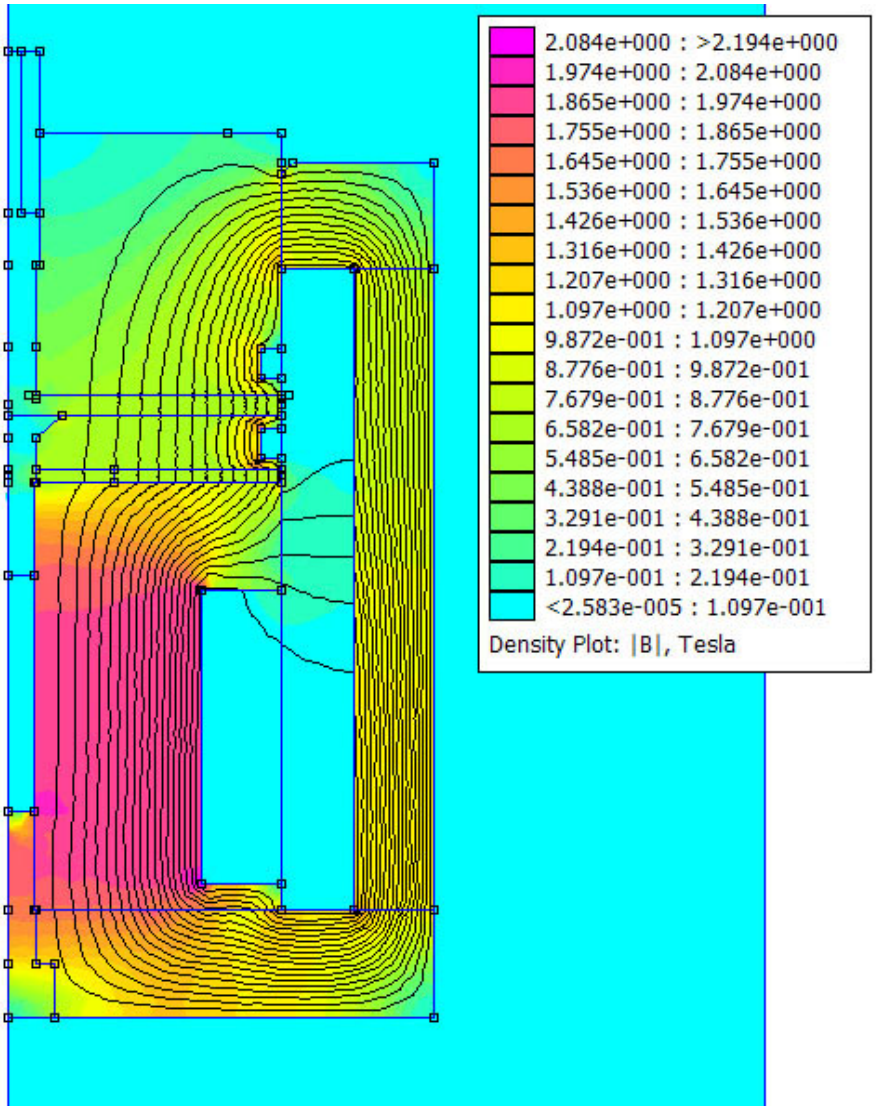

Figure 4-13. FEMM results with 3A of current supplied to the coil magnet

The areas of greatest interest are the Gauss-meter probe gap located above the magnet core and the MR fluid test chamber located below the piston. It is desirable to have a uniform flux density across the both of these areas. A comparison plot of the flux density distribution in these two areas is presented in Figure 4-14. This plot shows the flux density as function of the radius in the test chamber of the rheometer. It is clear from this plot that the flux density is constant and uniform through the majority of the radius. Also, the flux density in the gauss probe gap closely follows the density found in the MR fluid test chamber. This model indicates that flux density measurements taken in the air gap

below the test chamber should closely follow the conditions experienced through the MR fluid.

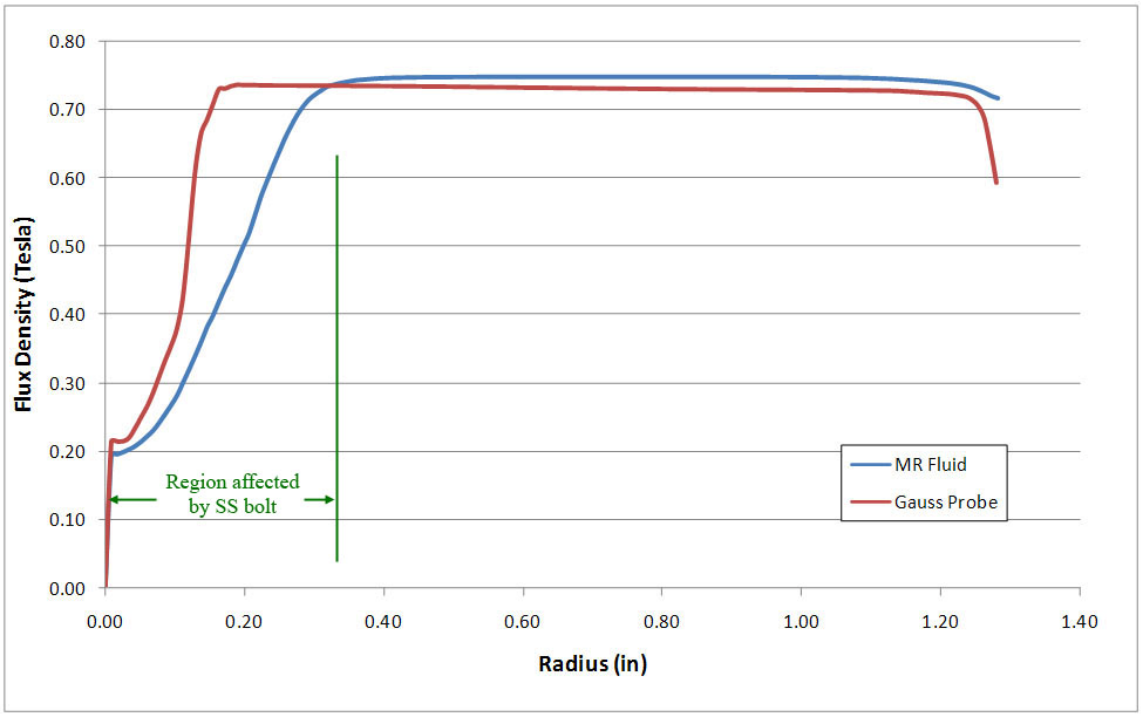

Figure 4-14. The flux density across both the MR fluid chamber and the Gauss-meter probe area for a current supply of 3 Amps

4.4 Rheometer Fabrication and Assembly

The section details the fabrication of the squeeze mode rheometer as well as instructions to assemble and install it on an MTS material testing rig.

4.4.1 Rheometer Fabrication

The squeeze mode rheometer consists of 13 custom machined pieces along with 32 off-the-shelf parts, as can be seen in Table 4-1 and Figure 4-15. The following paragraphs provide a brief description of the fabrication process for each of the 13 custom components in the rheometer.

Table 4-1. Bill of materials for squeeze mode rheometer

Bill of Materials			
Part Number	Qty	Description	Purchased/Custom
1	1	Top Strut - 6061 Aluminum	Custom
2	1	Piston Mount - 12L14 Steel	Custom
3	1	Piston - 12L14 Steel	Custom
4	1	Piston Stud - Steel	Custom
5	1	Upper Plate - 1018 Steel	Custom
6	1	Chamber Floor - 12L14 Steel	Custom
7	1	Magnet Core - 12L14 Steel	Custom
8	1	Outer Shell - 1018 Steel	Custom
9	1	Inner Shell - 6061 Aluminum	Custom
10	1	Bottom Plate - 1018 Steel	Custom
11	1	Base Mount - 6061 Aluminum	Custom
12	1	Gauss Probe Bracket - 1018 Steel	Custom
13	1	Gauss Probe Clamp - 6061 Aluminum	Custom
14	1	5/16 in Spherical Joint	Purchased
15	1	5/16-24 Jam Nut	Purchased
16	1	5/16-24 Hex Bolt	Purchased
17	1	5/16-24 Nylon Lock Nut	Purchased
18	1	Stainless Steel 1/4 in Flat Head Cap Screw	Purchased
19	1	Stainless Steel 1/4 in Washer	Purchased
20	3	1/4-28 Steel Socket Head Cap Screw	Purchased
21	16	8-32 Flat Head Cap Screw	Purchased
22	2	Buna-N O-ring size 142	Purchased
23	2	8-32 Socket head cap screws	Purchased
24	1	¼ in Male-Male Plastic Hose Barb	Purchased
25	1	¼ in Clear Vinyl Tubing	Purchased
26	1	Plastic Funnel with ¼ in connection	Purchased

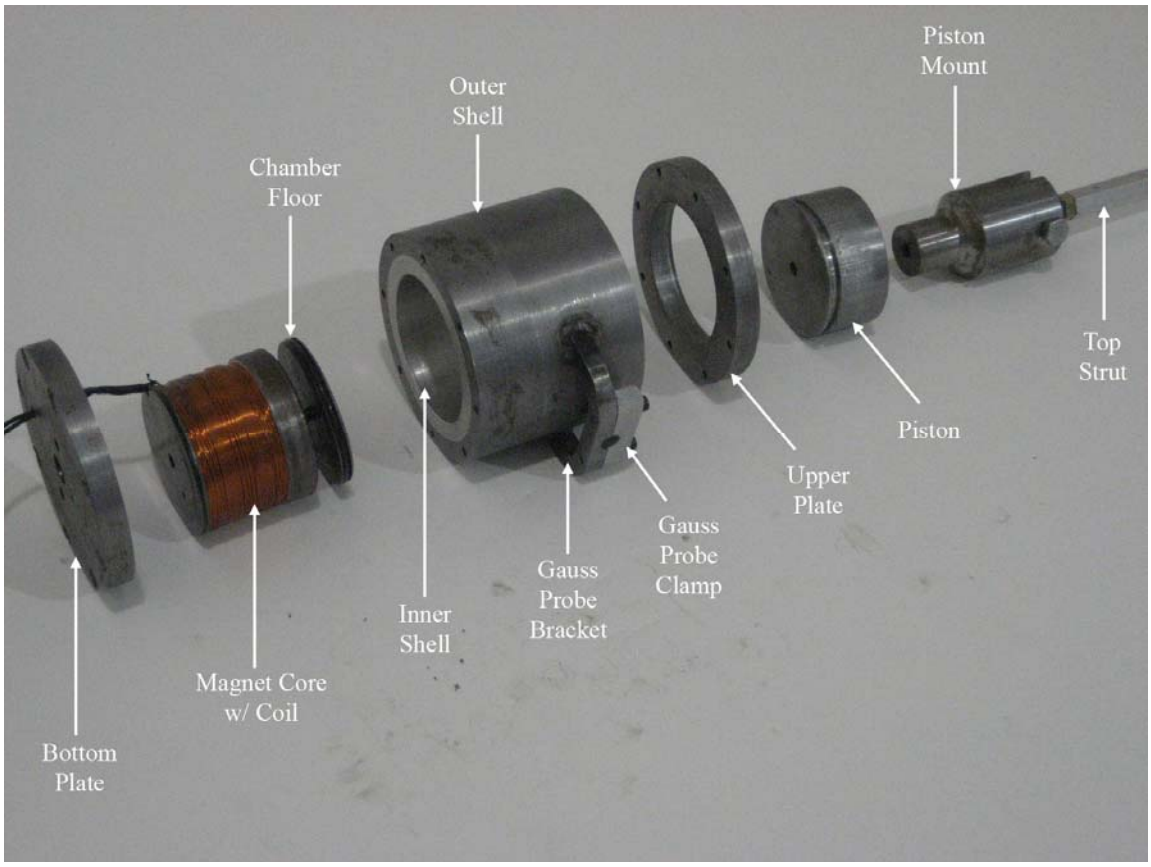

Figure 4-15. Exploded layout of the squeeze mode Rheometer (photo by Ryan Cavey)

The first of the custom components is the Top Strut shown in Figure 4-16, which connects the Piston Mount to the MTS load cell. This part is made from an Al 6061 hexagonal rod with a width of ½ in and a length of 11 in. One end of the hex rod is machined to form a clamping surface for the MTS load cell, while the other end is drilled and tapped with a 5/16-24 UNF thread for a spherical joint.

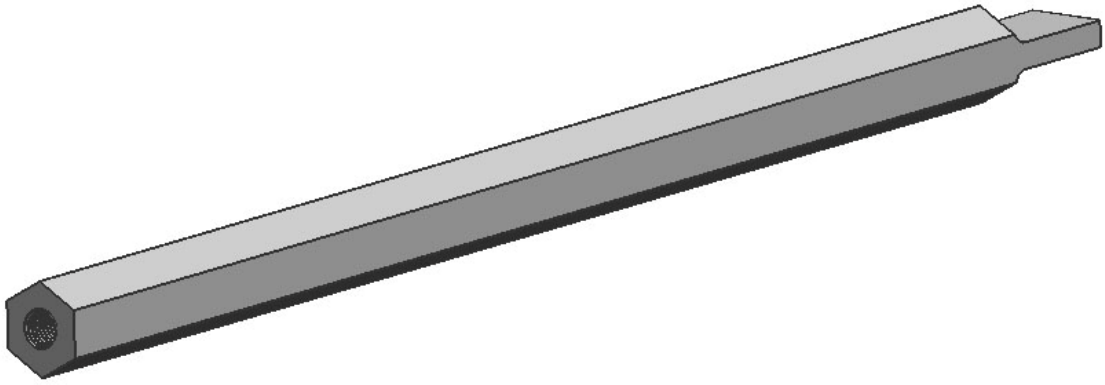

Figure 4-16. The Top Strut is made from aluminum hex rod

The Piston Mount, shown in Figure 4-17a, is constructed from 12L14 steel and serves as a rigid link between the Top Strut and the Piston. The Piston Mount also provides an exit passage for excess MR fluid via two connected holes through the part, as shown in Figure 4-17b. The edges of the cylinder are machined flat at the spherical joint connection to provide a sufficient grip surface for the nut and bolt.

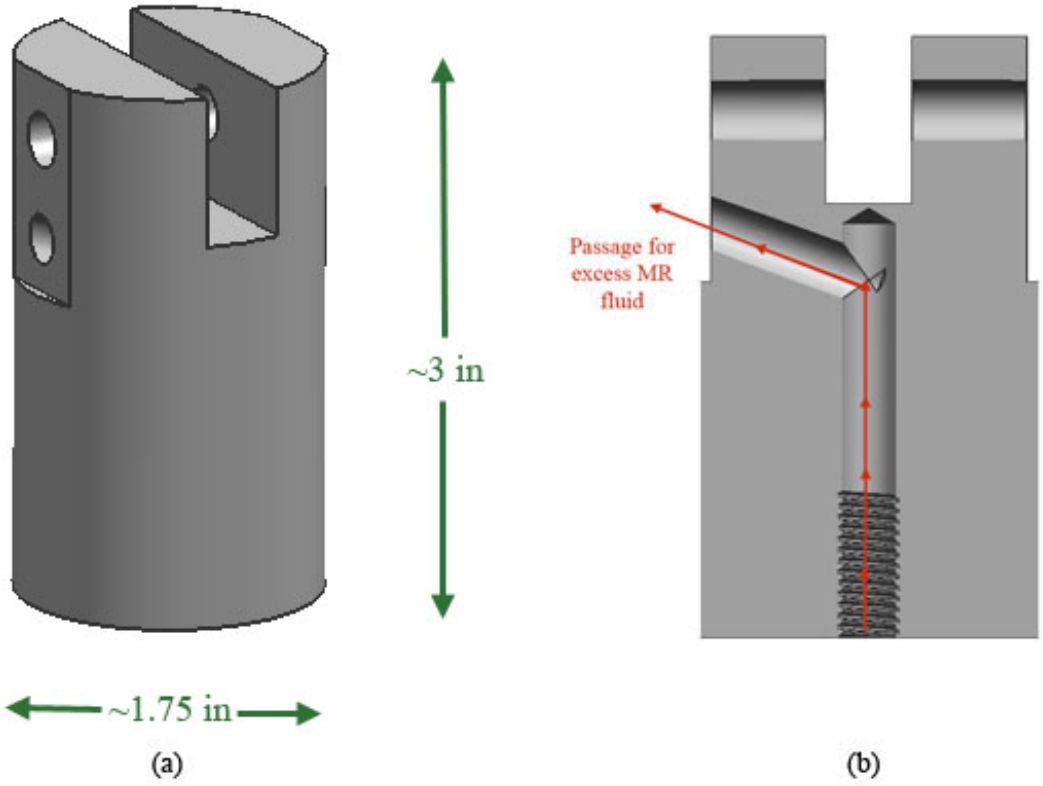

Figure 4-17. (a) The Piston Mount (b) Section view of the Piston Mount shows the passage for MR fluid

The Piston of the rheometer is a simple cylinder made from 12L14 steel, as can be seen in Figure 4-18. The Piston transmits force from the MTS load frame to the MR fluid chamber. The diametrical tolerances of this part are critical to the operation of the rheometer. The Piston diameter is matched to the inner bore of the Inner Cylinder with a clearance fit of 0.002 in. This provides enough clearance to allow for a free sliding piston, while also constraining it to purely axial motion. The Piston is attached to the Piston Mount via the Piston Stud, which is simply a threaded rod with a hole drilled through its center to allow excess MR fluid to pass out of the test chamber. The Piston Stud is shown in Figure 4-19.

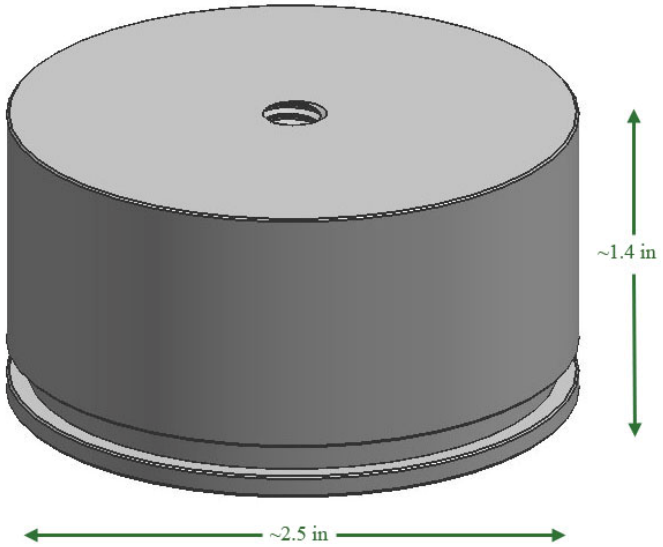

Figure 4-18. The Piston has a partially threaded thru hole for the Piston Stud as well as a groove for an O-ring

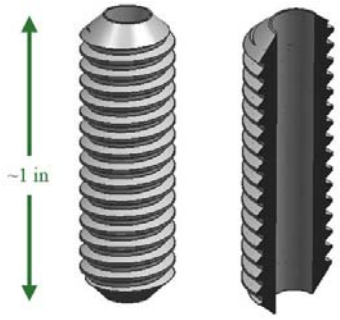

Figure 4-19. The Piston Stud allows MR fluid to pass through its center

The Upper Plate of the rheometer is shown in Figure 4-20. It provides the pathway for magnetic flux to transition from the core to the Outer Shell. The material of choice for this component is 1018 mild steel because of its favorable permeability properties.

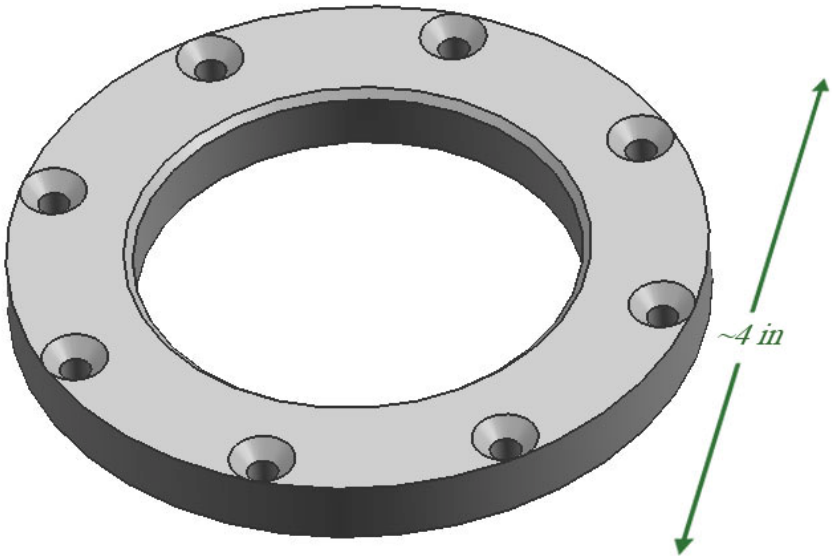

Figure 4-20. The Upper Plate of the rheometer

The next component is the Chamber Floor, which resembles a large thick washer, as seen in Figure 4-21. This component, as well as the Magnet Core, is made from 12L14 steel. The Magnet Core has a notch, approximately 1/8 in in size, machined into the outer diameter of its base to provide an entry and exit point for the coil wires, as shown in Figure 4-22. There is also a small hole drilled in the base for a dowel pin that is used to prevent the Magnet Core from spinning after assembly. If the Magnet Core were allowed to rotate, there is a risk that the wires leading the coil could be sheared. Once machined, the Magnet Core is wrapped with approximately 640 turns of 22 AWG coil wire. Each layer of wire is lightly coated with a quick set epoxy to fix the wire in place and reduce the chance of nicking the insulation coating on the wire.

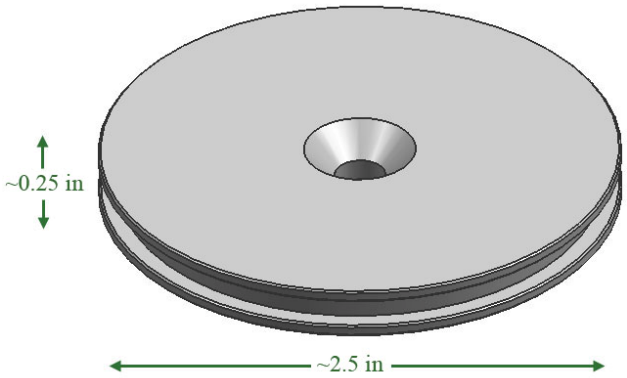

Figure 4-21. The Chamber Floor has a countersunk thru hole for a stainless steel flat head bolt as well as a groove for a sealing O-ring

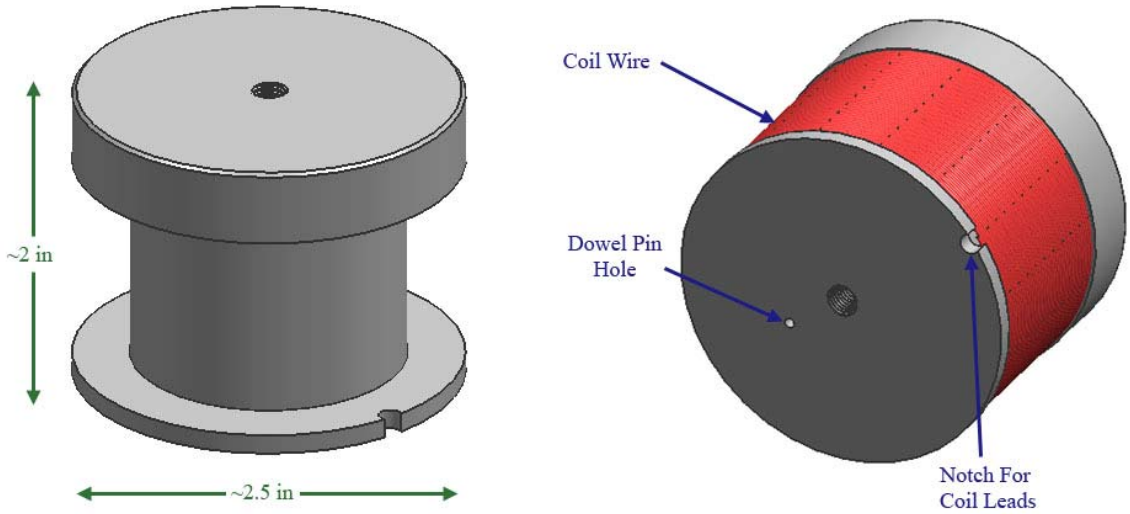

Figure 4-22. Magnet Core is wrapped with 22 AWG coil wire

The Outer Shell connects the upper and lower portions of the magnetic circuit; hence, it is machined from 1018 mild steel. The Upper and Lower Plates are attached using 16 (8 per side) 8-32 flat head screws, as shown in Figure 4-23. The Inner Shell serves as an insulator in the magnetic circuit and is made from Al 6061. This component also provides a sealing surface for both the Piston and Chamber Floor o-rings and also constrains the Piston to pure axial motion. For these reasons, the machining quality of the inner diameter, in terms of diametrical tolerance, run out, and surface finish, is critically

important. The outer diameter of the Inner Shell, which is shown in Figure 4-24, is also important as it provides the 0.004 in diametrical press fit with the Outer Shell.

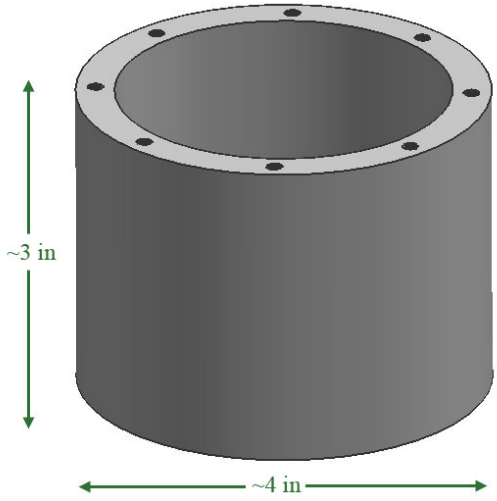

Figure 4-23. The Outer Shell has a total of 16 drilled and tapped holes

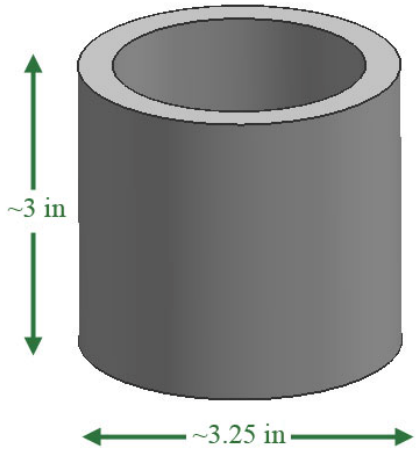

Figure 4-24. The aluminum Inner Shell is pressed into the steel Outer Shell

Similar to the Upper Plate, the Bottom Plate provides the pathway for magnetic flux to transition from the Outer Shell back to the Magnet Core. The plate is made from 1018 mild steel. The Bottom Plate, which is shown in Figure 4-25, incorporates a small hole for the Magnet Core dowel pin mentioned previously, as well as a thru hole for the coil leads.

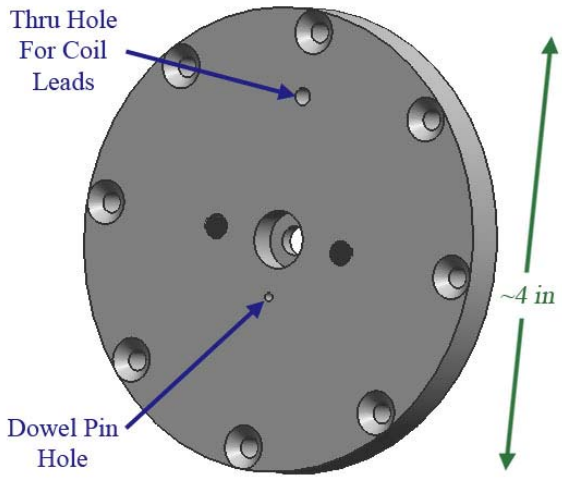

Figure 4-25. The Bottom Plate of the rheometer

Machined from Al 6061, the Base Mount, which can be seen in Figure 4-26, serves as a rigid link between the MTS load frame and the rheometer. It also offers a clamping surface for the jaws of the hydraulic actuator.

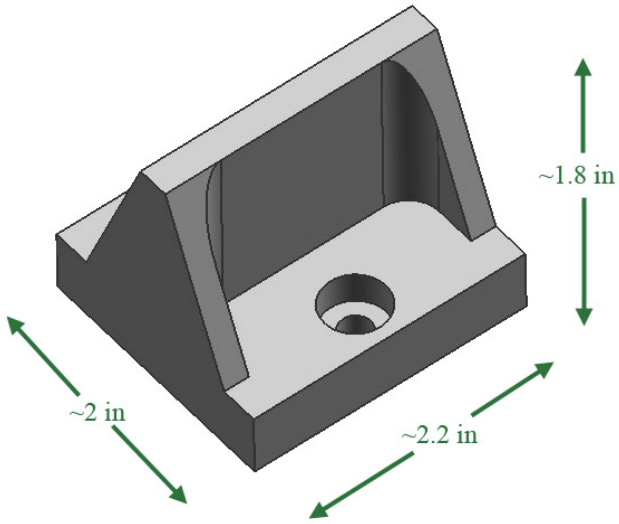

Figure 4-26. The Base Mount secures the body of the rheometer to hydraulic actuator

The last two components of the rheometer provide an adjustable mount for the Gauss-meter probe, as shown in Figure 4-27. The Gauss Probe Bracket is made from a square 1018 steel rod with a width of 3/8 in, while its counterpart, the Gauss Probe Clamp, is made from Al 6061. Together these components must firmly grip the Gauss-meter probe without crushing or otherwise damaging it. To accomplish this, the center of the hole machined in the Gauss Probe Clamp is located 0.010 in below the bottom edge of the part. This means that even though the diameter of the hole is matched to the diameter of the gauss probe, the clamp will apply pressure to the probe rather than bottoming out on the steel bracket.

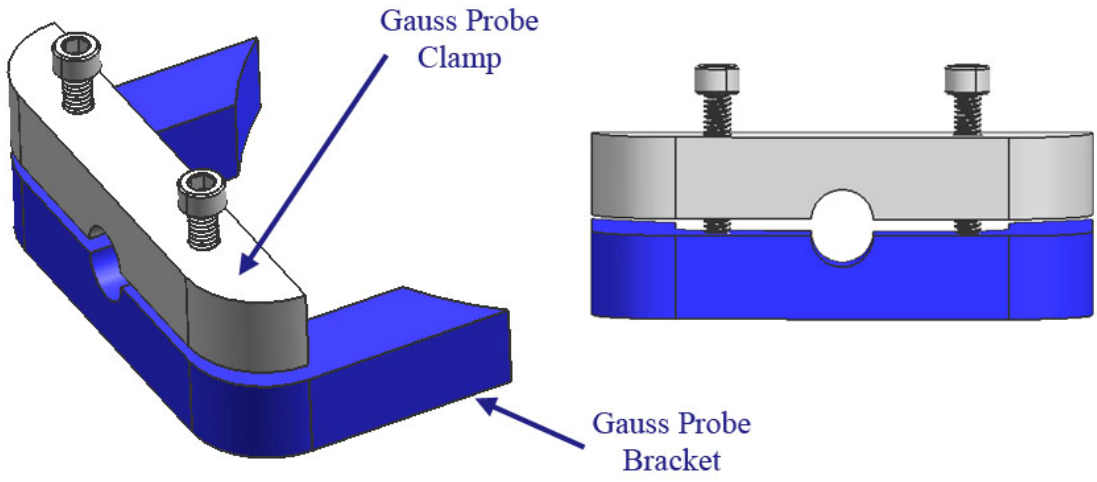

Figure 4-27. The Gauss Probe Clamp is designed to be able to compress the shaft of the probe only 0.010 in to ensure that it will not be damaged

4.4.2 Rheometer Assembly

This sub-section provides step by step instructions for assembling the squeeze mode rheometer, including assembly steps taken during the manufacturing process. An exploded view of the full assembly is shown in Figure 4-28.

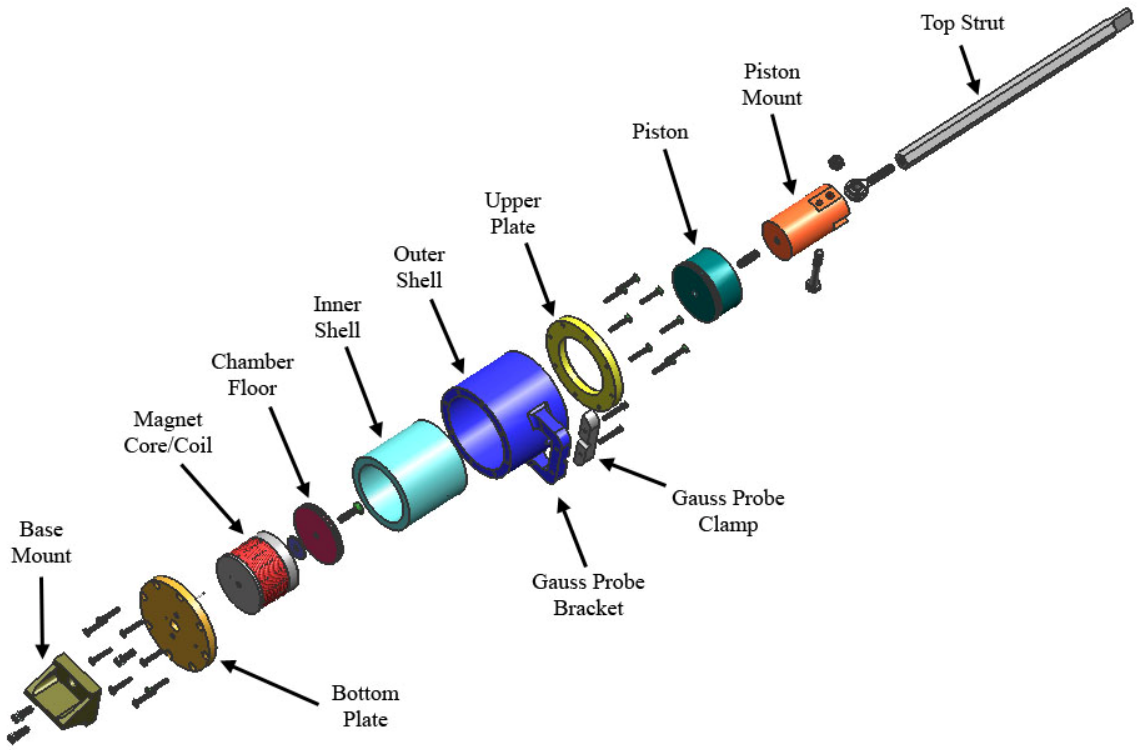

Figure 4-28. Exploded view of the rheometer components

The first step in assembly process actually takes place during the fabrication stage of the Inner and Outer Shells. After the inner bore of the Outer Shell and the outer diameter of the Inner Shell are machined, the parts are pressed together with an interference fit to form one cylinder, as shown in Figure 4-29. These parts are assembled before the finish machining operations to eliminate the possibility of dimensional distortion due to the press fit. Once the shells are joined, the ends are machined to the proper length and the sixteen holes used secure the Upper and Bottom Plates are drilled and tapped. At this point Upper Plate is bolted the shell via eight size 8-32 flat head screws. The shell-plate subassembly is placed back in a lathe for finish machining on the inner bore of both the Upper Plate and Inner Shell. These surfaces are dimensionally critical as they form the sealing and guide surface for the sliding piston. Finish machining these surfaces as an assembly ensures that no lip is inadvertently formed between the Upper Plate and Inner Shell due to slight misalignments that can occur while bolting the plate in place, as shown in Figure 4-30.

Figure 4-29. The Inner and Outer Shells pressed together (photo by Ryan Cavey)

Figure 4-30. By machining the inner bore as an assembly, no lip is formed at the joint between the Upper Plate and the Inner Shell (photo by Ryan Cavey)

The mount for the Gauss-meter probe is welded to the Outer Shell once the Inner Shell is press fit into the assembly. The Gauss probe mount is assembled using two 8-32 socket head cap screws to secure the aluminum Gauss Probe Clamp to the steel Gauss Probe Bracket, as shown in Figure 4-31. With a stepped hole already drilled into the shell

assembly at the proper height, as shown in Figure 4-32, the Gauss probe mount assembly is positioned for welding with the use of a polished alignment rod. The diameter of the alignment rod is matched to the larger diameter in the stepped hole to within a 0.001 in clearance fit. Using this rod ensures that the Gauss probe mount is properly aligned with the stepped hole in the shell, as shown Figure 4-33.

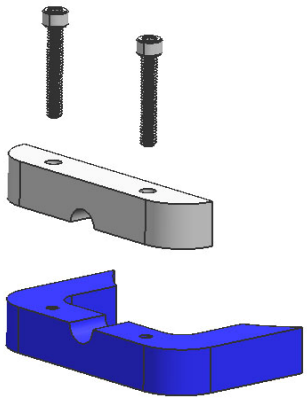

Figure 4-31. Exploded view of the Gauss Probe mount

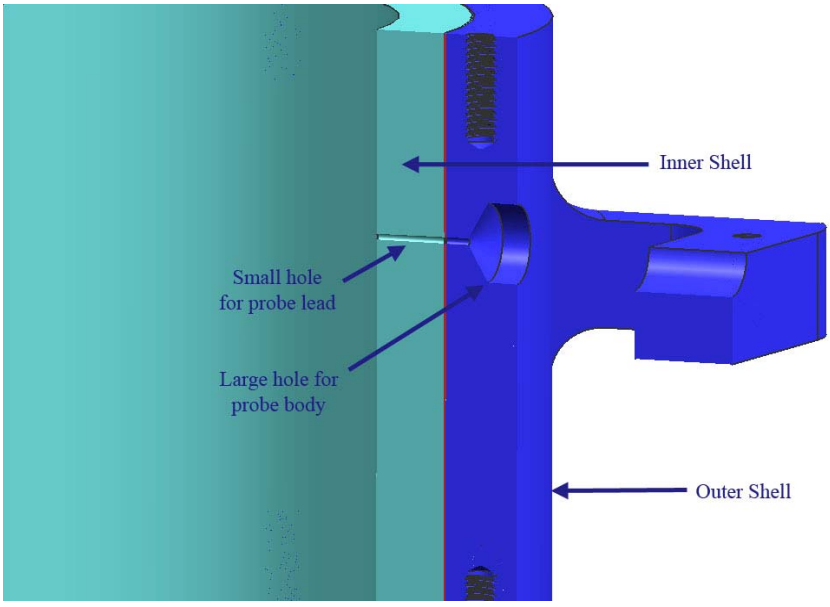

Figure 4-32. Cross-sectional view of the stepped hole drilled for the Gauss-meter probe

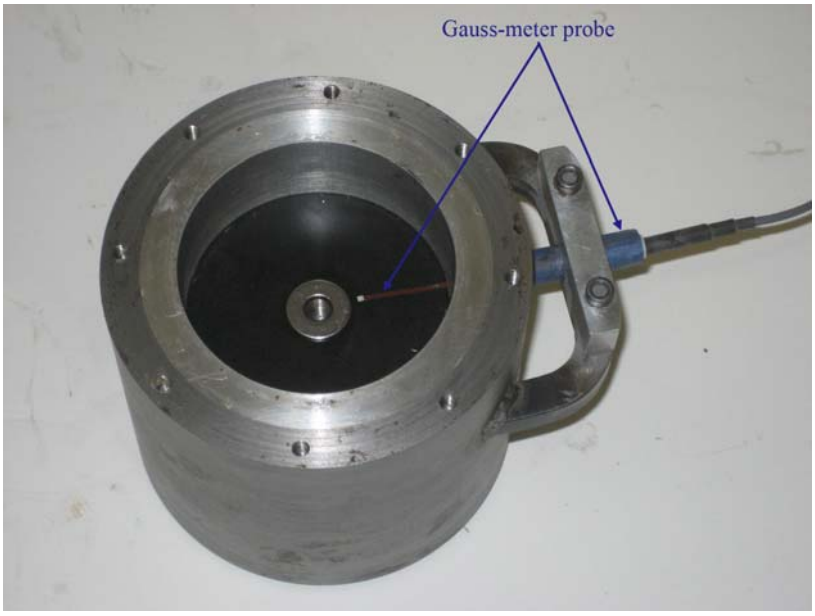

Figure 4-33. The Gauss-meter probe mount welded in place with adequate alignment (photo by Ryan Cavey)

With the Inner and Outer Shells pressed together, the Upper Plate secured, and the Gauss Probe Bracket welded, the rest of the components are now ready for assembly. The Magnet Core is placed on the Bottom Plate by threading the coil leads through a small hole in the plate and then carefully aligning the dowel pin and center bolt holes in each component, as can be seen in Figure 4-34. The core and plate are secured using a single ¼-28 socket head cap screw through the center of the components.

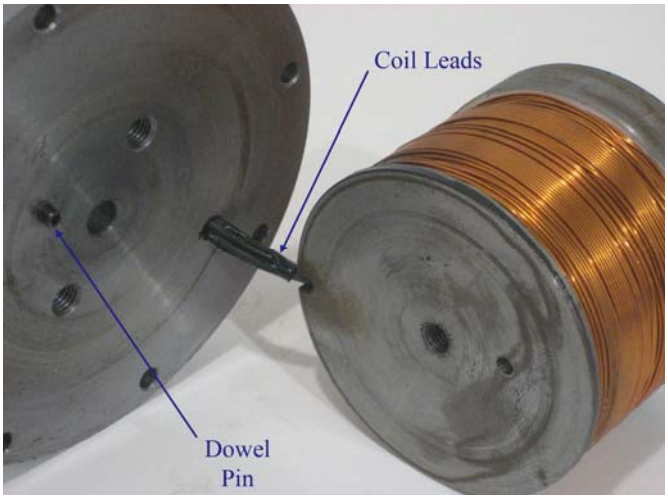

Figure 4-34. Mating surface between the Magnet Core and Bottom Plate (photo by Ryan Cavey)

The Chamber Floor, which has an O-ring installed around its circumference, is bolted to the top of the Magnet Core with the use of a ¼-28 stainless steel flat head cap screw and stainless steel flat washer. The stainless steel washer creates the 0.050 in tall air void between the Magnet Core and Chamber Floor that is used for the Gauss-meter probe, as shown in Figure 4-35.

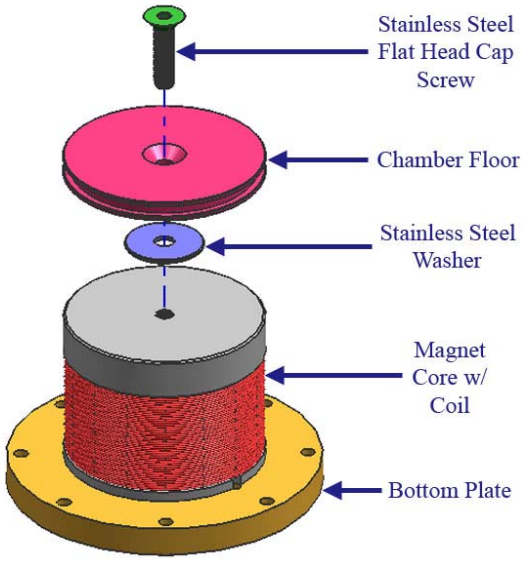

Figure 4-35. Exploded view of the core assembly

The Bottom Plate, Magnet Core, and Chamber Floor assembly, which is shown in Figure 4-36, is inserted through the bottom of the rheometer shell aligning the eight holes on the Bottom Plate to the threaded holes in the Outer Shell. Eight 8-32 flat head cap screws secure the Bottom Plate assembly to the shell of the rheometer, as shown in Figure 4-37.

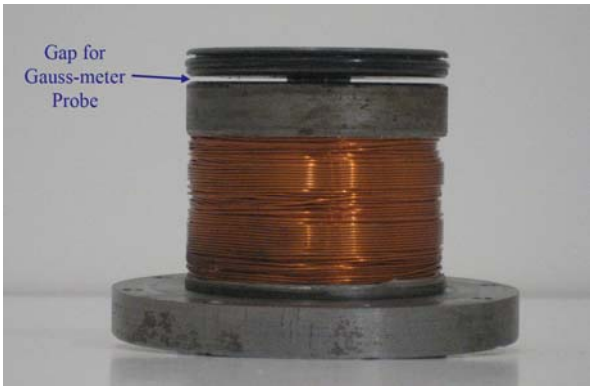

Figure 4-36. Coil magnet, Chamber Floor, and Bottom Plate assembled (photo by Ryan Cavey)

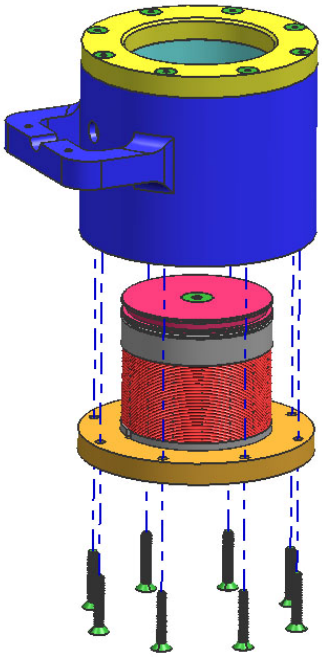

Figure 4-37. The core and Bottom Plate assembly is attached to the Outer Shell with 8 flat head screws.

The last component bolted to the main body of the rheometer is the aluminum Base Mount. Two ¼-28 socket head cap screws are used to fasten the Base Mount to the Bottom Plate, as shown in Figure 4-38.

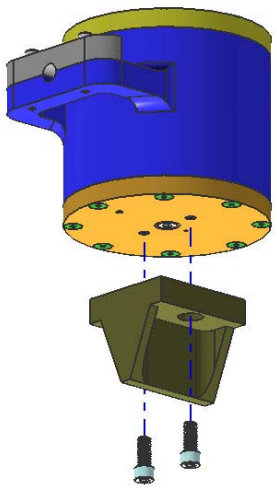

Figure 4-38. Exploded view of the Base Mount connection

The piston sub-assembly slides relative to the body components of the rheometer mentioned thus far. The piston sub-assembly starts with threading the Piston Stud into the Piston so that approximately half of the threads on the stud are still showing. The Buna-N O-ring is installed on the Piston before the Piston Mount is threaded onto the remaining threads of the Piston Stud, as shown in Figure 4-39. The piston sub-assembly is completed by attaching the aluminum Top Strut, which has a 5/16 in spherical joint locked into place by a jam nut, to the Piston Mount. This connection is made by a 5/16-24 hex bolt, which passes through the spherical joint, and nylon lock nut, as shown in Figure 4-39.

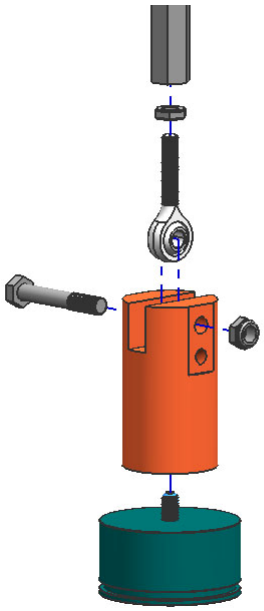

Figure 4-39. Exploded view of the piston sub-assembly

A plastic ¼ in male-to-male hose barb is attached to the Piston Mount with epoxy before the entire piston sub-assembly is inserted into the shell of the rheometer, as shown in Figure 4-40.

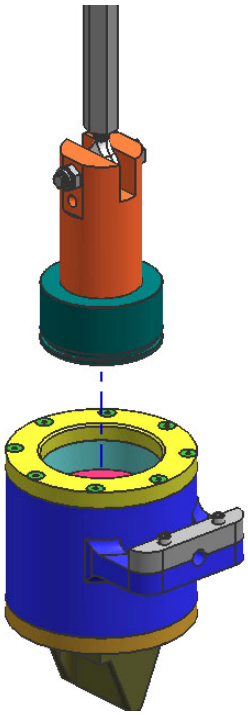

Figure 4-40. The piston sub-assembly with the rheometer body sub-assembly

4.4.3 Rheometer Installation

With the rheometer completely assembled, it is ready for installation on the Material Test Systems (MTS) load frame pictured in Figure 4-41. The MTS load frame is an 810 series Material Testing System mated with a 5.5-kip load cell and a hydraulic actuator capable of producing at least a 5.5 kip force with a dynamic stroke of ±5 in. The actuator is powered by an MTS Model 505.20 SilentFlo Hydraulic Power Unit. This hydraulic pump, shown in Figure 4-42, has a flow rate of 20 gal/min and an operating pressure of 3000 psi [51].

Figure 4-41. MTS 810 series Material Testing System (photo by Ryan Cavey)

Figure 4-42. MTS SilentFlo Hydraulic Power Unit (image adapted from [51])

The actuator is controlled via the MTS model 458.20 analog controller pictured in Figure 4-43. This controller is capable of producing a variety of signals including square, ramp, and sinusoidal waves of variable amplitudes and frequencies. Displacement and force measurements are passed from the controller to the PC-based dSPACE DS1102 data acquisition system. The dSPACE system is used in conjunction with Matlab/Simulink and Control Desk software to create user definable layouts to collect data from various channels. Along with the displacement and force channel, an additional channel is allocated for the Gauss-meter probe measurement. The probe is used to measure the magnetic flux density inside the rheometer. The probe is an "ultra-thin" (0.2mm x 1.5mm) transverse probe from F.W. Bell. This probe is connected to an F.W. Bell 5080 Gauss-meter as shown in Figure 4-44. The 5080 model provides an analog output, which is connected to the dSPACE system, for recording the flux density [51].

Figure 4-43. MTS 458 analog hydraulic controller (photo by Ryan Cavey)

Figure 4-44. Gauss-meter and "ultra-thin" transverse probe (image adapted from [51])

The rheometer is installed by placing the Base Mount in the center of the open jaws of the lower clamp on the MTS load frame, as shown in Figure 4-45. The piston sub-assembly is removed from the rheometer and the flat portion of the Top Strut is positioned in the center of the upper clamp on the load frame. Both clamps are locked into position using the hydraulic controls located on the front of the 810 load frame, as can be seen in Figure 4-45. The Gauss-meter probe is carefully threaded through the small hole in the rheometer shell that leads to the measurement gap. The Gauss Probe Clamp is locked down to secure the probe in one of the pre-determined positions, as shown in Figure 4-46.

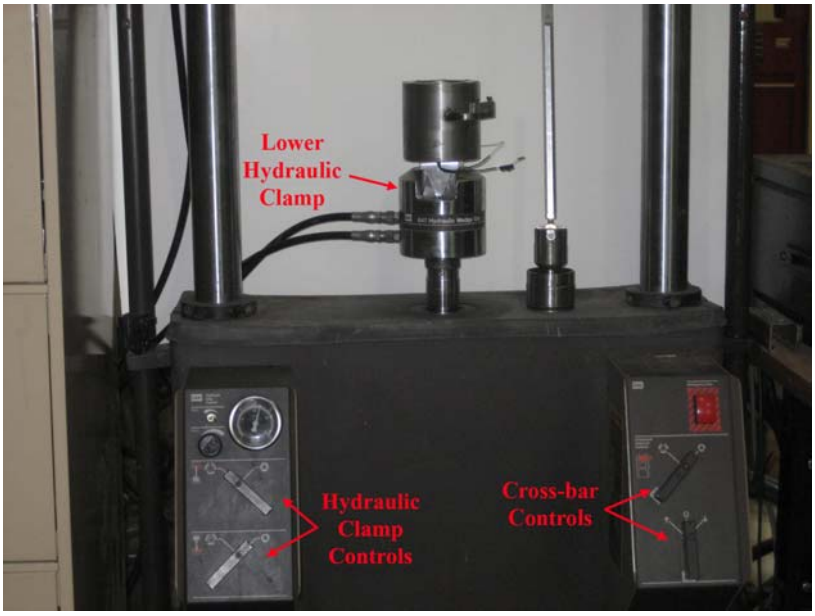

Figure 4-45. The rheometer body clamped in the MTS load frame (photo by Ryan Cavey)

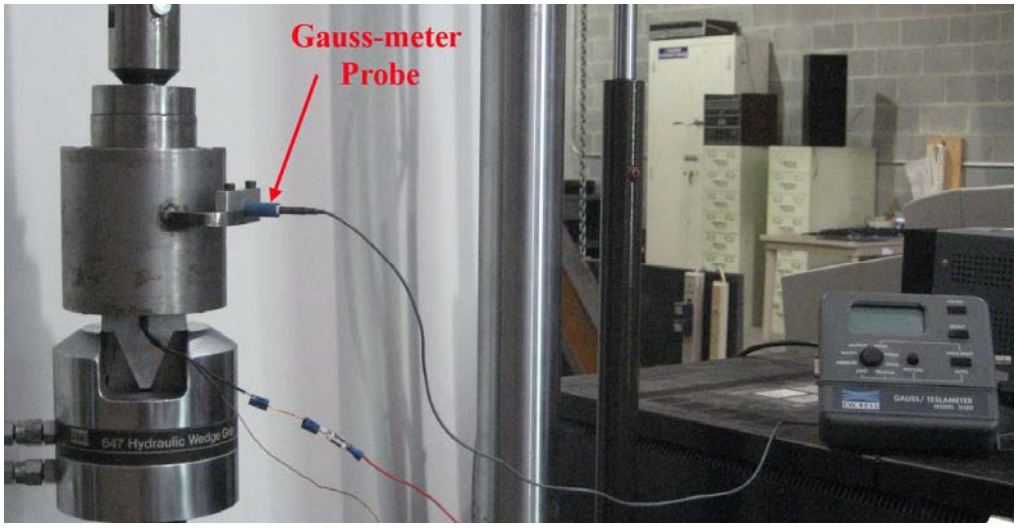

Figure 4-46. The Gauss-meter probe installed in the rheometer (photo by Ryan Cavey)

Clear vinyl tubing is used to connect the male hose barb protruding from the Piston Mount to the plastic funnel. The funnel serves as the overflow reservoir for excess MR fluid. Placing the overflow reservoir above the rheometer ensures that air is not trapped inside the system.

Finally, the leads from the coil magnet are connected to a DC power supply. The coil magnet is powered by a Protek DC Power Supply model 3005B, which has a choice of either voltage or current control. With the rheometer clamped into the load frame, the MTS 458 controlling the actuator, the power supply connected to the coil leads, and the dSPACE data acquisition system recording force, displacement, and magnetic flux density, the rheometer is ready for operation, as seen in Figure 4-47.

Figure 4-47. The rheometer installed in the load frame ready for testing (photo by Ryan Cavey)

4.5 Summary

Rheometers are used to study the relationship between stress and deformation in fluids. There are many types of rheometers that exist today, but thus far only the rotational shear mode rheometer is in common use for the characterization of MR fluids. The squeeze mode rheometer design addresses the challenges of managing the MR fluid, creating a beneficial magnetic circuit, applying force to the fluid, and collecting data. The squeeze mode rheometer is made primarily from 13 custom components machined from a combination of steels and aluminum. The rheometer is assembled using common hardware and fasteners. The assembled rheometer is easily installed in an MTS load frame, outfitted with a Gauss-meter probe, and connected to the dSPACE data acquisition system.

5. Rheometer Testing

This chapter begins with a description of the test setup and testing procedure. It is followed by a section that provides the results of these tests. The next section provides a discussion of the test results as well as additional observations made during the test phase. The following section is dedicated to the redesign of the rheometer piston. The test results for the redesigned piston are presented in the next section. The chapter concludes with a summary that highlights the key ideas presented in the chapter.

5.1 Test Setup

This section provides further detailed information about the test setup and test procedure. The test procedure is presented as a bulleted list in a user manual format.

The dSPACE DS1102 data acquisition system (DAQ) may be configured in a nearly endless number of different ways. It has the capability of serving as a real-time control system, accepting and recording incoming signals as well as outputting analog signals. The testing conducted with the squeeze mode rheometer only requires a simple 3-channel data recording configuration. The DS1102 pc-based DAQ is used in conjunction with Matlab/Simulink software to accomplish the desired data acquisition goals. The inputs and outputs of the system are handled by a Simulink model and then passed to the ControlDesk in dSPACE. The Simulink model used for the rheometer data collection can be seen in Figure 5-1. The model consists of an analog-to-digital conversion block that receives the input signals directly from 3 different channels, a simple low pass filter that attenuates frequencies above 100Hz, and a channel gain that is matched to each of the instruments used during testing.

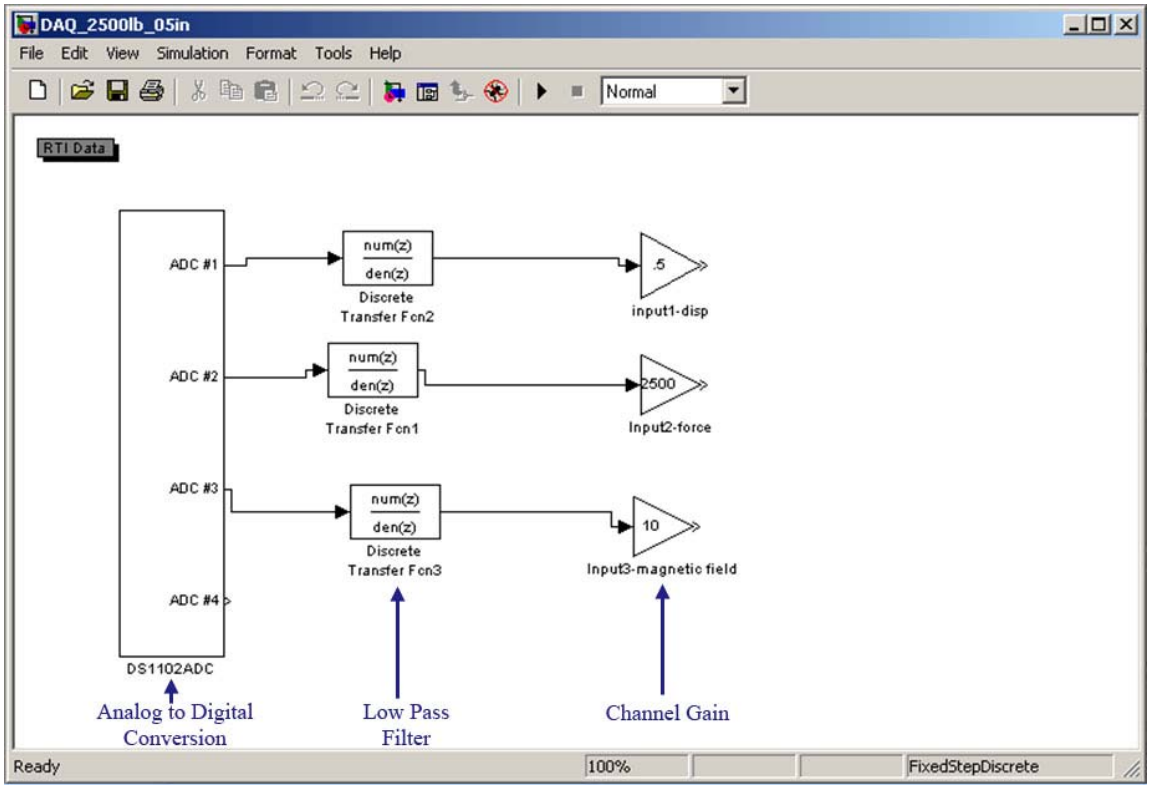

Figure 5-1. Simulink model for recording 3 data channels with the dSPACE DS1102

The Simulink model is used by the dSPACE ControlDesk software to complete the data acquisition configuration. The variables Input1-disp, Input2-force, and Input3-magnetic field found in the Simulink model represent the filtered and properly gained signals that are to be recorded. These are the variables used by the dSPACE software for sampling, recording, and displaying the selected outputs. The ControlDesk layout is also a widely configurable portion of the data acquisition system. The layout used during rheometer testing is shown in Figure 5-2. Each test run records 10 seconds of data sampling at a rate of 250Hz.

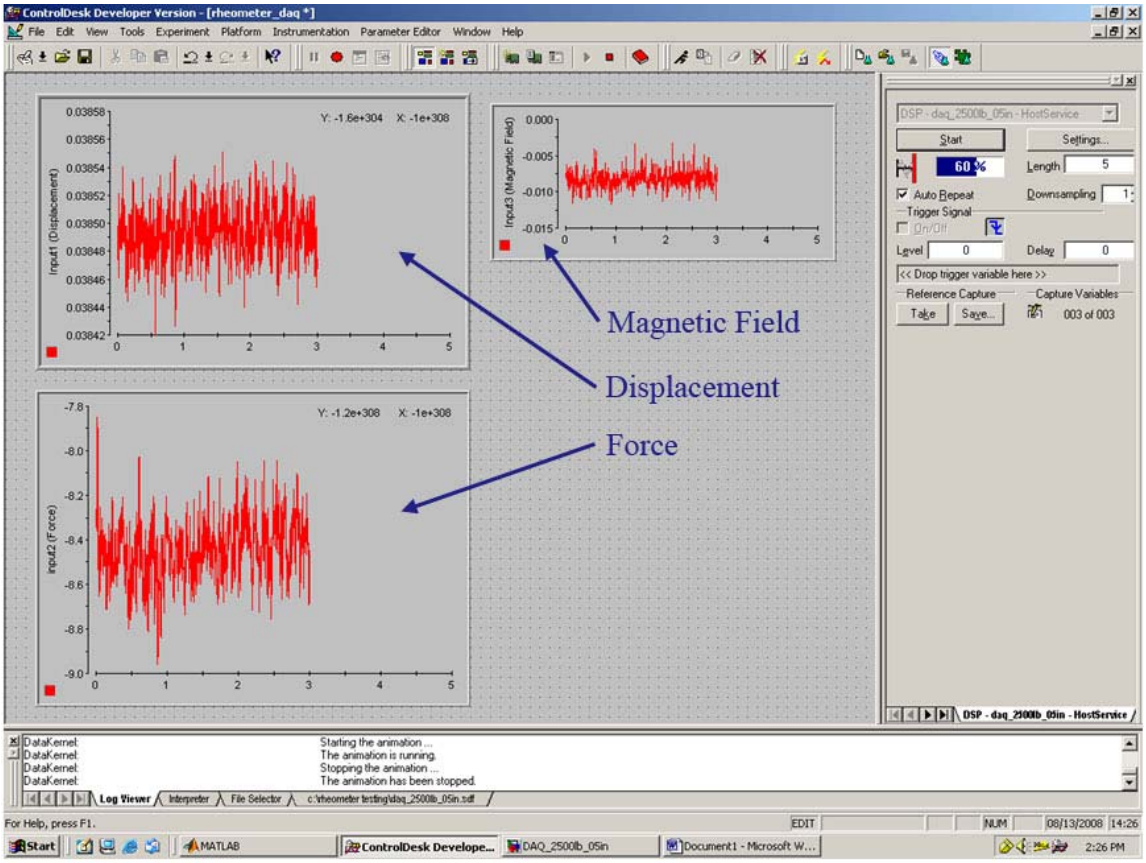

Figure 5-2. Data acquisition layout used in ControlDesk

The following test procedure assumes that the rheometer base and piston assembly are properly clamped in the MTS load frame as seen in Figure 5-3.

Figure 5-3. The rheometer assembly clamped in the MTS load frame is ready for testing (photo by Ryan Cavey)

Test Procedure:

1. Open the dSPACE ControlDesk software and load the Simulink model created for rheometer testing
2. Power on the MTS 458 controller and clear the limit switch errors
3. Before pressurizing the hydraulic actuator, the DC Error must be zeroed to prevent the actuator from moving undesirably. Controls for the MTS 458 are pictured in Figure 5-4.

Figure 5-4. Controls for the MTS 458 controller (photo by Ryan Cavey)

4. The DC Error is adjusted with the Zero turn knob labeled above.
5. Activate the hydraulic pump by pressing the High button on the Hydraulic Pressure portion of the controller.
6. Raise the actuator and rheometer base approximately 3 in by using the Zero adjustment knob.
7. Adjust the Set Point to the initial gap height desired between the Chamber Floor of the rheometer and the bottom of the piston. In most tests this initial gap is set to 0.100 in as seen in Figure 5-5.

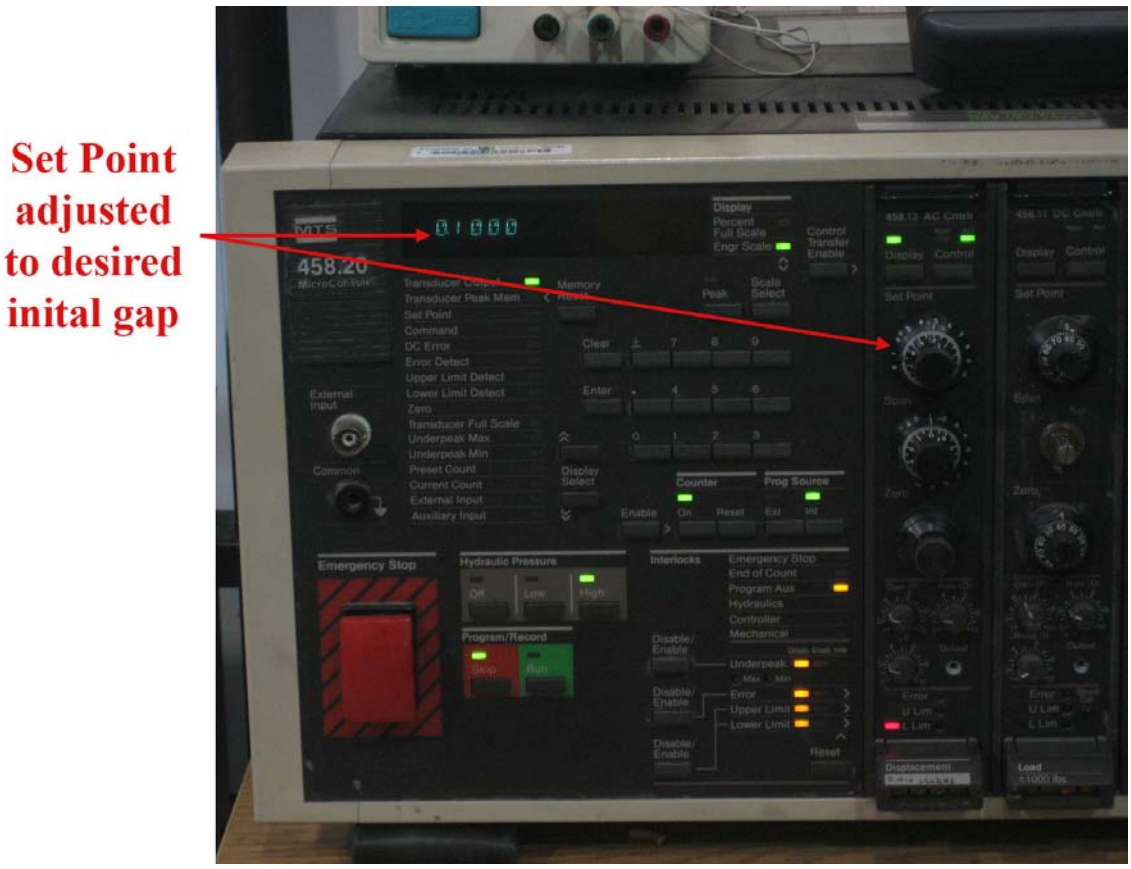

Figure 5-5. The Set Point marks the center point of the ramp wave used for testing (photo by Ryan Cavey)

8. A ramp wave is used for the displacement input to provide a constant velocity for each test run. Select the ramp wave on the right-hand side of the controller. Also choose the Invert option so that the initial motion compresses the fluid rather than separating. Set the frequency to the desired value using the turn knobs below the wave selection buttons. The majority of tests were performed with a frequency of 0.03Hz.
9. Adjust the span to the desired value. The span is given as a percentage of full range. With the ±0.5 in displacement module in place and a desired span of ±0.05 in, the adjustment knob is set to roughly 10%.
10. To complete the fine adjustment of the span, press the green Run button in the Program/Record area of the controller. The actuator and rheometer base will begin to oscillate according the wave settings selected previously.

The press the Peak button to display the measured peak and valley of the motion. Adjust the span until the desired value is reached, as shown in Figure 5-6.

Figure 5-6. The fine adjustment of the span is performed while the actuator is in motion (photo by Ryan Cavey)

11. Once the span adjustment is complete press the red Stop button in the Program/Record area of the controller.
12. Fill the rheometer chamber with well-mixed MR fluid. Ensure that the amount of MR fluid exceeds the initial gap height that is to be tested. This will prevent excess air from being trapped in the test chamber.
13. Using the Zero adjustment knob, slowly raise the rheometer base so that it slides around the piston assembly.
14. The initial gap height is set with digital calipers. Before the rheometer was clamped into the load frame, the piston was placed into the empty test chamber of the rheometer. With the chamber empty and the Piston sitting on the chamber floor, which corresponds to a zero gap height, the top of

the Piston sits above the top of the Upper Plate. This height was measured to be 0.134 in as shown in Figure 5-7. Adjust the calipers to this measurement and set the incremental zero on the calipers.

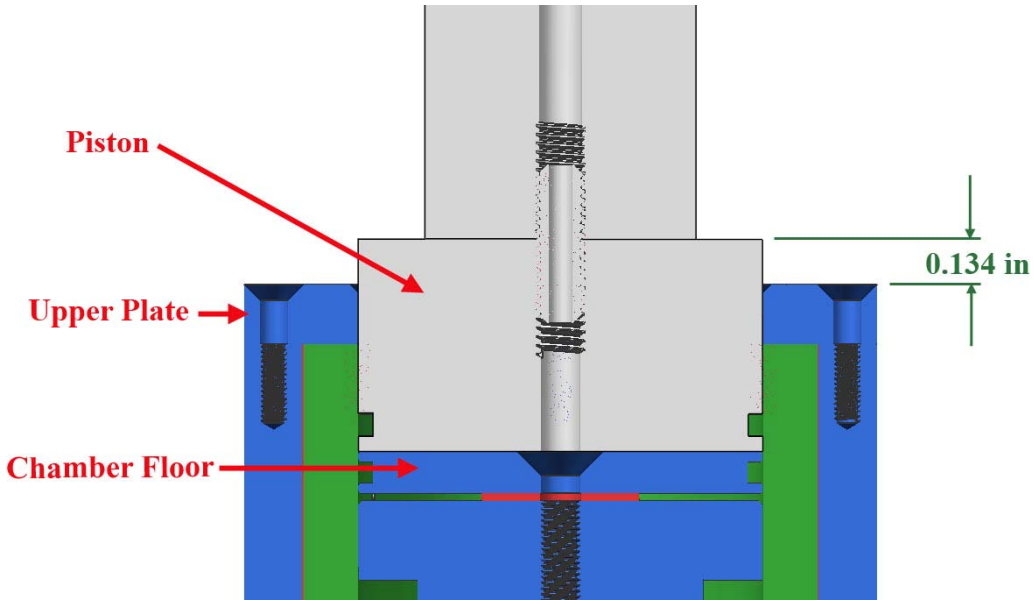

Figure 5-7. The height of the Piston top with a zero gap in the test chamber is used to set up the rheometer for testing.

15. With the incremental zero on the digital calipers corresponding to a zero gap height in the test chamber, raise the rheometer with the Zero adjustment knob on the MTS 458. Measure the height between the Piston and Upper Plate using the incremental setting on the calipers and adjust until the desired initial gap height is reached, as shown Figure 5-8. Most tests were performed with an initial height of 0.100 in.

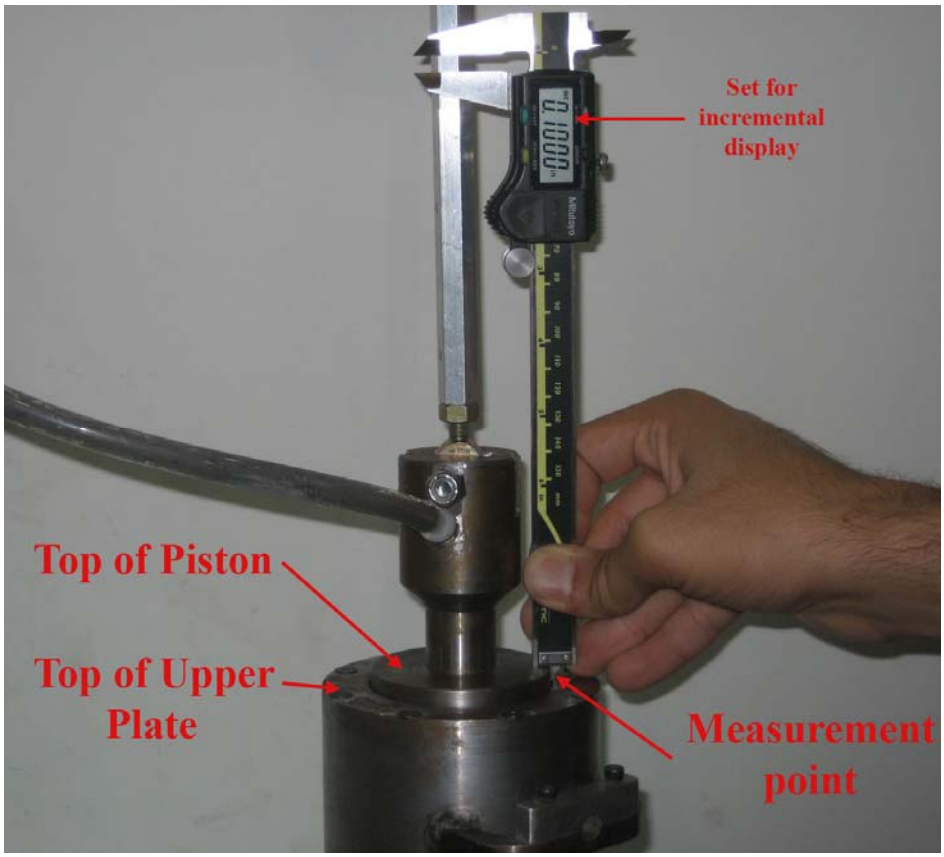

Figure 5-8. With the correct incremental zero, the display on the digital calipers corresponds to the gap height within the chamber (photo by Ryan Cavey)

16. Once the Piston and rheometer base are set at the correct gap height, ensure that there is excess MR fluid in the clear tubing leading to the reservoir. If there is not MR fluid in the tube that means there is likely not enough fluid inside the chamber and air in the chamber will affect the results. The tubing and reservoir for excess MR fluid is shown in

Figure 5-9. The reservoir for excess MR fluid is kept above the test chamber to allow air to escape (photo by Ryan Cavey)

17. Turn on the Gauss meter and perform the auto-zeroing function. Turn on the analog output for the meter.
18. Turn on the Protek 3005B power supply and use the current control to knob to adjust to the desired value. Coil currents of 1, 2, 3, and 4 Amps were tested with the rheometer. Turn off the power supply.
19. Turn on the now pre-set power supply when ready to begin the test run. The prepped data acquisition, controller, and power supply is pictured in Figure 5-10.

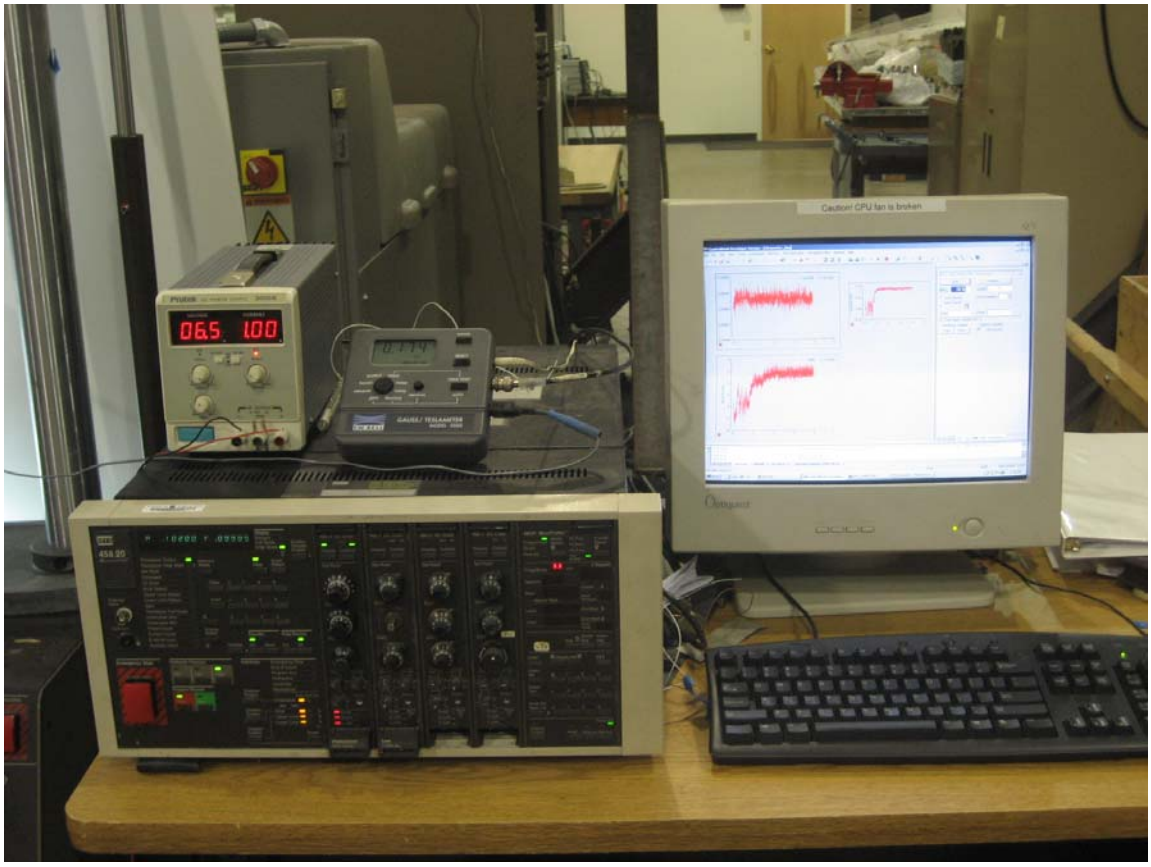

Figure 5-10. The power supply is maintains at a constant current throughout the test (photo by Ryan Cavey)

20. Press the Start button on the layout in ControlDesk to begin recording data.
21. Press Run on the MTS 458 controller to start the ramp wave motion.
22. After the wave motion reaches the minimum gap height and begins separating again, turn the power supply off. This relaxes the fluid while the gap size is growing and sucking in the MR fluid that was expelled during the test.

This test procedure was followed for the majority of tests performed with the rheometer. Deviations from this procedure will be stated along with the results in the following section.

5.2 Test Results

The test results section is divided into two parts. The first is dedicated to tests focusing the rheometer itself rather than MR fluid. The second part presents the test results from operating MR fluid in squeeze mode.

5.2.1 Rheometer Verification Tests

Before any tests were conducted on MR fluid, a series of verification tests were performed to ensure that the rheometer functioned as intended. One of the first tests conducted was for the purpose of comparing the magnetic flux density measured in rheometer to the FEMM model used during the design phase. For this experiment, the Gauss-meter probe was placed in 4 different locations along the radius of the rheometer. Three of these locations are pictured in Figure 5-11. The 4^{th} location, dubbed Outer Position 2, is located 0.050 in closer to the center than Outer Position 1. This additional data at the outer edge of the test chamber is needed to characterize the non-uniform magnetic flux density expected in this region due to the O-ring groove. Results for this test are presented in Figure 5-12. The flux density measurements appear to be in close agreement with the FEMM model and remain relatively uniform across the bulk of the test chamber. The most notable variation between the experimental results and FEMM model is the existence of a non-zero slope in the test data. The flux density appears to be higher than expected near the core center, while a bit lower near the perimeter of the test section. The root cause for this variation is unknown, however the degree of variation is not substantial enough to cause alarm and the model has been determined to be sufficiently accurate for the purposes of this research. Based on the test results, the FEMM model is assumed to be reasonably accurate and thus the magnetic flux density measured in the probe gap area is assumed to be similar to that in the test chamber.

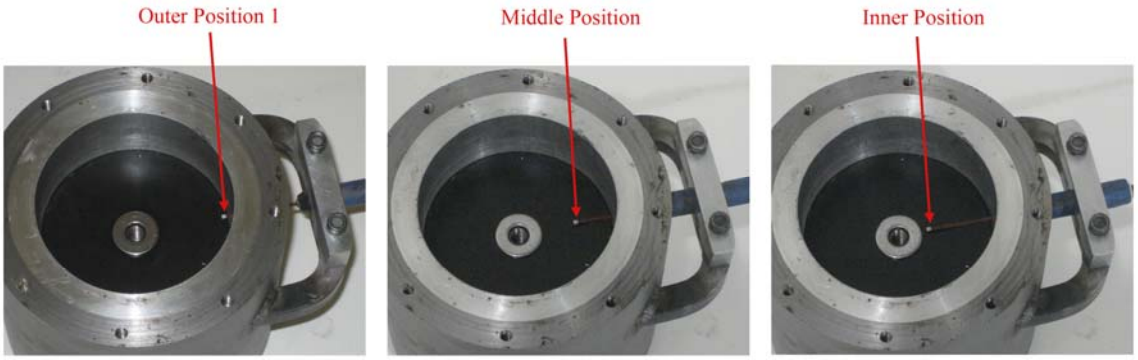

Figure 5-11. Measurement positions for the Gauss-meter probe (photo by Ryan Cavey)

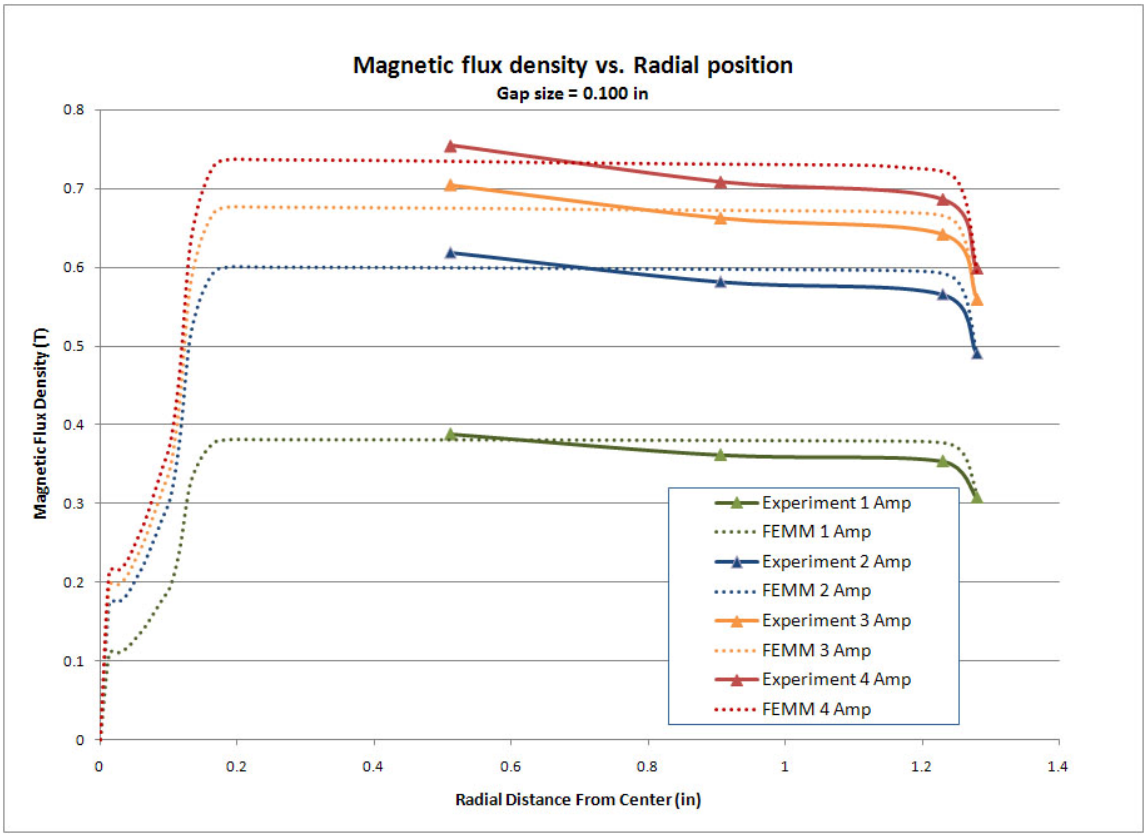

Figure 5-12. The magnetic flux density measured in the rheometer compared to the FEMM model

The next test was designed to investigate any hysteretic elements that may exist in relationship between coil current and magnetic flux density. At each probe location, the coil current is adjusted up through the operating range (0 to 4 Amps) while recording the flux density at every 1 Amp increment. Without turning the power supply off, the coil

current is adjusted back down the operating range (4 to 0 Amps) while again recording the flux density at each 1 Amp interval. The results of this test are shown in Figure 5-13. The magnetic flux density seems to exhibit a small degree of hysteresis in relation to the coil current. This is most pronounced at the lowest current setting of 1 Amp where the difference in measurements is approximately 0.05 T. As a result of this testing, the procedure for adjusting coil current during MR fluid tests includes a note to approach the desired coil current from a lower setting. For example, it is acceptable to adjust the coil current from 1 Amp to 3 Amps, but not from 3 Amps to 1 Amp.

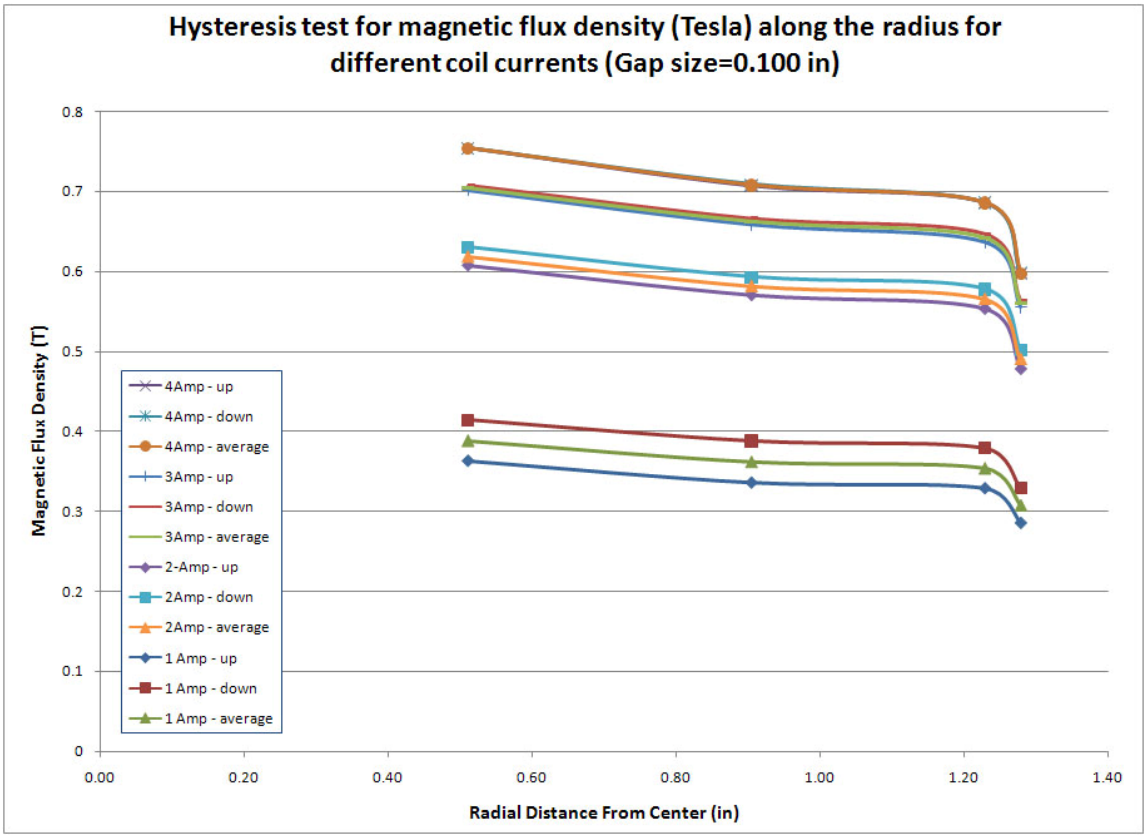

Figure 5-13. The magnetic flux density results after sweeping the coil current up and down the operating range along with the average value for each probe position

In another test, the magnetic flux density was recorded while the gap size was decreased from an initial value of 0.200 in to 0.050 in with an empty test chamber. The purpose of this test was to investigate how the magnetic flux density changes with the gap size. The results shown in Figure 5-14 confirm that there is a significant rise in the flux

density (approximately 35%) as the gap height is decreased. This dramatic increase is to be expected when the medium filling the gap is air. Air has a high reluctance value compared to steel or MR fluid. The magnetic flux density was also recorded during MR fluid testing, as shown in Figure 5-15. The flux density still increases with decreasing gap height, but the rise is reduced to approximately 15% over the full range of displacement (0.200 in to 0.050 in).

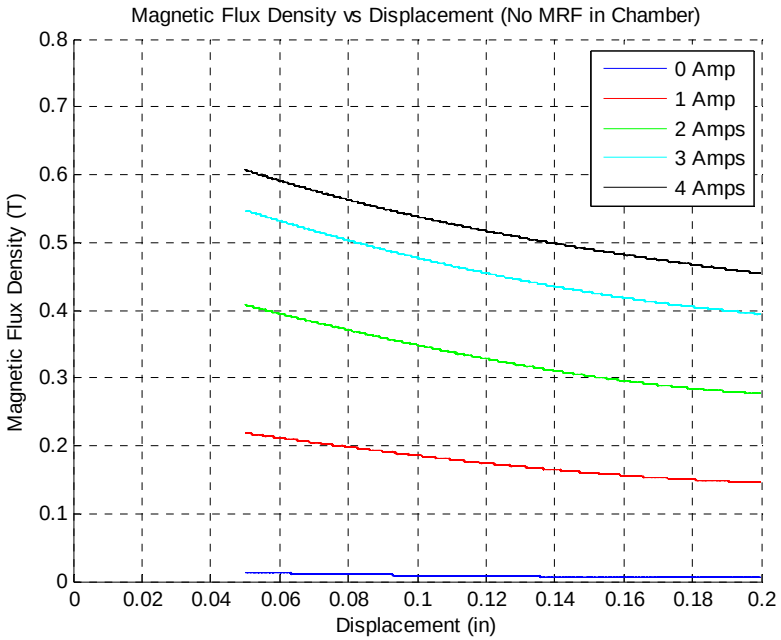

Figure 5-14. Magnetic flux density vs. Air gap height in the test chamber

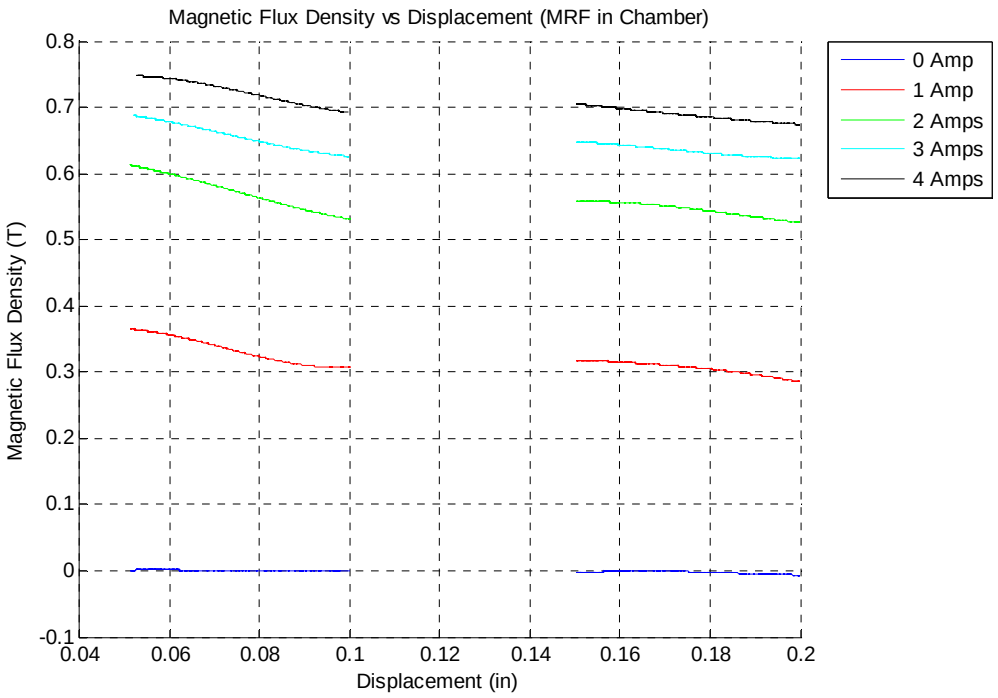

Figure 5-15. Magnetic flux density vs. Gap height with MR fluid in the test chamber

The next tests are concerned with the friction force created between the sliding piston and the rheometer base. The first test is performed with an empty chamber where the gap height is varied through the full range of operation (0.200 in to 0.050 in) and the coil current is also adjusted through its full range (0 to 4 Amps). As can been seen in the test results in Figure 5-16, the increased coil current produces an increasingly positive force on the piston. It should be noted that a positive force corresponds to a tension force while a negative value corresponds to a compressive force. The test of greatest interest is the one performed with 0 Amps supplied to the coil magnet. This represents the friction force generated by the sliding action of the piston and rheometer base. The friction force appears to remain constant at -10 lbs during the compressive stroke of the test.

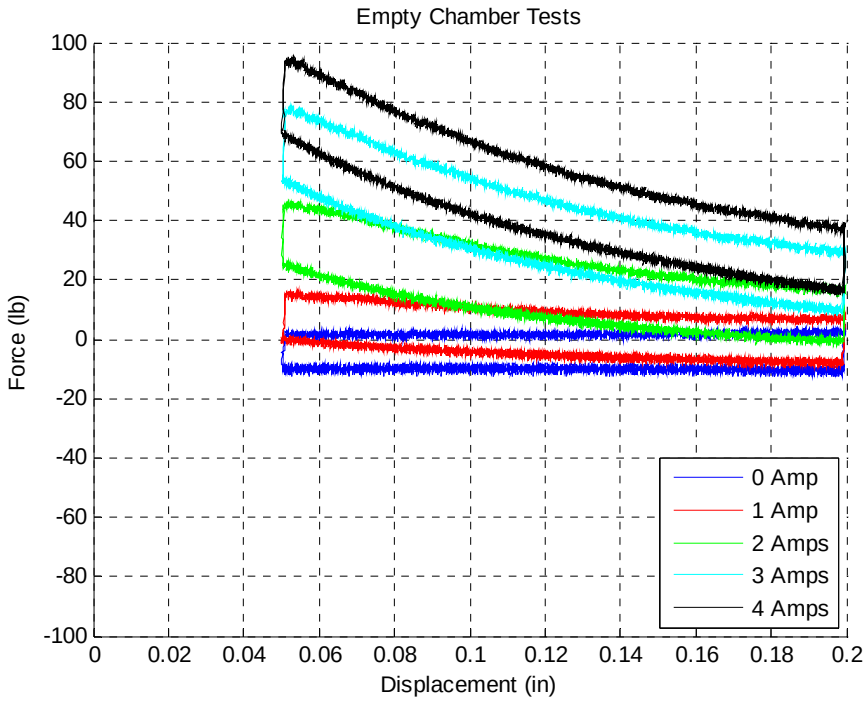

Figure 5-16. Force vs. Gap height with an empty test chamber and a piston velocity of 0.06 in/s

A similar test was also performed with MR fluid in the test chamber. The coil current was set to zero while the gap size was adjusted through its full range. The results can be seen in Figure 5-17. The total resistance force remains relatively constant at approximately -20 lbs during the compression stroke. This means that in future tests any compressive force greater than 20 lbs is a result of the MR fluid stiffness in squeeze mode.

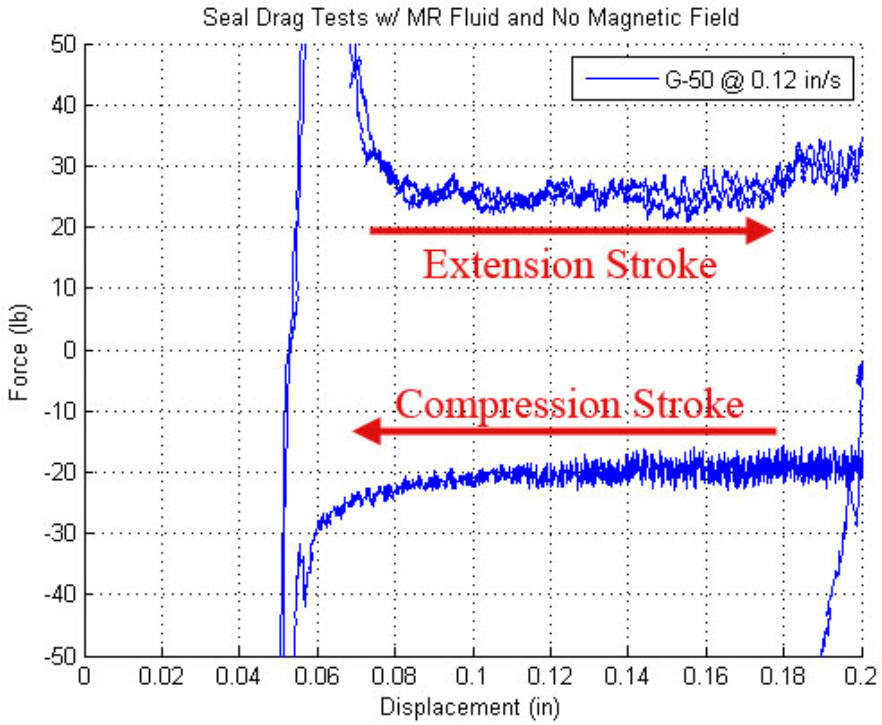

Figure 5-17. The friction force related to piston seal in conjunction with the resistance force generated by the relaxed MR fluid

5.2.2 Squeeze Mode Tests

The first MR fluid used for testing was a blend from a major auto manufacturer that consists of 50% ferrous particles by volume. Limited data is available for this fluid, but what is available can be found in the appendix of this document. This fluid will be referred to as G-50 for the remainder of this chapter. The initial tests with this fluid were performed with 1 Amp of coil current and a gap height ranging from 0.100 in to 0.050 in, as shown in Figure 5-18. The G-50 fluid demonstrates impressive compressive resistance at just 1 Amp of coil current. The interesting points of this plot are the "sawtooth" features and the progressively increasing peak compressive force for each consecutive run.

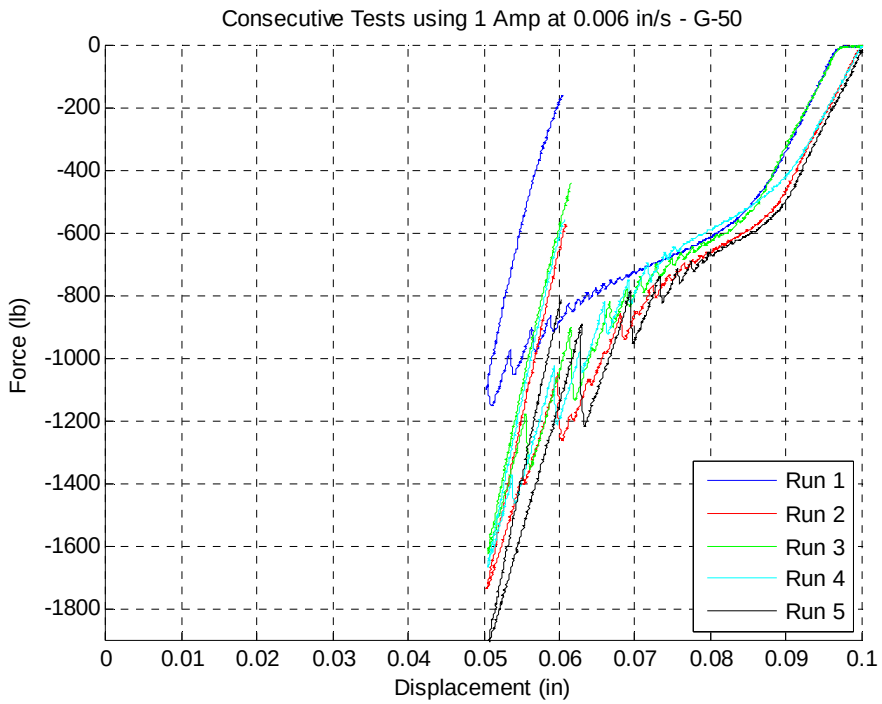

Figure 5-18. G-50 fluid with 1 Amp of coil current at a gap height ranging from 0.100 in to 0.050 in

Because of fears that the rheometer may fail structurally at such high loads, the next tests were performed at a larger gap size. The stroke was held constant at 0.050 in, but the initial gap was shifted from 0.100 in to 0.200 in. Tests were conducted at coil currents of 1, 2, 3, and 4 Amps. The test results for the G-50 fluid at the larger gap height are shown in Figure 5-19, Figure 5-20, and Figure 5-21 with plot overlaying all of these results in Figure 5-22. A similar "sawtooth" pattern can also be found in these plots as well as the progressive increase in peak force from one consecutive test run to the next.

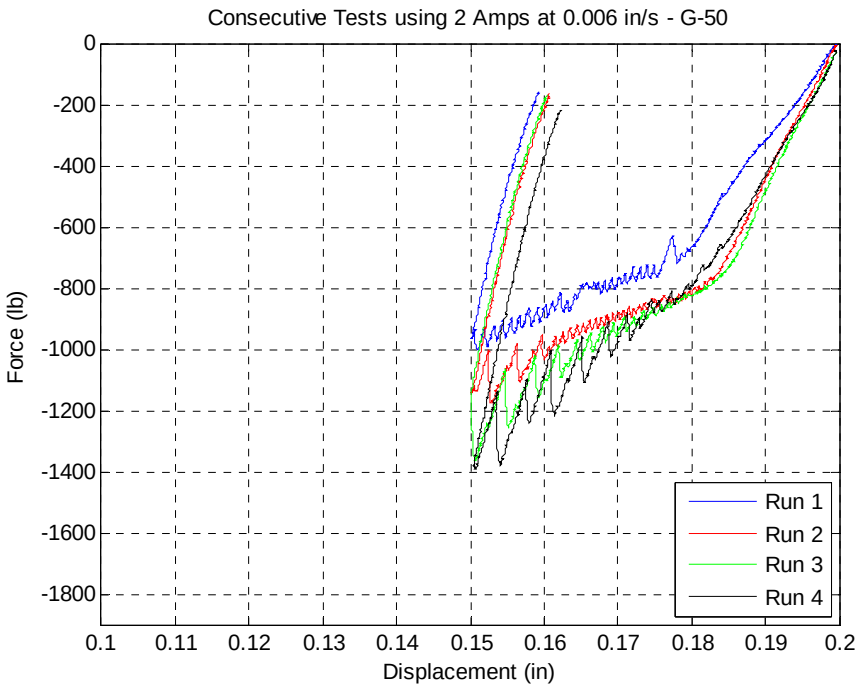

Figure 5-19. G-50 fluid with 2 Amps of coil current at a gap ranging from 0.200 in to 0.050 in

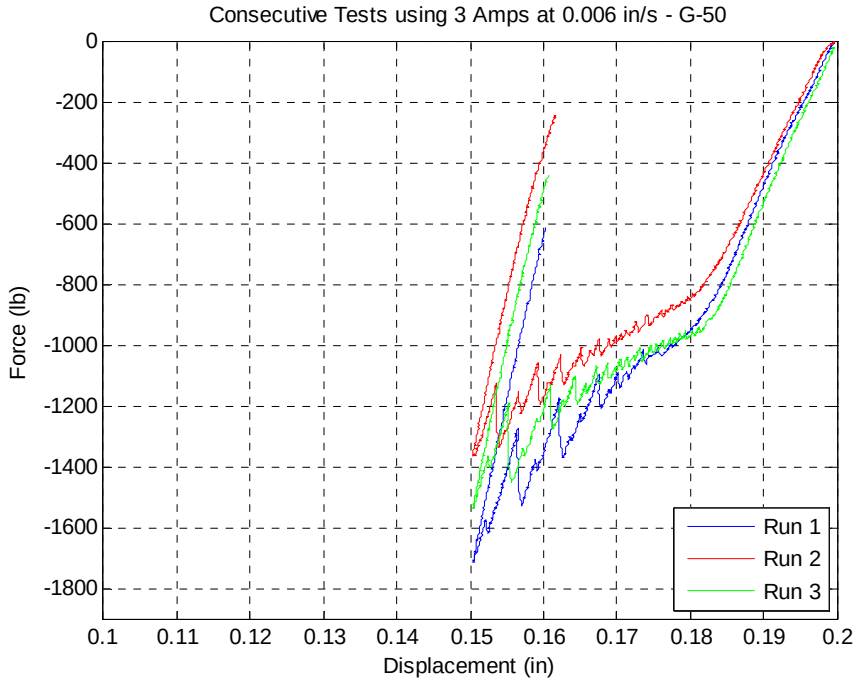

Figure 5-20. G-50 fluid with 3 Amps of coil current at a gap ranging from 0.200 in to 0.050 in

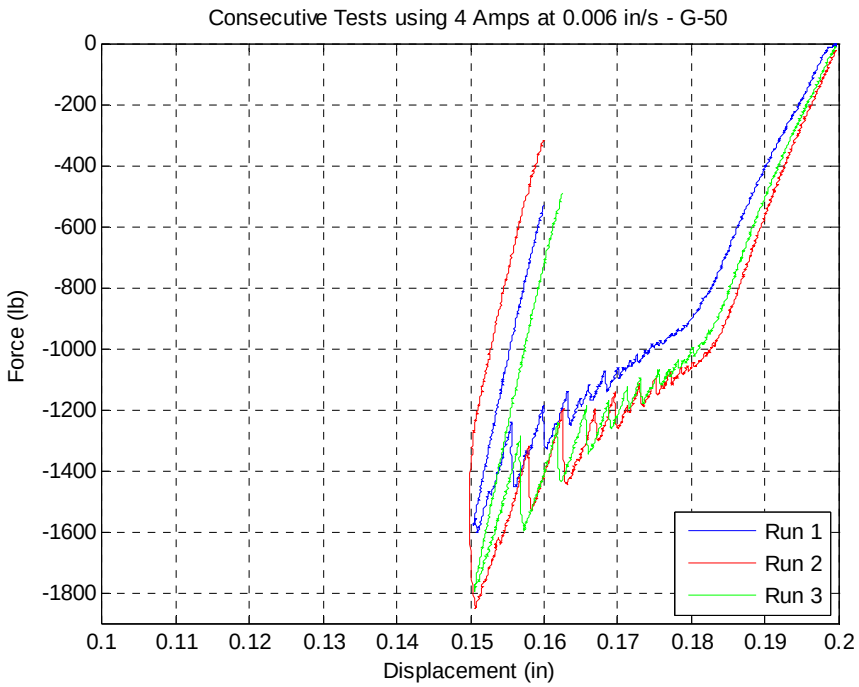

Figure 5-21. G-50 fluid with 4 Amps of coil current at a gap ranging from 0.200 in to 0.050 in

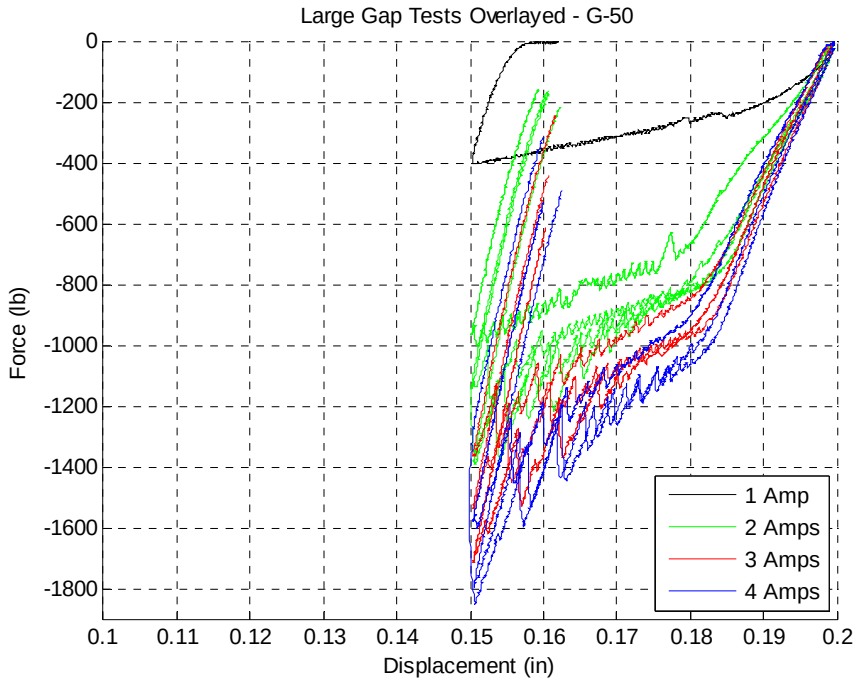

Figure 5-22. G-50 fluid tests at larger gap height overlayed

The next MR fluid that was investigated contained a significantly lower percentage of iron particles. The MRF-120RD fluid, which is manufactured by the Lord Corporation, contains approximately 20% ferrous particles by volume. Reducing the iron content allows for a more free-flowing fluid in its relaxed state, but also reduces the rheological effect of the applied magnetic field. Testing for this fluid consisted of a series of 10 consecutive test runs performed at each coil current level. The initial gap height was set at 0.100 in and then reduced at a constant velocity of 0.006 in/s to a final height of 0.050 in. The results from testing 1, 2, 3, and 4 Amps are shown in Figure 5-23, Figure 5-24, Figure 5-25, and Figure 5-26, respectively. Some of the interesting points to note about these plots are that the "sawtooth" patterns are not present, the results for the 1 Amp setting are very consistent, and the results at both the 3 and 4 Amp settings exhibit a progressive increase in compressive force for each consecutive test run.

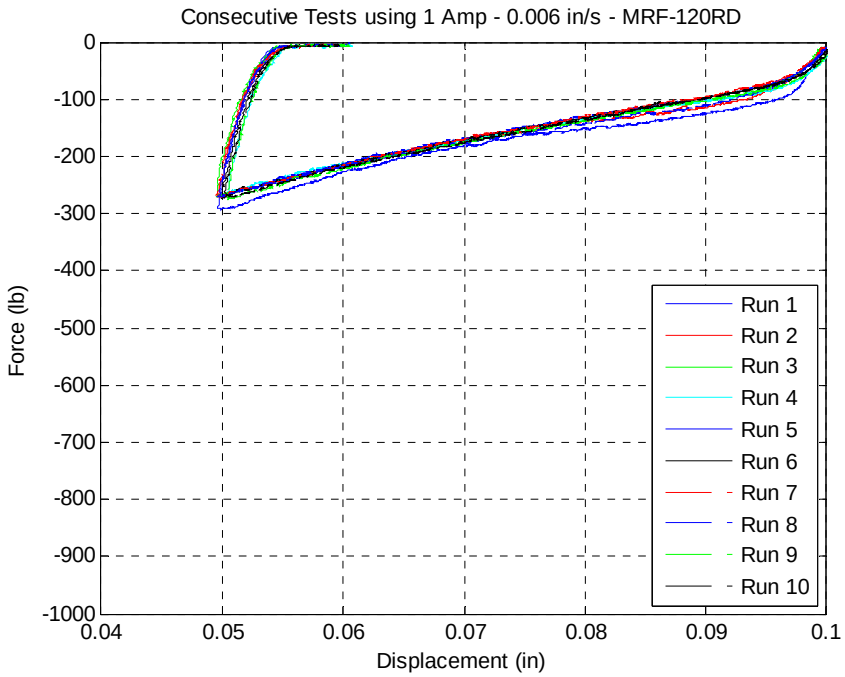

Figure 5-23. MRF-120RD fluid with a 1-Amp coil current at a gap ranging from 0.100 in to 0.050 in

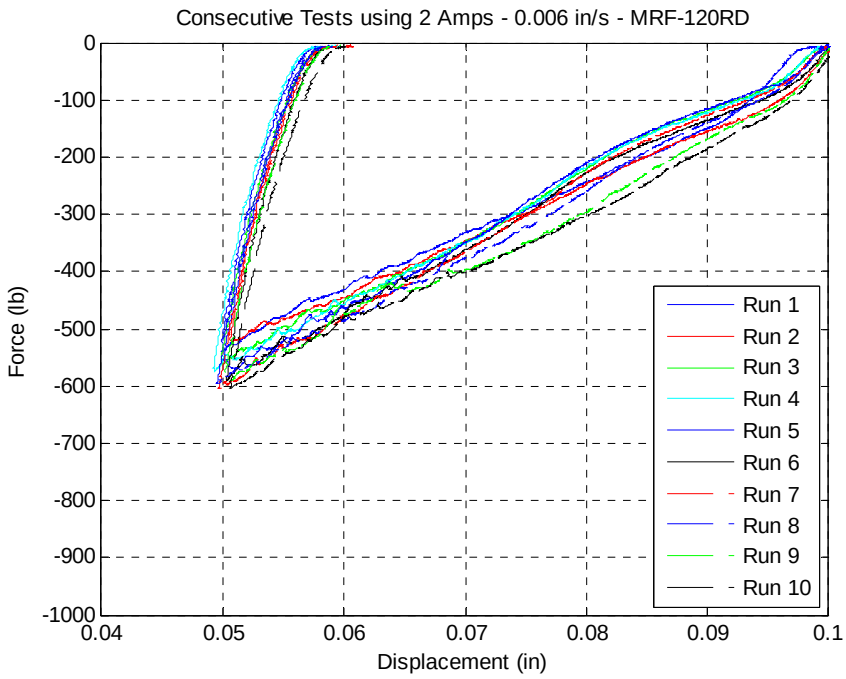

Figure 5-24. MRF-120RD fluid with a 2-Amp coil current at a gap ranging from 0.100 in to 0.050 in

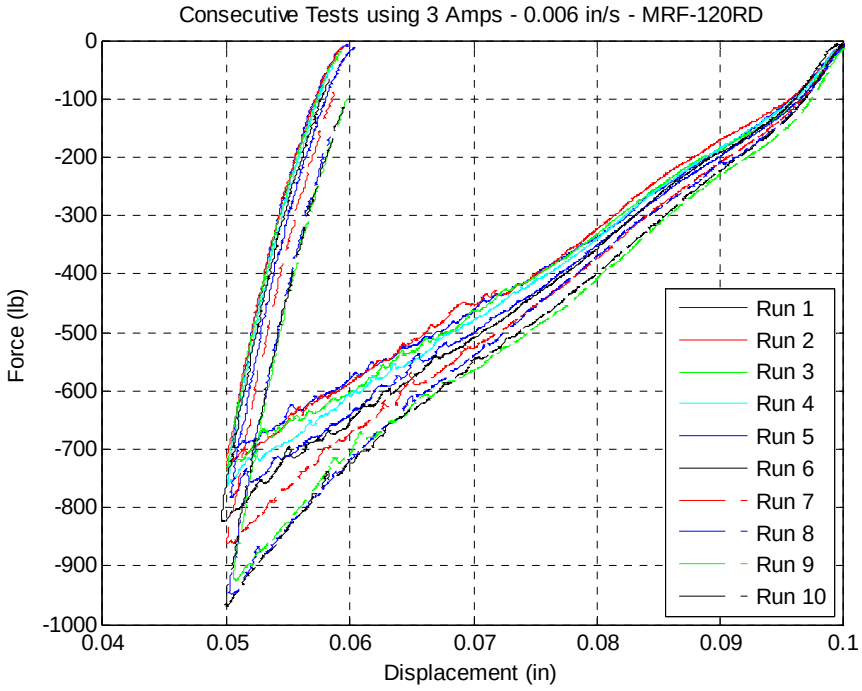

Figure 5-25. MRF-120RD fluid with a 3-Amp coil current at a gap ranging from 0.100 in to 0.050 in

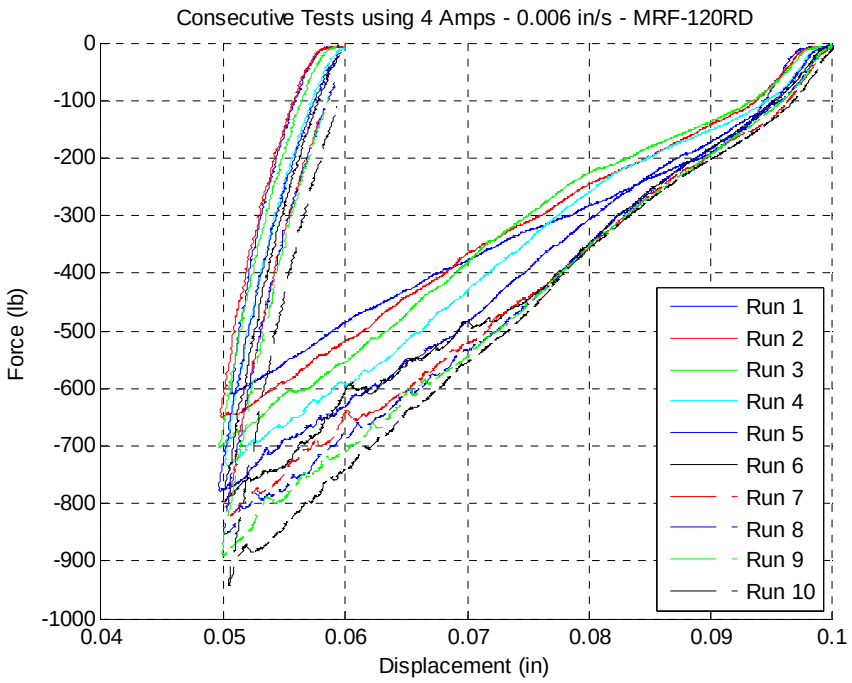

Figure 5-26. MRF-120RD fluid with a 4-Amp coil current at a gap ranging from 0.100 in to 0.050 in

A plot with all 40 test runs overlayed is given in Figure 5-27. It is clear from this plot that the MRF-120RD fluid does not benefit from increasing coil current from 3 Amps to 4 Amps. It is likely that the fluid is fully saturated at the 3 Amp setting, which means that any increase in magnetic field beyond this point will not significantly change the rheology of the fluid. A plot of magnetic flux density measurements for each of the 40 test runs is also provided in Figure 5-28. The flux density is very consistent for the 3 Amp setting, while the 4 Amp setting exhibits variation in the flux density over the course of 10 test runs. Because the force-displacement plots for both the 3 and 4 Amp settings exhibit the same progressive increase in force over consecutive runs, it is reasonable to assume that variation in flux density is not the sole cause for this progressive increase.

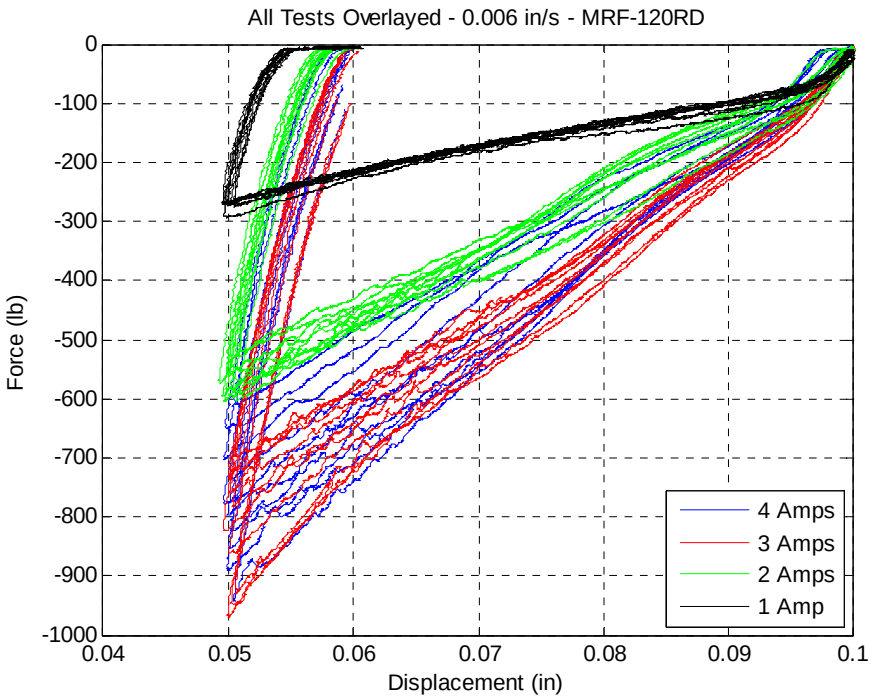

Figure 5-27. MRF-120RD fluid tests overlayed

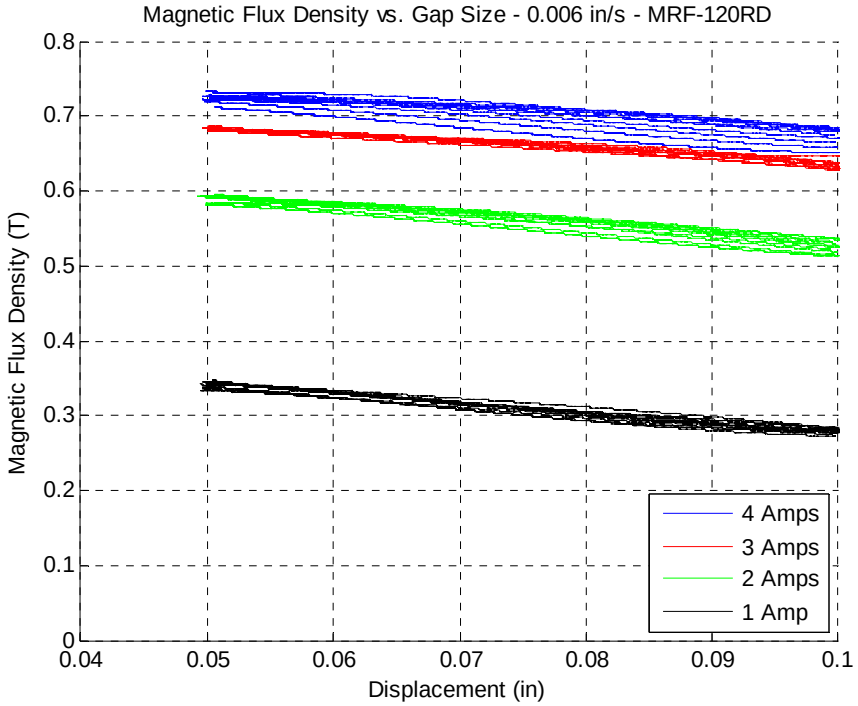

Figure 5-28. Magnetic flux density vs. gap size for MRF-120RD

The next test with the MRF-120RD fluid was designed to monitor how the fluid behaves when allowed to oscillate repeatedly without any adjustment to the coil current during the test. The actuator was set up so that the gap height in the test chamber oscillated between 0.050 in and 0.100 in with a ramp function producing a constant velocity of 0.003 in/s. The test allowed the for approximately 10 complete wave cycles. The results of this test performed at a coil current of 1, 2, 3, and 4 Amps are shown in Figure 5-29, Figure 5-30, Figure 5-31, and Figure 5-32, respectively. An overlay plot with all of the results from the oscillatory tests is given in Figure 5-33. The same trends arise once more in these plots with a consistent force-displacement at lower current settings, while the 3- and 4-Amp settings produce a progressive increase in force as the wave cycles progress.

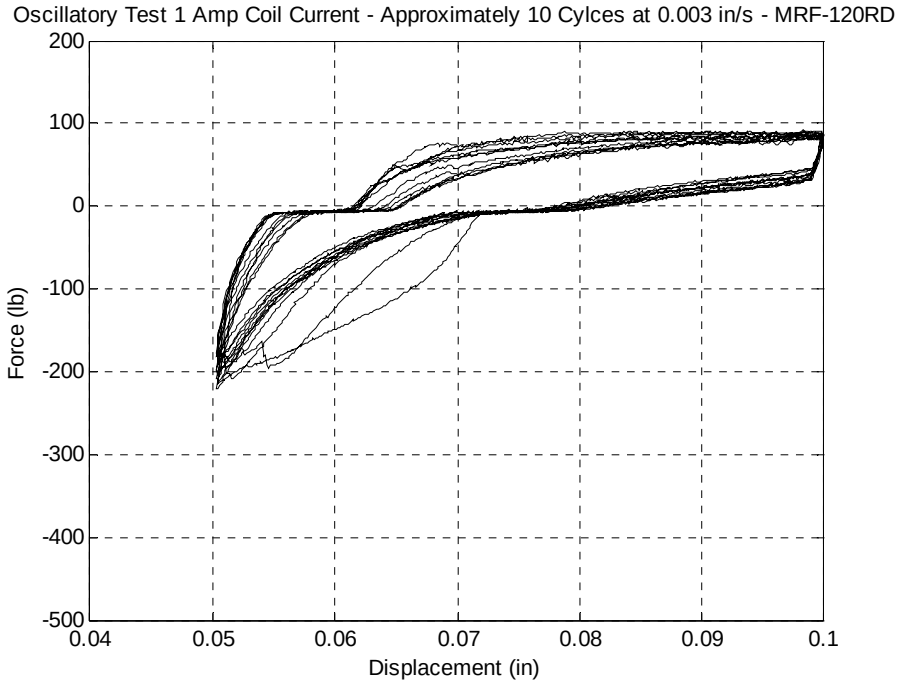

Figure 5-29. MRF-120RD oscillatory test with a coil current of 1 Amp

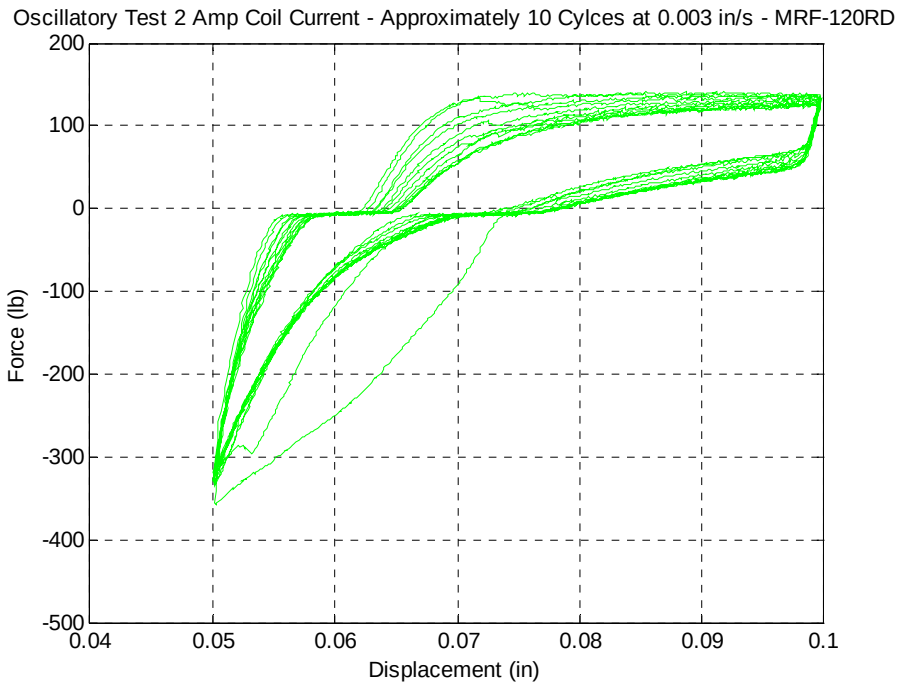

Figure 5-30. MRF-120RD oscillatory test with a coil current of 2 Amps

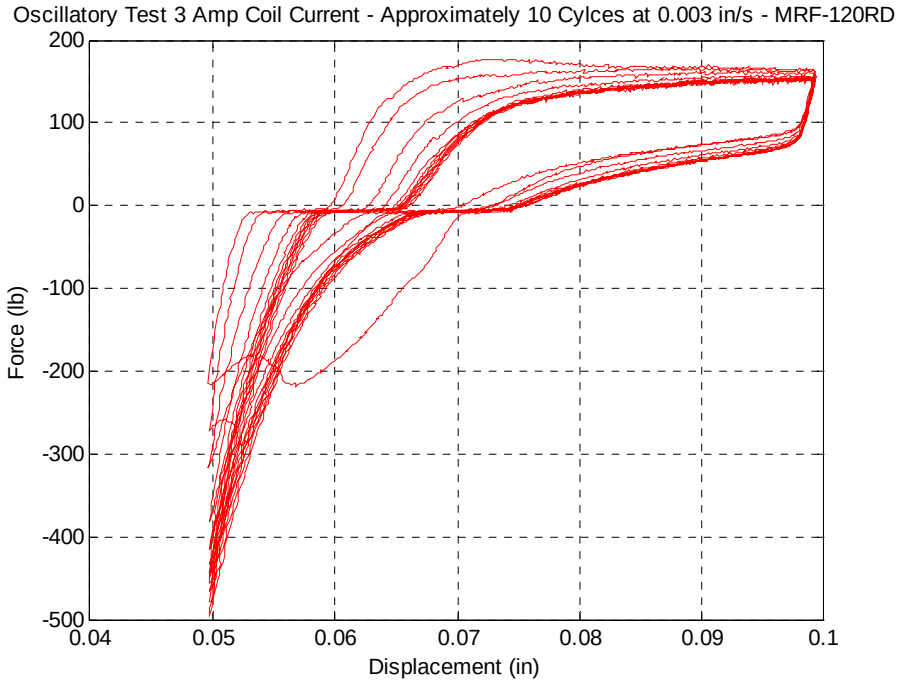

Figure 5-31. MRF-120RD oscillatory test with a coil current of 3 Amps

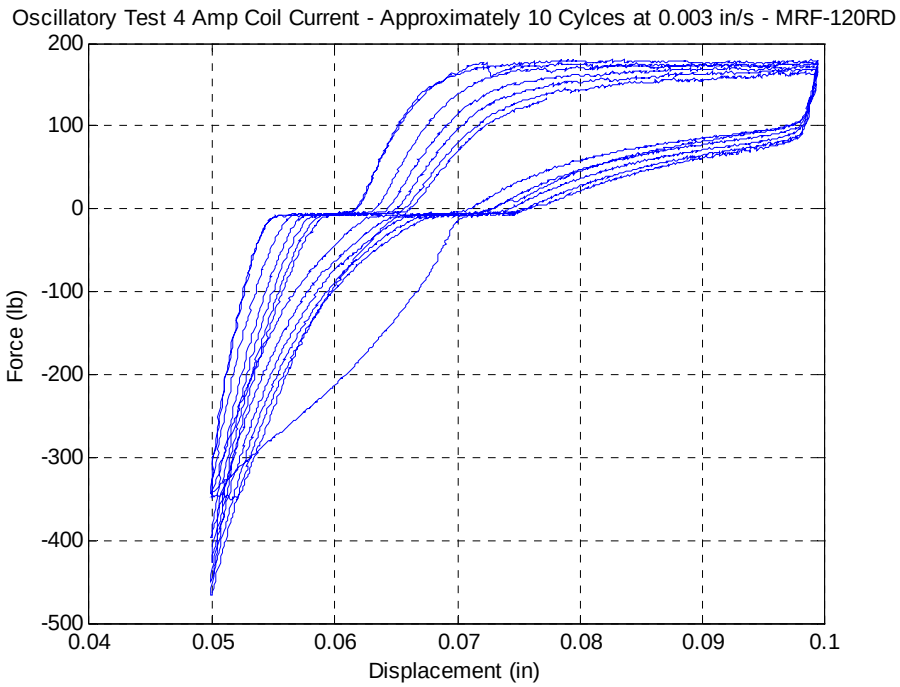

Figure 5-32. MRF-120RD oscillatory test with a coil current of 4 Amps

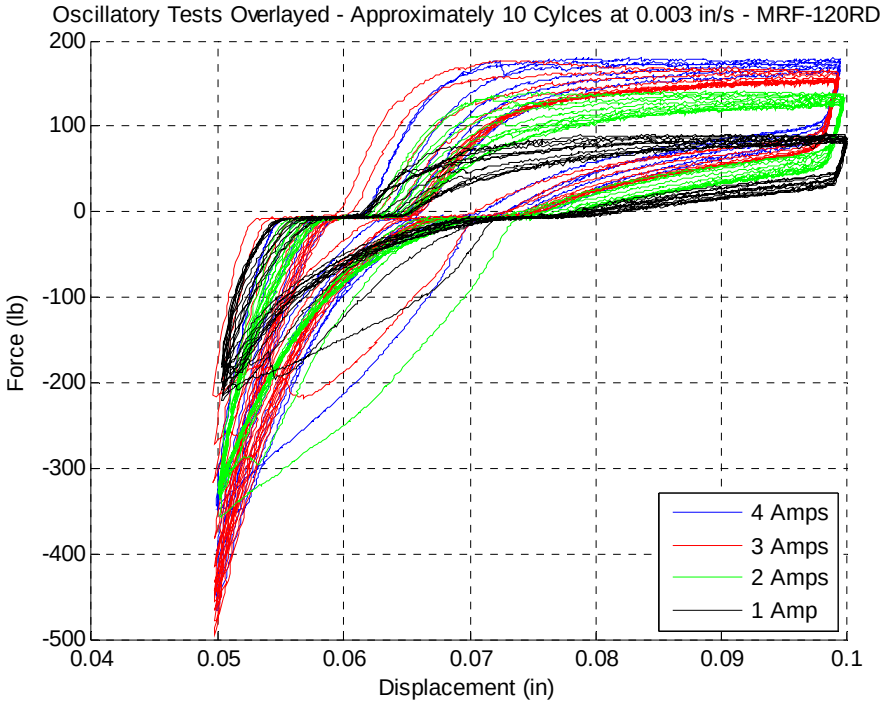

Figure 5-33. MRF-120RD oscillatory tests overlayed

The next fluid that was investigated with the squeeze mode rheometer was another mix from the same major auto manufacturer that consisted of approximately 20% ferrous particles by volume. This fluid is referred to as G-20 hereafter. A similar array of tests was performed with this fluid. The purpose was to determine whether the behavior exhibited in previous tests varied, depending on the elements in the MR composition other than the iron particle fraction. Such elements include the use and type of surfactants in the fluid. Surfactants coat the ferrous particles to aid in suspension within the carrier fluid. A series of 10 consecutive test runs at a coil current level were performed with a gap height ranging from 0.100 in to 0.050 in at a constant 0.006 in/s velocity. The resulting test plots from coil current levels of 1, 2, 3, and 4 Amps are shown in Figure 5-34, Figure 5-35, Figure 5-36, and Figure 5-37 respectively. An overlay of all tests with the G-20 fluid is given in Figure 5-38. The results from this testing are nearly identical to those from the MRF-120RD tests. The trends concerning consistency at lower coil currents and progressively increasing force at higher currents is present once again. Moreover, the compressive force values found in the force-displacement plots also match well with those found in the MRF-120RD tests.

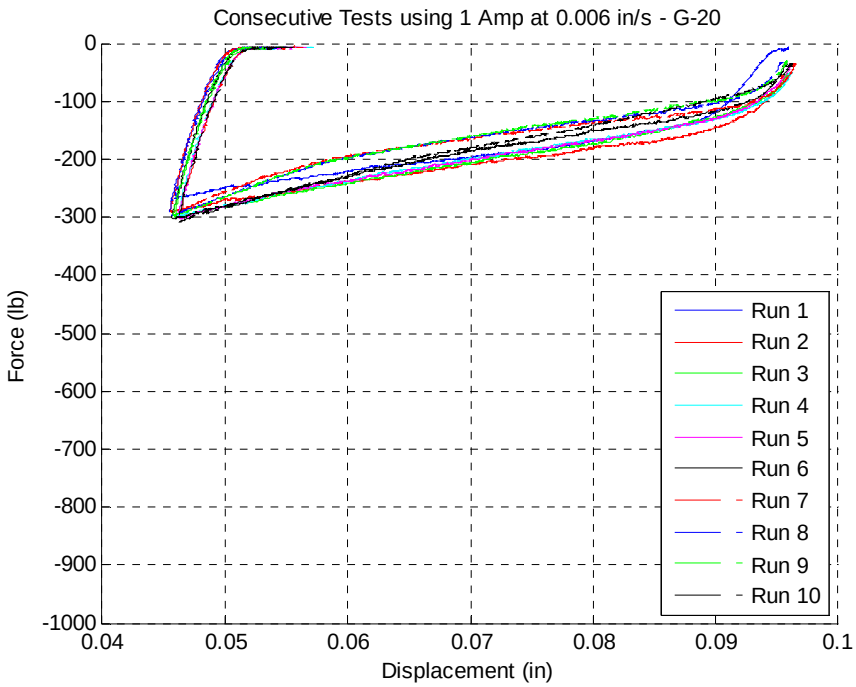

Figure 5-34. G-20 fluid with 1 Amp of coil current at a gap ranging from 0.100 in to 0.050 in

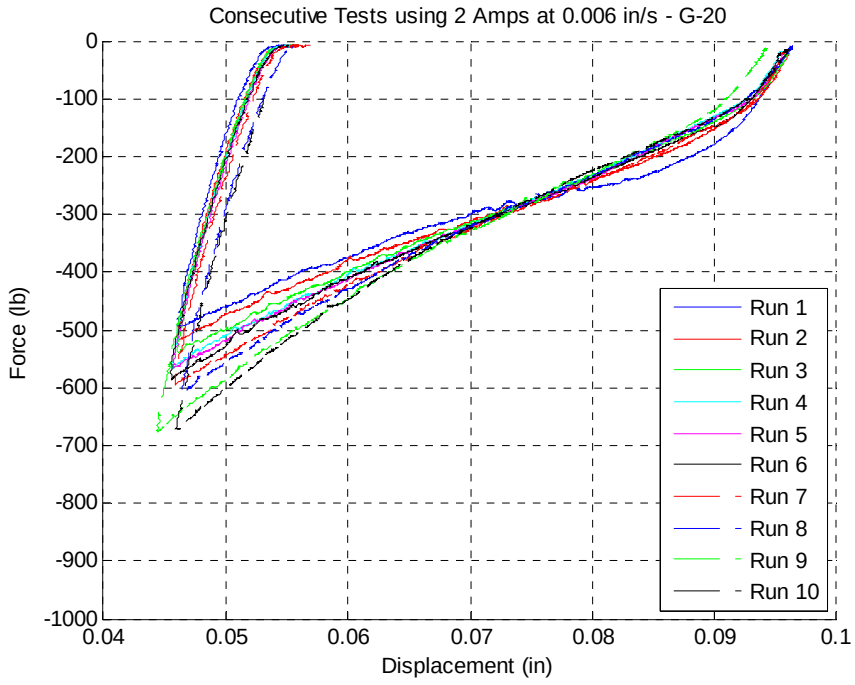

Figure 5-35. G-20 fluid with 2 Amps of coil current at a gap ranging from 0.100 in to 0.050 in

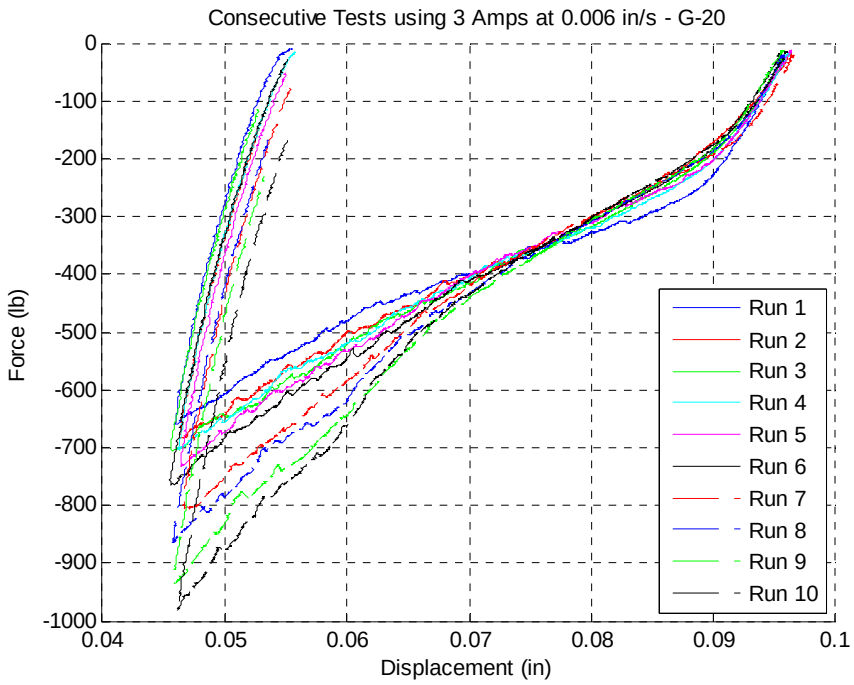

Figure 5-36. G-20 fluid with 3 Amps of coil current at a gap ranging from 0.100 in to 0.050 in

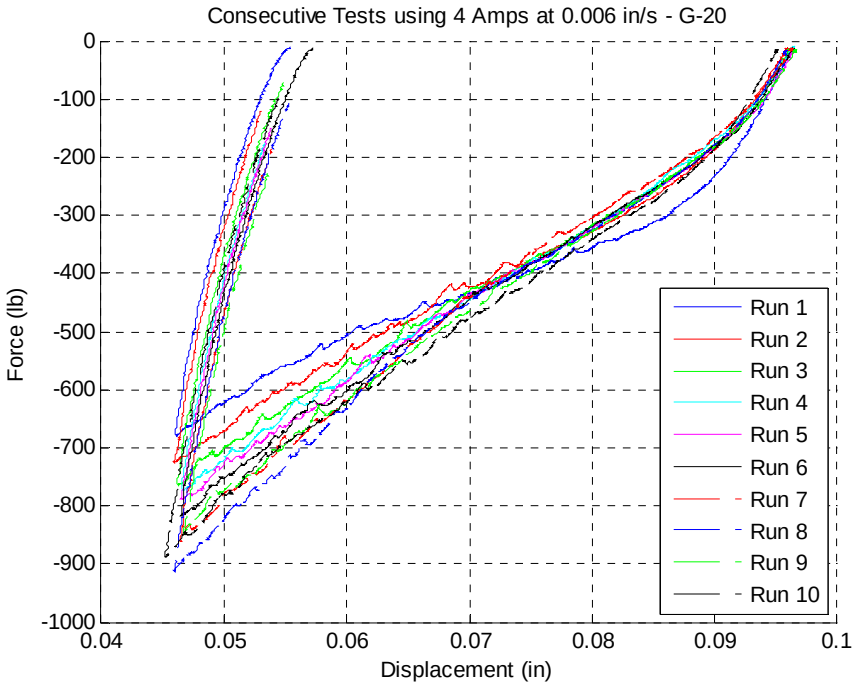

Figure 5-37. G-20 fluid with 4 Amps of coil current at a gap ranging from 0.100 in to 0.050 in

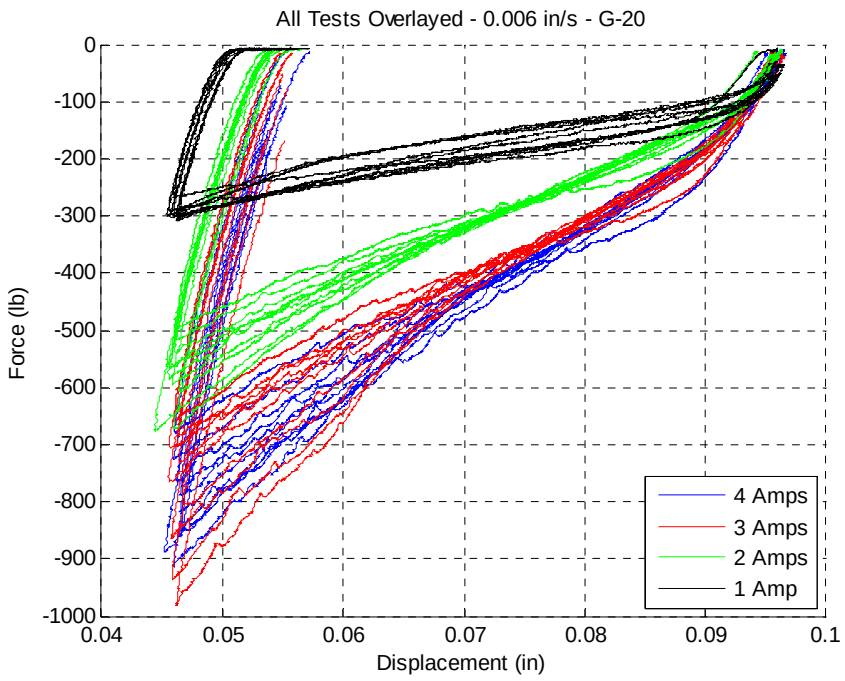

Figure 5-38. G-20 tests overlayed

Next, another MR fluid from Lord Corporation was selected for testing. This particular mix, which is called MRF-122EG, has a 22% ferrous particle volume fraction. Data sheets for this fluid can be found in the appendix of this document. This fluid was tested at a coil current setting of 1 and 2 Amps at a gap height ranging from 0.100 in to 0.050 in with a constant velocity of 0.006 in/s. The plots for tests conducted at 1 and 2 Amps are given in Figure 5-39 and Figure 5-40 respectively. These plots are also presented together as an overlay in Figure 5-41. The most striking aspect of these particular graphs is the rate at which the force increases from one run to the next. Also, in previous tests with a fluid of similar volume fraction, the results with 1 Amp of coil current were relatively consistent from run to run. It should be noted that the number of test runs was cut short due to fears of structural failure in rheometer.

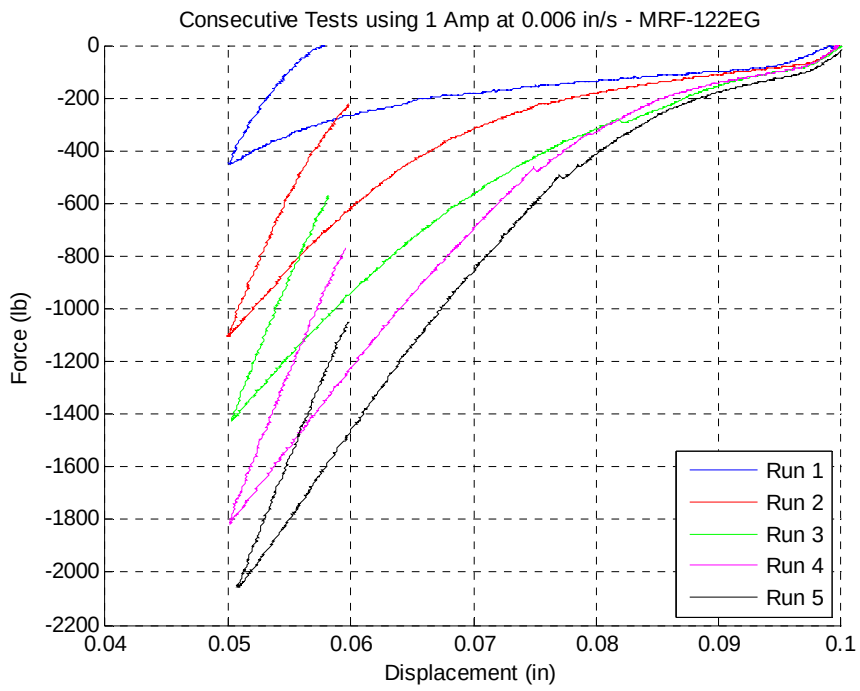

Figure 5-39. MRF-122EG fluid with a 1-Amp coil current at a gap ranging from 0.100 in to 0.050 in

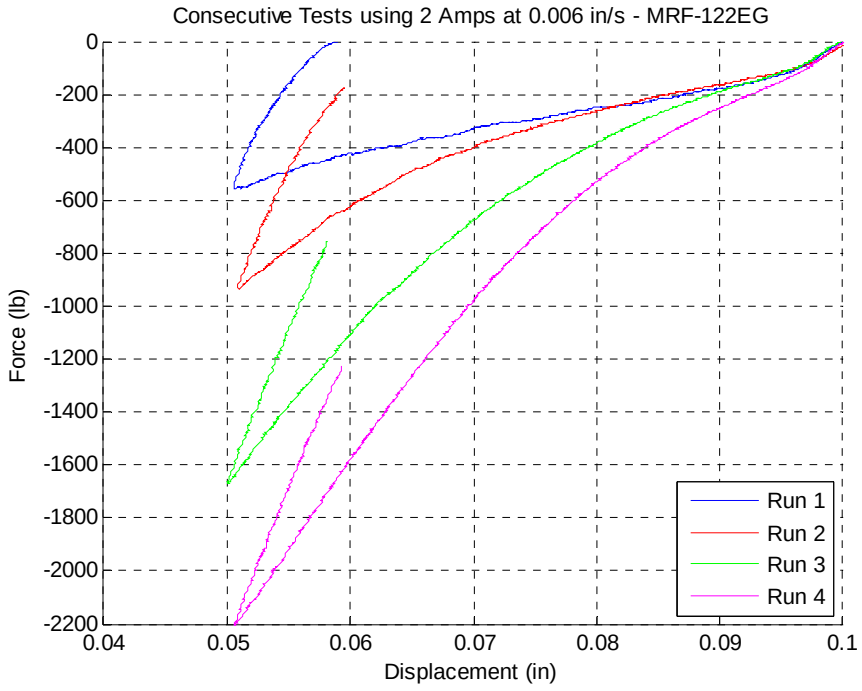

Figure 5-40. MRF-122EG fluid with a 2-Amp coil current at a gap ranging from 0.100 in to 0.050 in

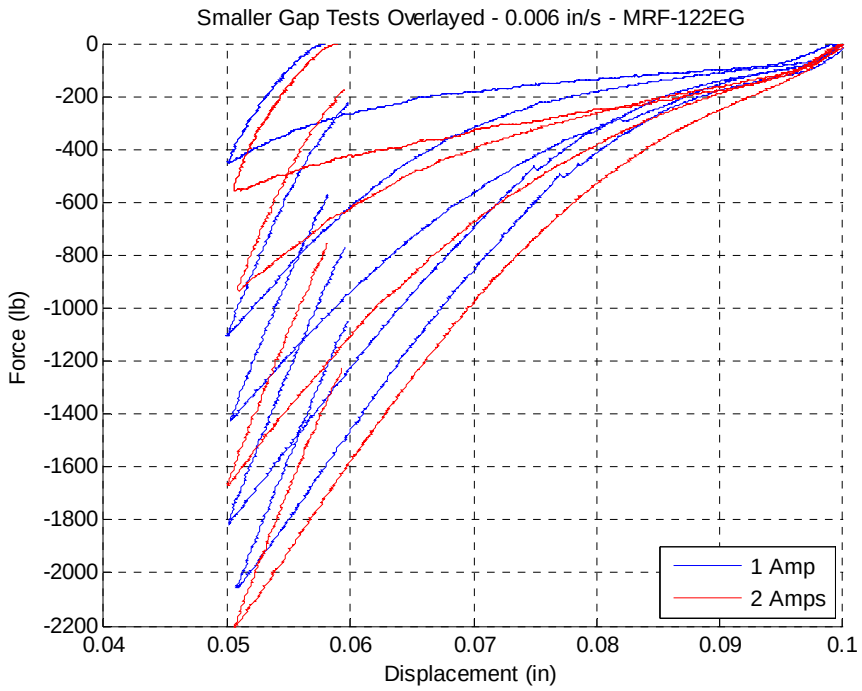

Figure 5-41. MRF-122EG small gap tests overlayed

Additional testing was performed with the MRF-122EG fluid at a larger gap size to investigate the role that gap height plays in the behavior of the fluid. The test procedure remained the same as in the previous testing with the only deviation being that the gap height ranged from 0.200 in to 0.150 in. The results from these tests are plotted in Figure 5-42, Figure 5-43, and Figure 5-44. The increase in gap height dramatically reduces the progressive force increase found in the lower gap height tests. The results are consistent for test runs with 1 Amp of coil current, while the 2-Amp setting still exhibits some degree of the progressively increasing force trend.

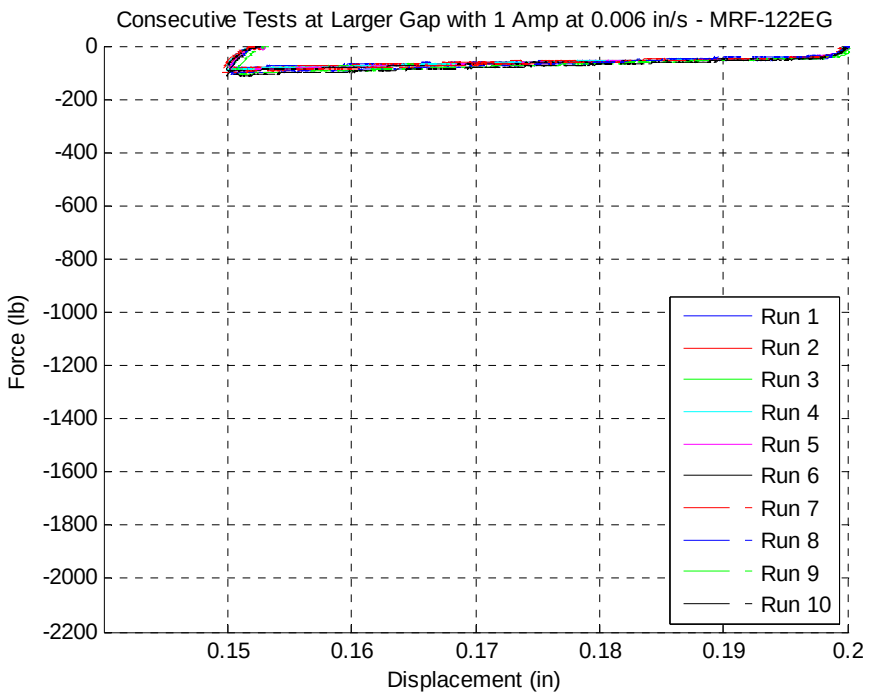

Figure 5-42. MRF-122EG fluid with a 1-Amp coil current at a gap ranging from 0.200 in to 0.150 in

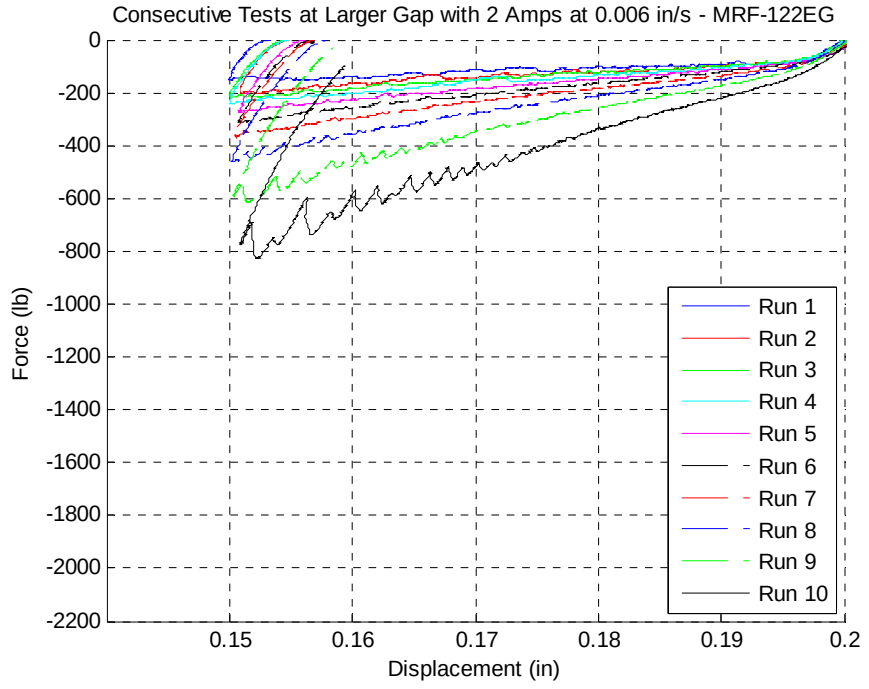

Figure 5-43. MRF-122EG fluid with a 2-Amp coil current at a gap ranging from 0.200 in to 0.150 in

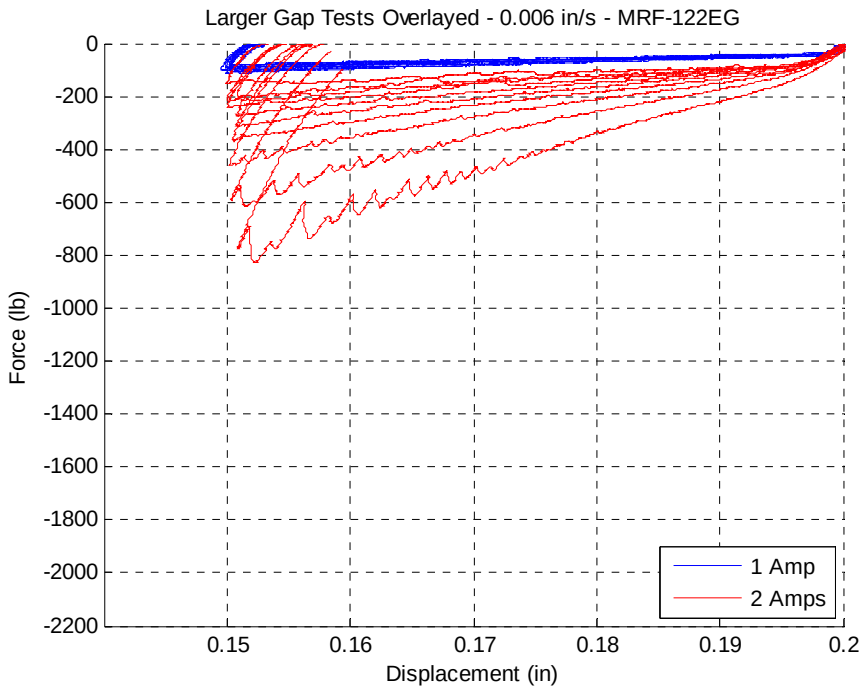

Figure 5-44. MRF-122EG large gap tests overlayed

The final fluid tested in the rheometer is MRF-132DG produced by Lord Corporation, which contains 32% volume fraction of ferrous particles. The data sheets for this fluid can be found in the appendix of this document. Tests with this fluid mimic those performed with the MRF-122EG fluid. The first set of testing was conducted with coil currents of 1 and 2 Amps at a gap height ranging from 0.100 in to 0.050 in with a constant velocity of 0.006 in/s. The resulting test plots are shown in Figure 5-45, Figure 5-46, and Figure 5-47. There is a progressive increase in force between consecutive runs, but the effect at 1 Amp is not as pronounced as it was with the MRF-122EG fluid. The effect at a coil current of 2 Amps is quite similar to the one found in the 22% volume fraction fluid tested previously.

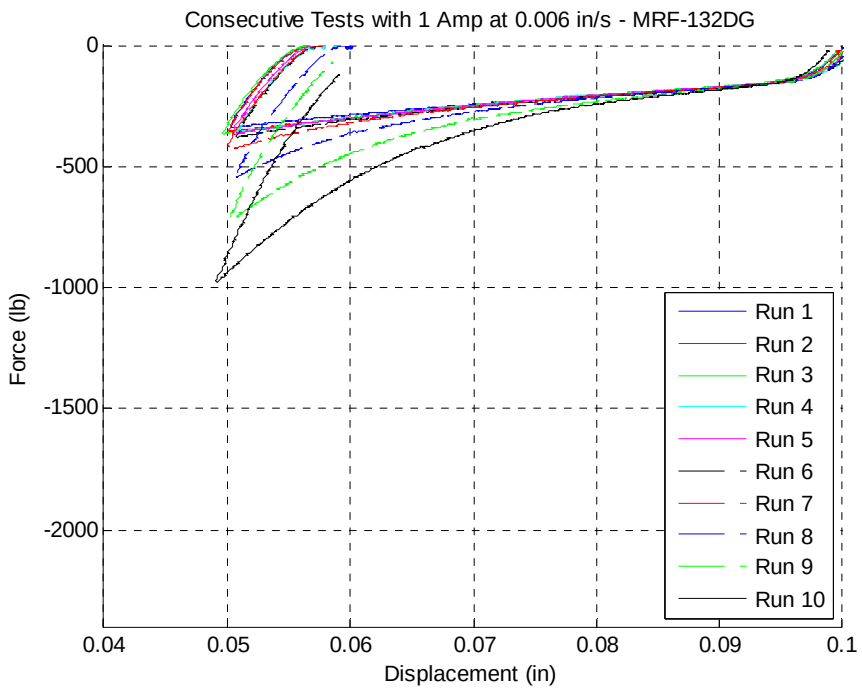

Figure 5-45. MRF-132DG fluid with a 1-Amp coil current at a gap ranging from 0.100 in to 0.050 in

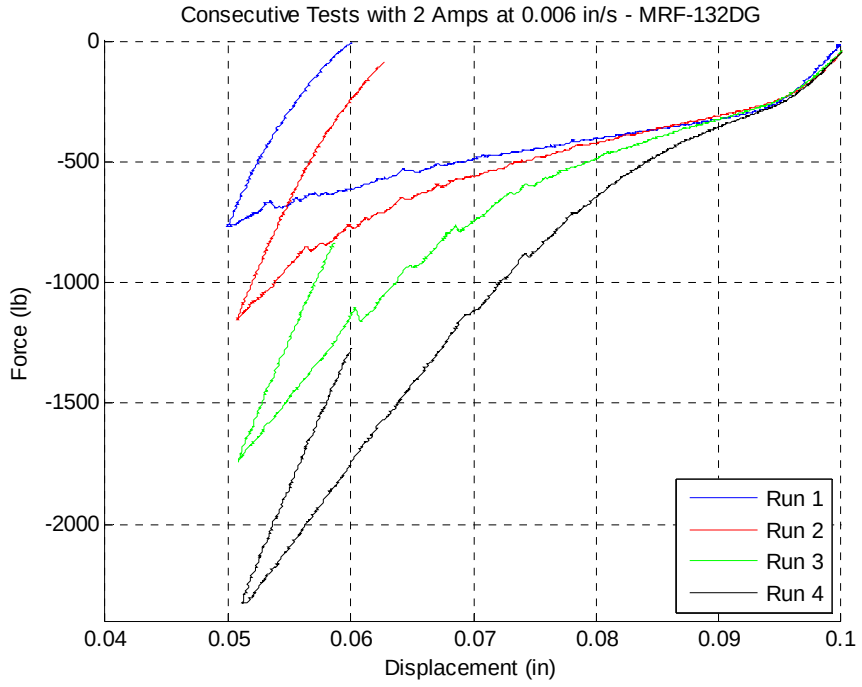

Figure 5-46. MRF-132DG fluid with a 2-Amp coil current at a gap ranging from 0.100 in to 0.050 in

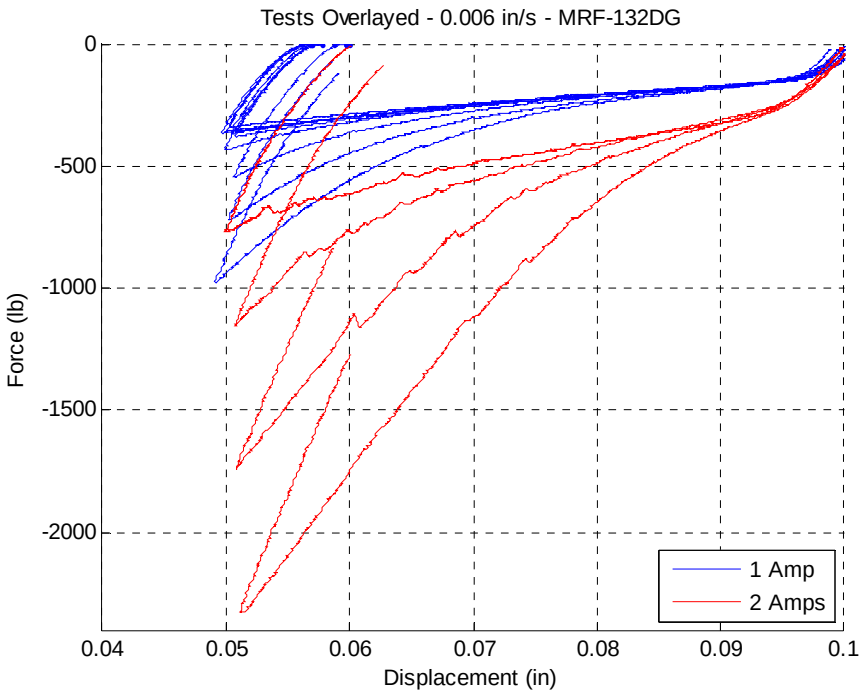

Figure 5-47. MRF-132DG small gap tests overlayed

The MRF-132DG fluid was also tested at a gap height ranging from 0.200 in to 0.150 in with a constant velocity of 0.006 in/s. These test results are plotted in Figure 5-48, Figure 5-49, and Figure 5-50. The force-displacement plots at the larger gap height are relatively consistent of the course of 10 runs. The coil current setting of 2 Amps shows only a mild increase in force over the test set.

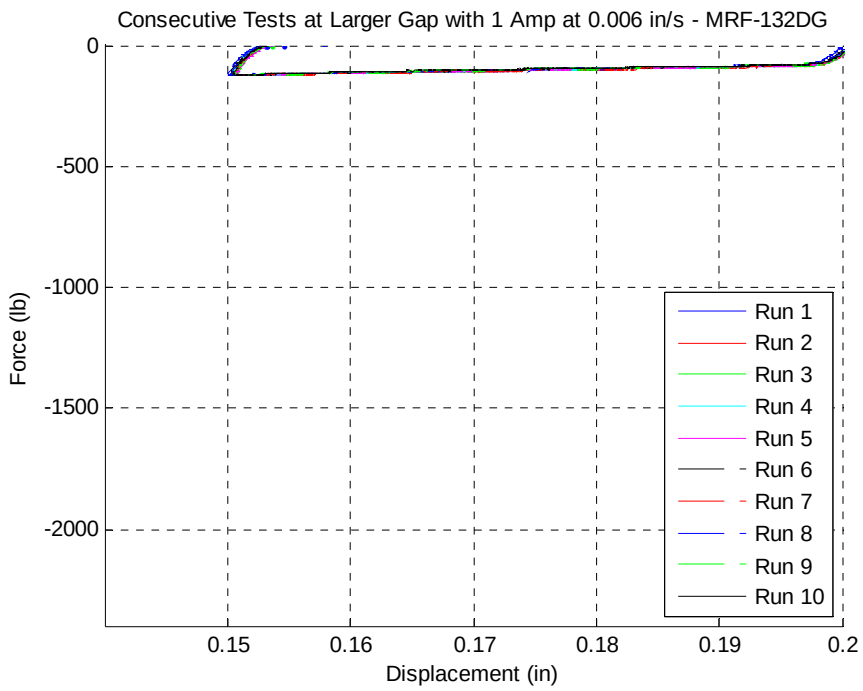

Figure 5-48. MRF-132DG fluid with a 1-Amp coil current at a gap ranging from 0.200 in to 0.150 in

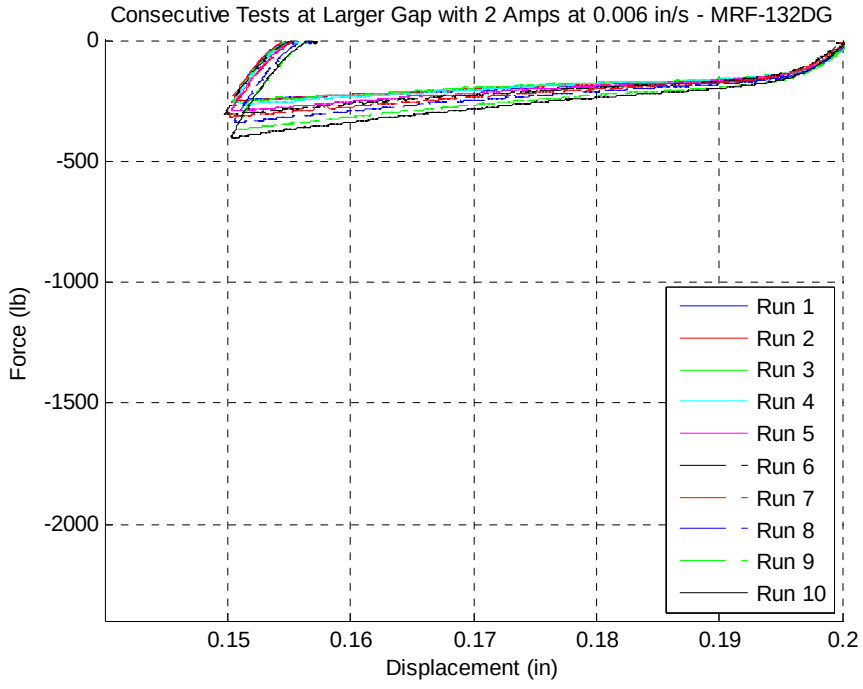

Figure 5-49. MRF-132DG fluid with a 2-Amp coil current at a gap ranging from 0.200 in to 0.150 in

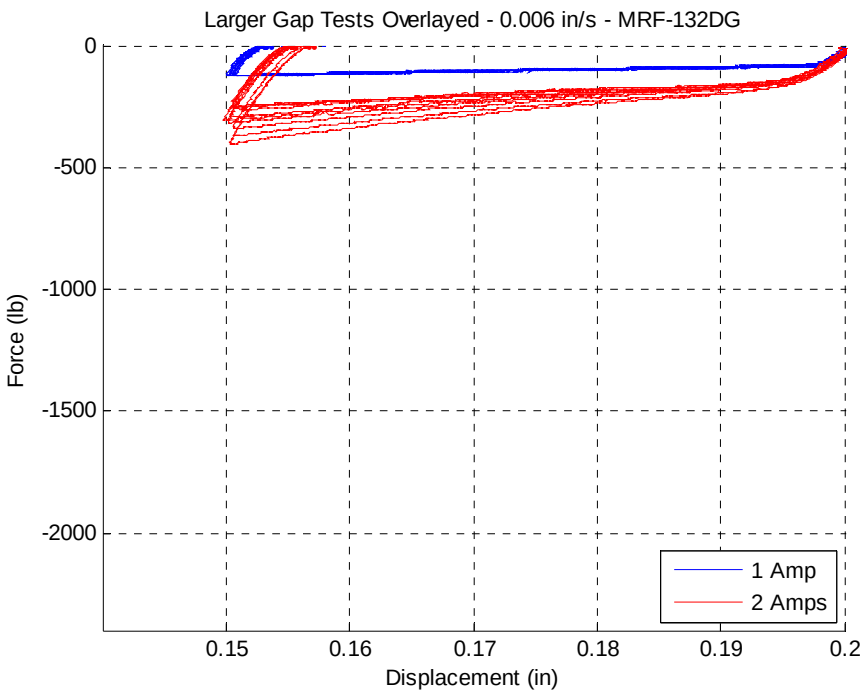

Figure 5-50. MRF-132DG large gap tests overlayed

5.3 Test Observations

This section provides additional subjective observations that were noted during the testing as well as a summary of the results reported in the previous section.

The anomalies found in the first set of tests, which involved the G-50 fluid, include a progressively increasing force for consecutive runs under the same test conditions and a "sawtooth" or "stick-slip" pattern in the force-displacement plots. The "sawtooth" pattern will be addressed first. Upon closer examination of the force-displacement plot, one notices that the force instantaneously decreases in multiple points along the stroke. This sudden loss in compressive force generates the "sawtooth" pattern noted previously. The likely cause for this phenomenon is air bubbles trapped inside the test chamber. The G-50 fluid is particularly susceptible to this scenario due to its relatively high viscosity in the relaxed state. The G-50 fluid in its relaxed state has a consistency that is similar to yellow mustard. It will flow relatively easy if acted on by an outside force and will eventually

settle to a smooth even level, but it does flow naturally and is difficult to work with. During testing with this fluid, the excess MR fluid was expelled up through the clear vinyl tubing as intended. When the gap reaches its minimum height and begins the upstroke, it effectively sucks the expelled fluid back into the chamber, thus refilling it to the original volume. The G-50 fluid did not flow easily back down into the chamber. Rather, it adhered to the wall of the vinyl tubing while an "air tunnel" was formed that lead directly to the test chamber. Tests with less viscous free-flowing fluids did not exhibit the "sawtooth" pattern described in the G-50 fluid plots.

The second anomaly discovered in initial testing with the G-50 fluid is the trend of progressively increasing force when consecutive tests are performed without mixing the fluid. This trend is common to some degree in all the MR fluids tested. It should be noted that during these tests, the temperature of the fluid and rheometer remained at a temperature close to ambient. Temperature does not seem to be a driving force in this trend. This trend, however, does present a challenge for applying squeeze-mode operation to practical applications.

The MRF-120RD fluid was tested in an oscillatory mode, where the gap height was allowed to complete 10 displacement cycles without turning off the coil current. The results were nearly identical to the test runs that were conducted one at time. Another interesting feature revealed by the testing was that the MR fluid was becoming saturated at the 3-Amp coil current level.

The tests performed with the MRF-122EG fluid produced very surprising results. The fluid has a similar volume fraction and consistency to that of the G-20 and MRF-120RD fluids, but the test results were drastically different. The progressively increasing force phenomenon observed in previous tests was magnified greatly in the MRF-122EG fluid. While mixing the fluid after a sequence of test runs, it was discovered that semi-solid aggregate clumps were forming in the test chamber. The fluid was in a relaxed state, but semi-solid clumps were spread around the perimeter of the test chamber predominantly sticking to the cylinder wall and chamber floor, as shown in Figure 5-51 . An example of an aggregate clump that was extracted from the MR fluid chamber is shown in Figure 5-52. It should be noted that the consistency of these clumps did not appear to have a magnetic quality to them. There was no obvious attraction of ferrous

particles or any sort of reformation when breaking the clumps apart. Based on these observations, it does not appear that remanence, which is the magnetization left behind in a medium after an external magnetic field is removed, is the sole cause for the clumping effect. From a combination of observations and multiple test results, it appears that the semi-solid aggregate clumps are the cause for the trend of progressively increasing force in consecutive test runs.

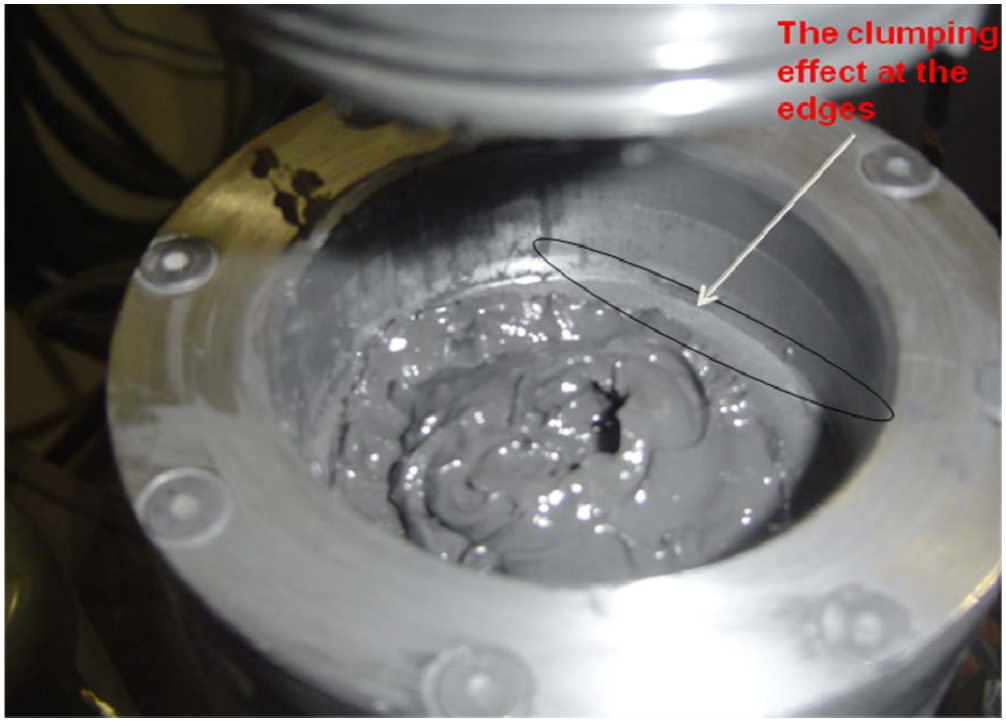

Figure 5-51. Semi-solid aggregate ring is formed on the floor around the perimeter of the test chamber (photo by Ryan Cavey)

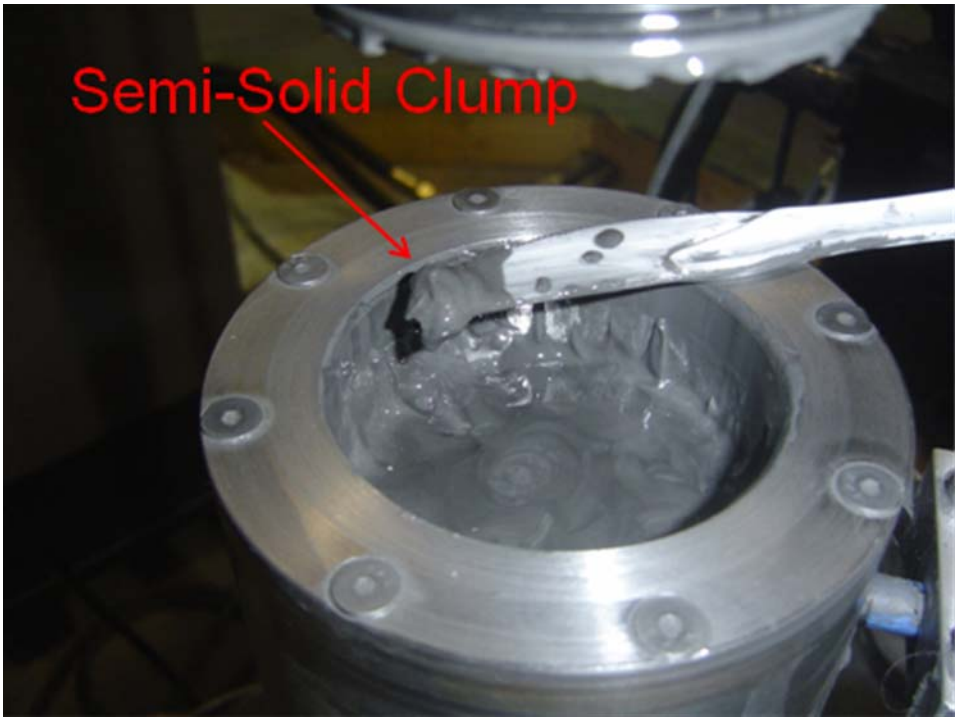

Figure 5-52. A pea-sized aggregate clump that has formed in the MR fluid test chamber (photo by Ryan Cavey)

The MRF-122EG fluid was retested at a larger height to investigate the effect that gap size has on the formation of the aggregate clumps. The clumping effect was somewhat reduced as the semi-solid aggregates that did form were not as tightly compacted as in the tests at a lower gap height. Similar clumping formations were observed with the MRF-132DG fluid as well. It should be noted that the trend towards a progressive increase in force was reduced in the MRF-132DG fluid when compared to the MRF-122EG fluid. This leads one to assume that the clumping effect is not solely due to the volume fraction of ferrous particles in the fluid.

5.4 Piston Redesign

In an attempt to understand, reduce, and possibly solve the problem of clump formation in the squeeze mode rheometer, the piston design is reexamined. As stated in the previous section, a semi-solid aggregate ring is consistently formed around the perimeter of the test chamber. The design of the piston is such that the only means of escape for the MR fluid is a single hole located in the center of the chamber. The aggregate clumps seem to form

at the points in the chamber which are the furthest distance away from that exit point. When the MR fluid is placed in compression, excess fluid is expelled through the exit hole. The fluid being expelled is assumed to be at atmospheric pressure while also having the largest flow rate of any region in the test chamber. It goes to show that the opposite is true for the extreme perimeter of the test chamber. During the compression stroke the fluid in the region is expected to be placed under the greatest pressure while exhibiting virtually no fluid flow. It is thought that this may lead to a large pressure gradient within the test chamber, as shown in Figure 5-53. It is possible that this pressure gradient encourages separation of the ferrous particles from the carrier fluid. With an applied magnetic field, the ferrous particles may resist flow while the base fluid is essentially squeezed out from the test chamber. During tests where clumping was observed, the excess MR fluid in the clear vinyl tubing became increasingly less viscous eventually becoming oil-like. This condition would likely lead to a localized increase in ferrous particle volume fraction and in turn may lead to the increased stiffness that was also observed.

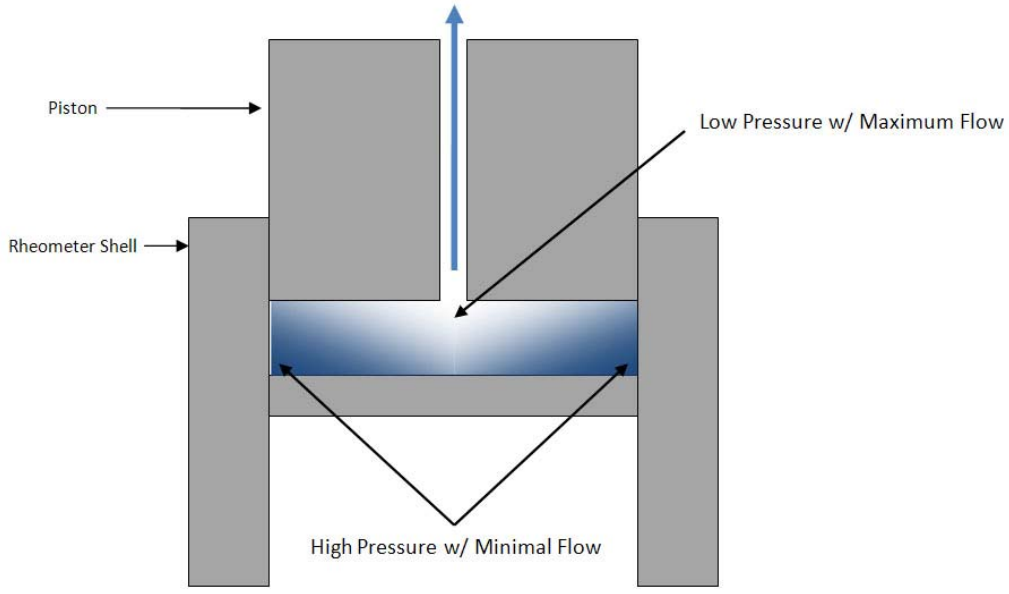

Figure 5-53. A piston with a single exit hole may create a large pressure gradient inside the test chamber

The design on a new piston incorporates and addresses the ideas presented in the previous paragraph. The new design is aimed at reducing the pressure gradient across the MR fluid. The piston is constructed from the same 12L14 solid steel stock chosen for the original piston. In order to reduce the pressure gradient, multiple holes are placed in an array around the face of the piston. A model of the Multi-hole Piston is shown in Figure 5-54. Eight holes, which each have a diameter of 0.150 in, are drilled through the body of the piston in two circular arrays that are offset 45 degrees to each other. The piston area was not held constant to the original piston design. The primary focus for the redesigned piston is to investigate to the aggregate clumping effect as opposed to directly comparing force magnitudes between pistons.

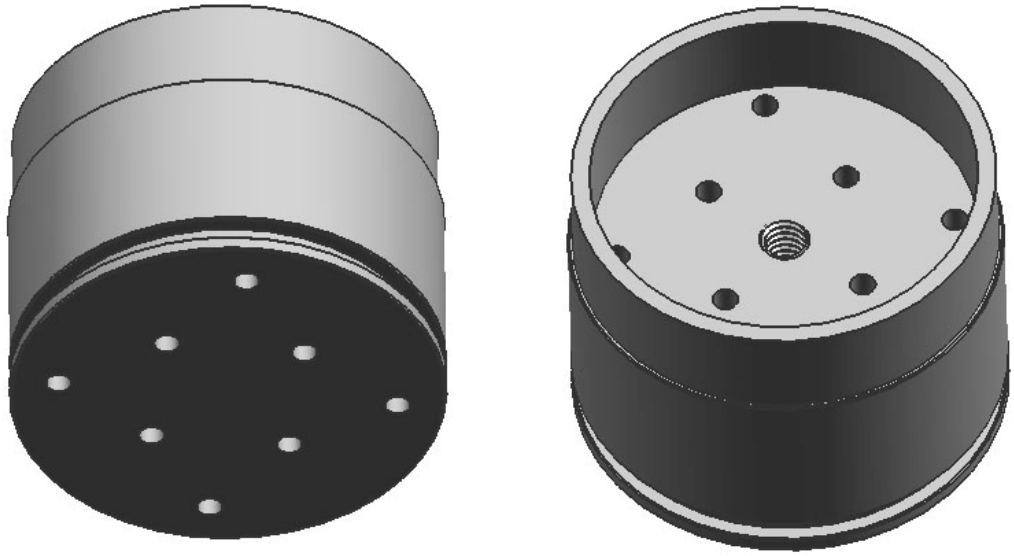

Figure 5-54. The Multi-hole Piston is interchangeable with the original piston

With the addition of 8 exit holes, the next challenge in the design is to control the excess MR fluid that is expelled during testing. In the end, a simple metal tube was welded to the top of the piston body to form a small cup-like reservoir for the fluid.

5.5 Multi-hole Piston Test Results

The first test that was performed with the Multi-hole Piston was friction or seal drag test. The test chamber was filled with MRF-132DG fluid with a gap height that ranged from

0.100 in to 0.050 in. The velocity was held constant at 0.006 in/s and the MR fluid was kept in its relaxed state as there was no magnetic field applied. The results from the seal drag test as well as a repeat of that test are shown in Figure 5-55. The off-state resistance force is reasonably consistent at approximately -7 lbs across the range of gap heights.

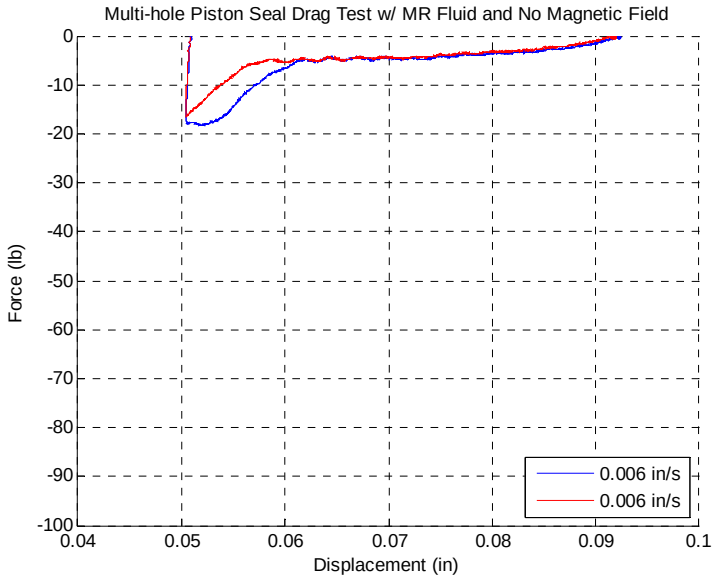

Figure 5-55. Resistance force for the Multi-hole Piston MRF-132DG fluid with no applied magnetic field

The Multi-hole Piston was tested with MRF-132DG fluid in a similar manner to the original piston design. Testing was performed with coil currents of 1 and 2 Amps with an initial gap height of 0.100 in. The gap height was reduced at a constant 0.006 in/s velocity to a final height of 0.050 in. The resulting plots from this testing are given in Figure 5-56, Figure 5-57, and Figure 5-58. The plots indicate that the progressive increase in force over consecutive runs is still dominant and that the Multi-hole design does not have the desired effect.

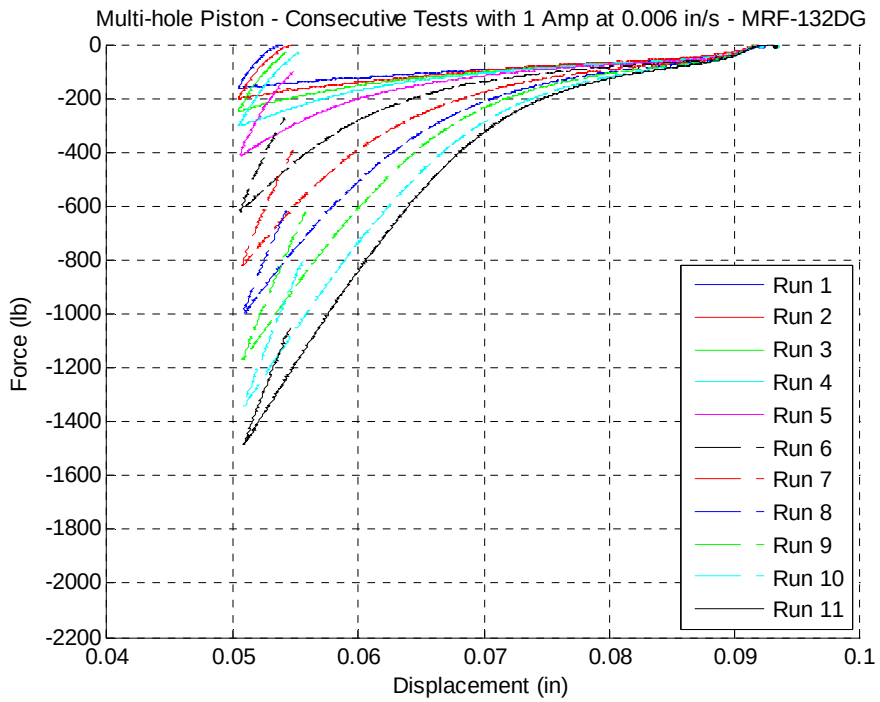

Figure 5-56. MRF-132DG fluid with the Multi-hole Piston at a coil current of 1 Amp

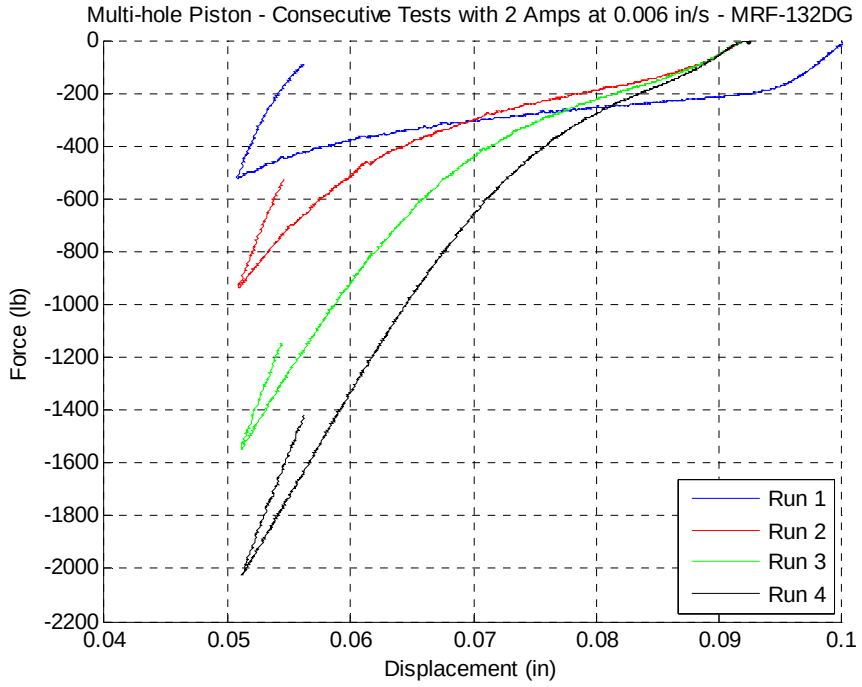

Figure 5-57. MRF-132DG fluid with the Multi-hole Piston at a coil current of 2 Amps

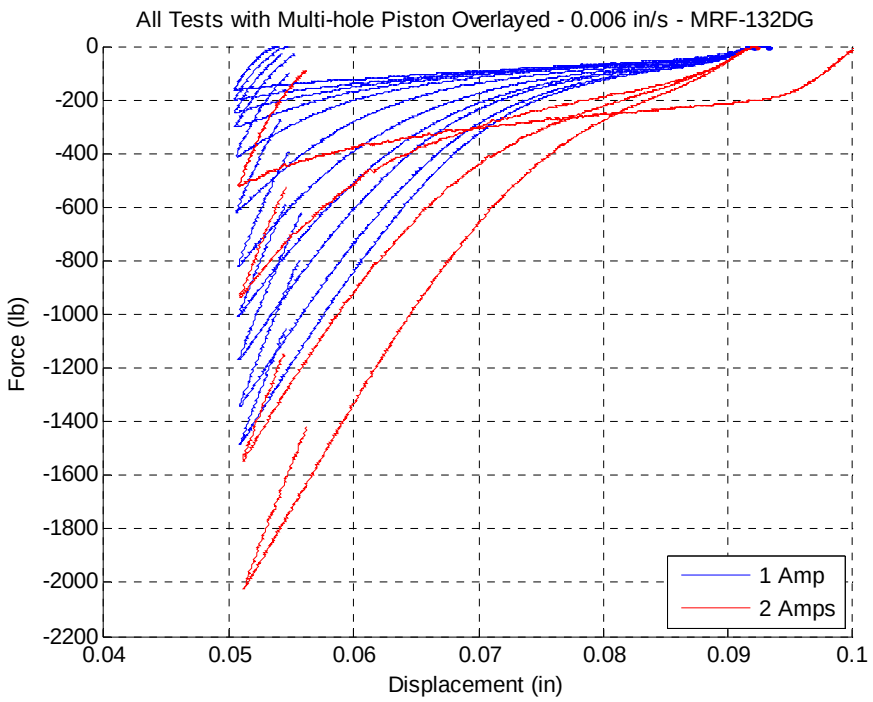

Figure 5-58. MRF-132DG fluid tests with the Multi-hole Piston overlayed

A pair of comparison plots between the tests performed with the Multi-hole piston and the identical tests performed with the single-hole piston are presented in Figure 5-59 and Figure 5-60. It is clear from these plots that the Multi-hole piston design intensifies the progressive increase in force trend. This is most notable in the 1 Amp coil current setting.

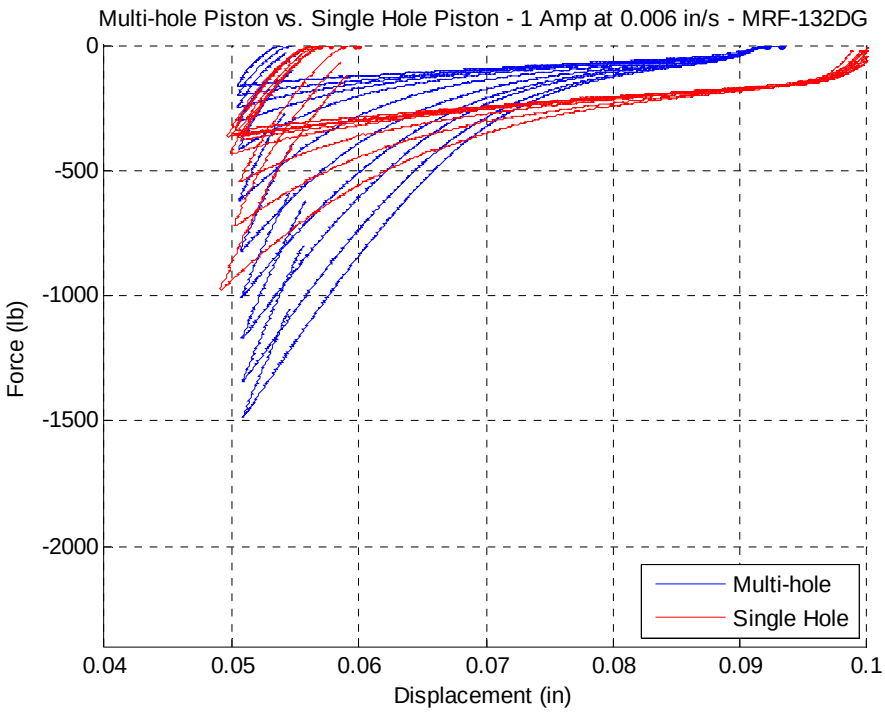

Figure 5-59. Multi-hole Piston results vs. single hole piston with a coil current of 1 Amp

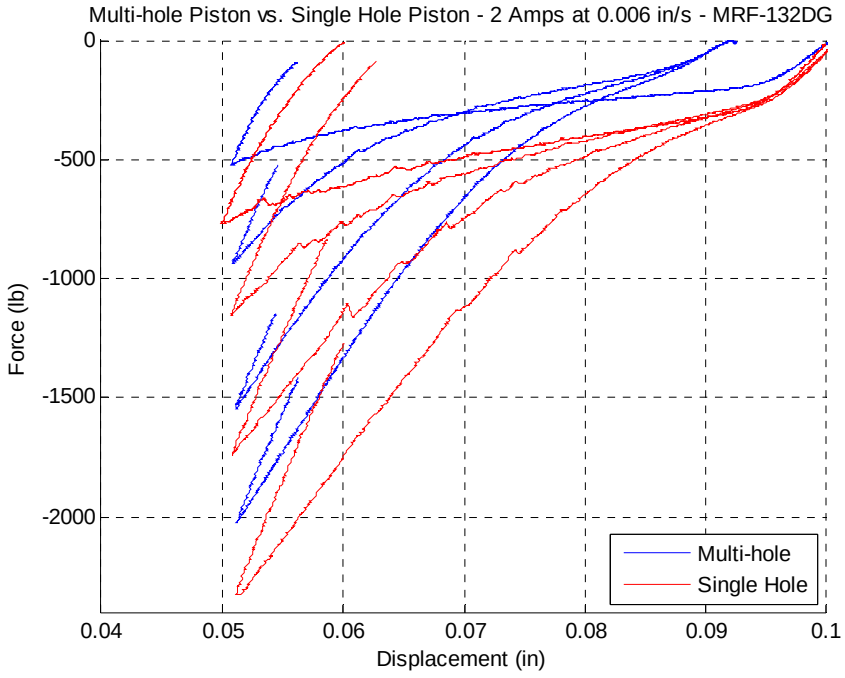

Figure 5-60. Multi-hole Piston results vs. single hole piston with a coil current of 2 Amps

Upon further inspection at conclusion of this testing, the aggregate clumping effect was confirmed to be increased over the single-hole piston tests. The pattern of aggregation changed from a simple ring to something that resembled a lattice structure across the piston face, as shown Figure 5-61. Severe fluid separation was also observed during testing, as shown in Figure 5-62. It appears that the carrier fluid is separating from the ferrous particles and being expelled from the test chamber. From the observations, it seems as though there is a column of nearly pure carrier fluid that leads all the way to the test chamber sitting below each one the dark brown spots.

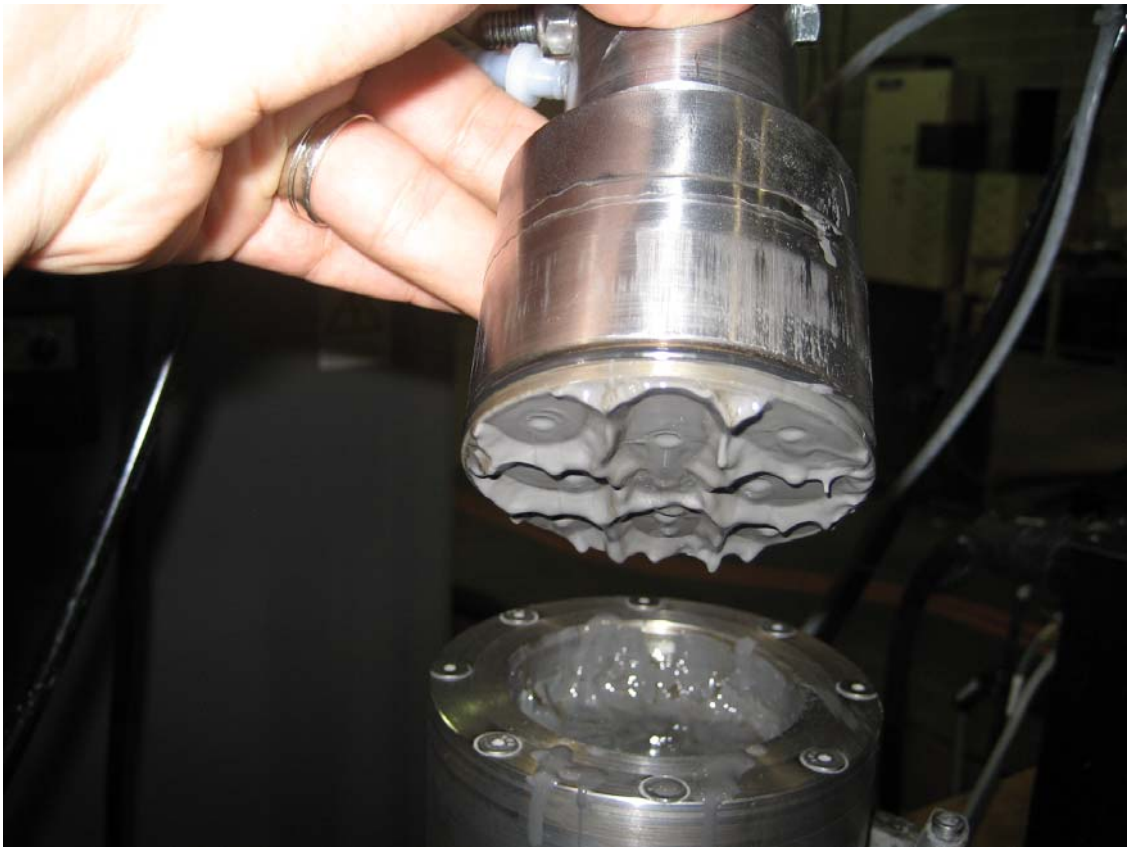

Figure 5-61. Semi-solid clumps form around multiple sites in the Multi-hole Piston (photo by Ryan Cavey)

Figure 5-62. Columns of separated carrier fluid appear to form directly over the eight thru holes in the piston (photo by Ryan Cavey)

While the aggregate clumping effect is not fully understood, it appears as though the Multi-hole Piston design created multiple pressure gradient sites that each encouraged separation in the MR fluid.

5.6 Summary

The squeeze mode rheometer uses a highly configurable data acquisition system to obtain test data. A simple 3 channel recording layout was developed for this testing. A test procedure was also developed and followed to provide consistency throughout the testing phase. The results of the rheometer testing are mixed. The rheometer proves that MR fluids operated in squeeze mode are capable of resisting very high compressive loads. The rheometer testing also proves that there are some seemingly adverse characteristics that must be addressed before squeeze mode sees wider implementation. The progressive increase in stiffness and aggregate clumping effect remain a challenge that requires further study.

6. Conclusion and Recommendations

The purpose of this chapter is to summarize the body of work that was produced for this thesis. The results from testing are discussed in reference to the research objectives set forth in Chapter 1. The chapter concludes with recommendations for future work in the area of MR fluid squeeze mode operation.

6.1 Summary

The first research objective mentioned in Chapter 1 was with regard to the design and fabrication of a squeeze mode rheometer. Currently, there are no known commercial instruments that may be used for squeeze mode rheometry with MR fluids. A rheometer that is intended for use with magnetorheological fluids has additional design requirements over its conventional counterpart, namely the management of the magnetic circuit that activates the fluid.

Another aspect that is unique to the design of a squeeze mode rheometer is fluid management during testing. The volume of fluid required in the test chamber varies as the piston moves relative to the body of the rheometer. There are many options available for accomplishing this task and ultimately the method chosen was the one that worked the best with the magnetic circuit design in the rheometer.

The design fundamentals as well the fabrication and assembly of the rheometer are discussed at length in this thesis. The detailed documentation provided allows for anyone that reads this to duplicate or design a squeeze mode rheometer for use with MR fluids.

The second research objective stated in Chapter 1 deals with providing a preliminary evaluation of MR fluids operated in the squeeze mode. A series of tests were performed with the rheometer to provide a foundation for understanding what the capabilities and limitations are for MR fluids in squeeze mode. The testing revealed that squeeze mode operation is able to provide substantial resistance to compressive loading in its activated state. The tests also revealed that thicker, more viscous MR fluids are susceptible to introducing unwanted air into the test chamber. This is due to the fact that they do not easily flow back into the chamber when the rheometer is in its extension stroke.

The primary observation from the preliminary testing is the trend of progressively increasing stiffness in the MR fluid. The trend was discovered while attempting to

perform repeat tests to confirm initial results. Each time a test was repeated without mixing the MR fluid, the peak compressive force produced by fluid increased over the previous run. This trend dominates the performance of the MR fluid in squeeze mode and was further investigated.

The final goal of this research was to investigate the factors that govern squeeze mode performance. Upon further testing and observation, it was discovered that semi-solid aggregate clumps were being formed in the test runs that produced a trend of increasing stiffness. Furthermore, the clumping effect appeared to be at its most extreme in the regions experiencing the least amount of fluid flow, namely the perimeter of the test chamber when using the single-hole piston.

A new piston was designed to reduce the large pressure gradient that was suspected of creating the aggregate clumps and to promote fluid remixing at multiple points in the test chamber. Testing revealed that the new design did not function as intended, but rather promoted the clumping effect in the fluid. The pattern of aggregation changed from a ring, which formed with the original piston, to a grid structure that followed the pattern of the 8 holes drilled in the new piston. It is clear that control over the formation of these semi-solid clumps is key to the success of operating MR fluid in squeeze mode.

6.2 Recommendations for Future Research

Based on the test results of this research, it is clear that squeeze mode operation in MR fluids warrants further research. The squeeze mode shows excellent potential in having a highly tunable method for controlling compressive loads. The future research in this area should be focused on generating predictable and reliable results in squeeze mode operation. In particular, a better understanding of the performance of the fluid after repeated cyclic loading is desired. Additionally, a model that characterizes the fluid with a stress-strain relationship, as well as a force-velocity relationship, in squeeze mode is also of great interest. The rheometer developed for this research should be adequate for collecting data to aid in the initial development of a model characterizing MR fluid in squeeze mode, although further verification testing should be preformed to fully document the limitations of the rheometer, i.e. structural compliance. At this point, it seems as though understanding how and why the clumping effect occurs is the critical path to

producing consistent performance in squeeze mode operation. Further research is needed to better understand and solve this challenging problem.

References

1. Goncalves, F.D., “Characterizing the Behavior of Magnetorheological Fluids at High Velocities and High Shear Rates,” Ph.D. Dissertation, Virginia Polytechnic Institute and State University: Blacksburg, VA, 2005.
2. Rabinow, J., “The magnetic fluid clutch.” AIEE Trans. 67, p. 1308, 1948.
3. Southern, B.M., “Design and Characterization of Tunable Magneto-Rheological Fluid-Elastic Mounts,” M.S. Thesis, Virginia Polytechnic Institute and State University, Blacksburg, VA, 2008.
4. Lange, U., Richter, L., Zipser, L., “Flow of Magnetorheological Fluids,” *Journal of Intelligent Material Systems and Structures*, Vol. 12, p. 161-164, 2001.
5. Lord Corporation, www.lord.com
6. Carlson, J.D., Weiss, K.D., “A growing attraction to magnetic fluids,” *Machine Design*, Vol. 66, No. 15, p. 61-64, 1994.
7. Weiss, K.D., Duclos, T.G., Carlson, J.D., Chrzan, M.J., and Margida, A.J., “High strength magneto - and electro - rheological fluids,” *Society of Automotive Engineers*, Vol. 932451, 1993.
8. Lord Corporation, “LORD Product Selector Guide,” 2008.
9. General Motors Corporation, “Magnetic Selective Ride Control,” 2008.
10. Audi, “Audi Magnetic Ride Suspension,” 2008.
11. Halverson, H., “Magnetic Ride - Star Wars Meets the 50th Car,” www.corvetteactioncenter.com, 2003.
12. Ahmadian, M., Vahdati, N., “Transient Dynamics of Semiactive Suspensions with Hybrid Control,” *Journal of Intelligent Material Systems and Structures*, Vol. 17 (No.2), p. 145-153, 2006.
13. Farjoud, A., Vahdati, N., Fah, Y.F., “Mathematical Model of Drum-type MR Brakes using Herschel-Bulkley Shear Model,” *Journal of Intelligent Material Systems and Structures*, Vol. 00, 2007.
14. Lee, U., Kim, D., Hur, N., Jeon, D., “Design Analysis and Experimental Evaluation of an MR Fluid Clutch,” *Journal of Intelligent Material Systems and Structures*, Vol. 10 (No. 9), p. 701-707, 1999.

15. Morrison, F.A., Understanding Rheology, Oxford University Press, New York, New York, 2001.
16. Materials Research Laboratory, University of California, Santa Barbara, http://www.mrl.ucsb.edu/mrl.
17. National Institute of Standards and Technology, http://ciks.cbt.nist.gov/.
18. Walters, K., Rheometry, Chapman and Hall Ltd, London, 1975.
19. Ciocanel, C., Naganathan, N.G., Viera, S.L., Hideki, Y., Molyet, K., "MR Fluid Behavior Under Constant Shear Rates And High Magnetic Fields Over Long Time Periods," *2004 ASME International Mechanical Engineering Congress and Exposition*, Vol. 69, p. 221-226, 2004
20. Carlson, J.D., Jolly, M.R., "MR fluid, foam and elastomer devices," *Mechatronics*, Vol. 10, p. 555-569, 2000.
21. Carlson, J.D., Catanzarite, D.M., Clair, K.A.S., "Commercial Magneto-Rheological Fluid Devices," *Proceedings 5th International Conference on ER Fluids, MR Suspensions and Associated Technology*, W. Bullough, Ed., World Scientific, Singapore, 1996.
22. Carlson, J.D., "What Makes a Good MR Fluid?," *Journal of Intelligent Material Systems and Structures*, Vol. 13, p. 431-435, 2002.
23. Lord Materials Division, "Designing with MR Fluids," *Engineering Note*, p. 1-5, 1999.
24. Jolly, M.R., Bender, J.W., Carlson, J.D., "Properties and Applications of Commercial Magnetorheological Fluids," *SPIE 5th Annual Symposium on Smart Structures and Materials*, San Diego, CA, March 1998.
25. Poynor, J.C, "Innovative Designs for Magneto-Rheological Dampers," M.S. Thesis, Virginia Polytechnic Institute and State University, Blacksburg, VA, 2001.
26. Olabi, A.G., Grunwald, A., "Design and application of magneto-rheological fluid," *Materials and Design*, Vol. 28 (No. 10), p. 2658-2664, 2007.
27. Lord Rheonetic Magnetically Responsive Technology, MR Damper, RD-1005-3 Product Bulletin, 2003.
28. Biedermann Motech GmbH, www.biedermann.com

29. Carlson, J.D., Matthis, W., Toscano, J.R., “Smart Prosthetics Based on Magnetorheological Fluids,” *Proceedings of SPIE*, Vol. 4332, p. 308-316, 2001.
30. Lord Rheonetic Magnetically Responsive Technology, MR Brake MRB-2107-3, Product Bulletin, 2003.
31. Phillips, R.W., “Engineering Applications of Fluids With a Variable Yield Stress,” Ph.D. Thesis, University of California, Berkeley, 1969.
32. Mazlan, S.A., Ekreem, N.B., Olabi, A.G., “The performance of magnetorheological fluid in squeeze mode,” *Smart Materials and Structures*, Vol. 16, p. 1678-1682, 2007.
33. Jolly, M.R., Carlson, J.D., Actuator 96. In: Borgmann H, Lenz K, editors. Proceedings of the 5th International Conference on New Actuators. Bremen, Germany: Axon Technologie Consult GmbH, 1996.
34. Carlson, J.D., US Patent No. 5,492,312 1996.
35. Forte, P., Parterno, M., Rustighi, E., “A magnetorheological fluid damper for rotor applications,” *International Journal of Rotating Machinery*, Vol. 10, p. 175-182, 2004.
36. Carmignani, C, Forte, P., Rustighi, E., “Design of a novel magneto-rheological squeeze film damper,” *Smart Materials and Structures*, Vol. 15, p. 164-170, 2006.
37. Ahn, Y.K., Ha, J.Y., Yang, B.S., “A new type controllable squeeze film damper using an electromagnet,” *Journal of Vibration and Acoustics*, Vol. 126, p. 380-383, 2004.
38. Wang, J., Meng, G., Feng, N, Hahn, E.J., “Dynamic performance and control of squeeze mode MR fluid damper-rotor system,” *Smart Materials and Structures*, Vol. 14, p. 529-539, 2005.
39. Wang, J., Feng, N., Meng, G., Hahn, E.J., “Vibration conrol of rotor by squeeze film damper with magnetorheological fluild,” *Journal of Intelligent Material Systems and Structures*, Vol. 17, p. 353-357, 2006.
40. Wang, X., Gordaninejad, F., Hitchcock, G., “A magneto-rheological fluid elastomer vibration isolator,” *Smart Structures and Materials*, Proc. of SPIE Vol. 5760, p. 217-225, 2005.

41. Goncalves, F.D., Koo, J.H., Ahmadian, M., "A Review of the State of the Art in Magnetorheological Fluid Technologies – Part 1: MR fluid and MR fluid models," *The Shock and Vibration Digest*, Vol. 38, 2006.
42. York, D., Wang, X., Gordaninejad, F., "A New MRF-E Vibration Isolator," *Journal of Intelligent Material Systems and Structures*, Vol. 18, p. 1221-1225, 2007.
43. Global Spec Inc., http://test-equipment.globalspec.com/
44. Malvern Instruments Ltd., www.malvern.com
45. TA Instruments, www.tainstruments.com
46. RheoTec Messtechnik GmbH, "Falling Ball Viscometer KF10 (DIN 53015)," *RheoTec Product Bulletin*, 2008.
47. Mazlan, S.A., Ekreem, N.B., Olabi, A.G., "Apparent stress-strain relationships in experimental equipment where magnetorheological fluids operate under compression mode," *Journal of Physics D: Applied Physics*, Vol. 41 (No. 9), Article No. 095002, 2008.
48. Tang, X., Wang X.J., Li, W.H., Zhang, P.Q., "Testing and Modeling of an MR Damper in the Squeeze Flow Mode," *Proceedings 6th International Conference on ER Fluids, MR Suspensions and Their Application, Yonezawa, Japan, 1997* p. 870-878, World Scientific, Singapore, 1998.
49. Zhu, J.G., "Magnetic Circuit Analysis," *48550 Electrical Energy Technology: Lecture Note*, University of Technology, Sydney (UTS), 1999.
50. Meeker, D., Finite Element Method Magnetics (FEMM), Foster-Miller, Inc., http://www.foster-miller.com/magnetic_modeling.htm, 2006.
51. Goncalves, F.D., "Dynamic Analysis of Semi-Active Control Techniques for Vehicle Applications," M.S. Thesis, Virginia Polytechnic Institute and State University, Blacksburg, VA, 2001.
52. Lord Corporation, "MRF-122EG Product Bulletin," *Lord Technical Data*, 2008.
53. Lord Corporation, "MRF-132DG Product Bulletin," *Lord Technical Data*, 2008.

Appendix A: MR Fluid and Rheometer Specifications

This appendix provides the available information regarding the material properties of the MR fluids tested in this research. The B-H plot for both the G-50 and G-20 MR fluids is provided in Figure A - 1. A plot of yield stress as is corresponds to flux density is shown in Figure A - 2.

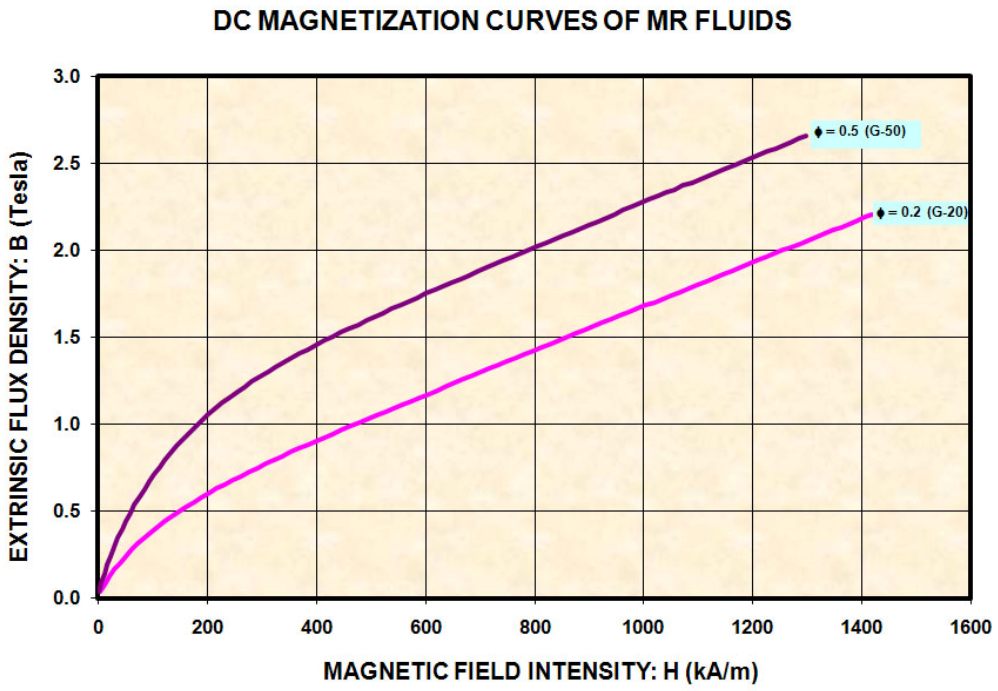

Figure A - 1. B-H curves for G-50 and G-20 MR fluids

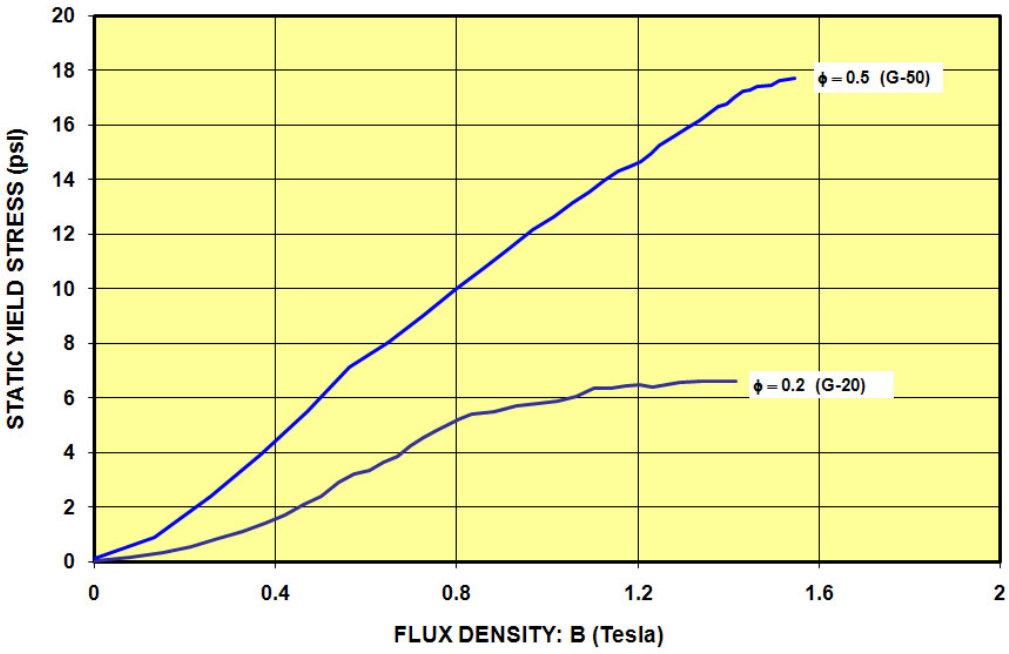

Figure A - 2. Yield stress characteristics of G-50 and G-20 MR fluids

The magnetic properties of MRF-122EG are shown in Figure A - 3. A plot of the MR fluid's yield stress versus the magnetic field intensity is shown in Figure A - 4.

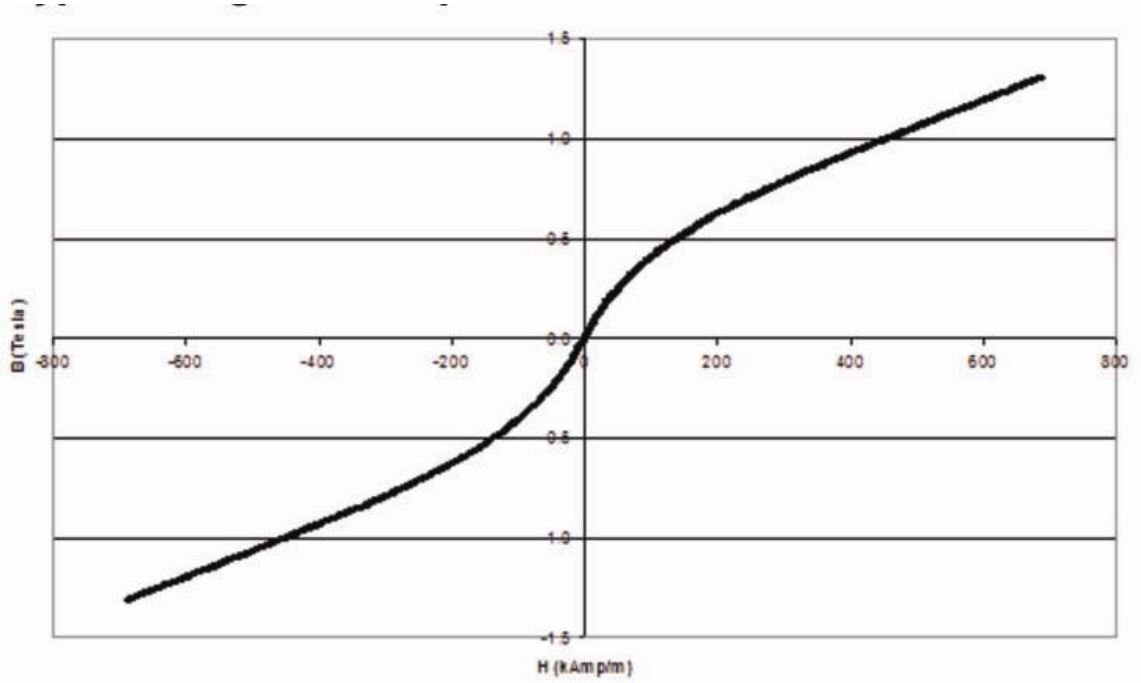

Figure A - 3. B-H curve for MRF-122EG [52]

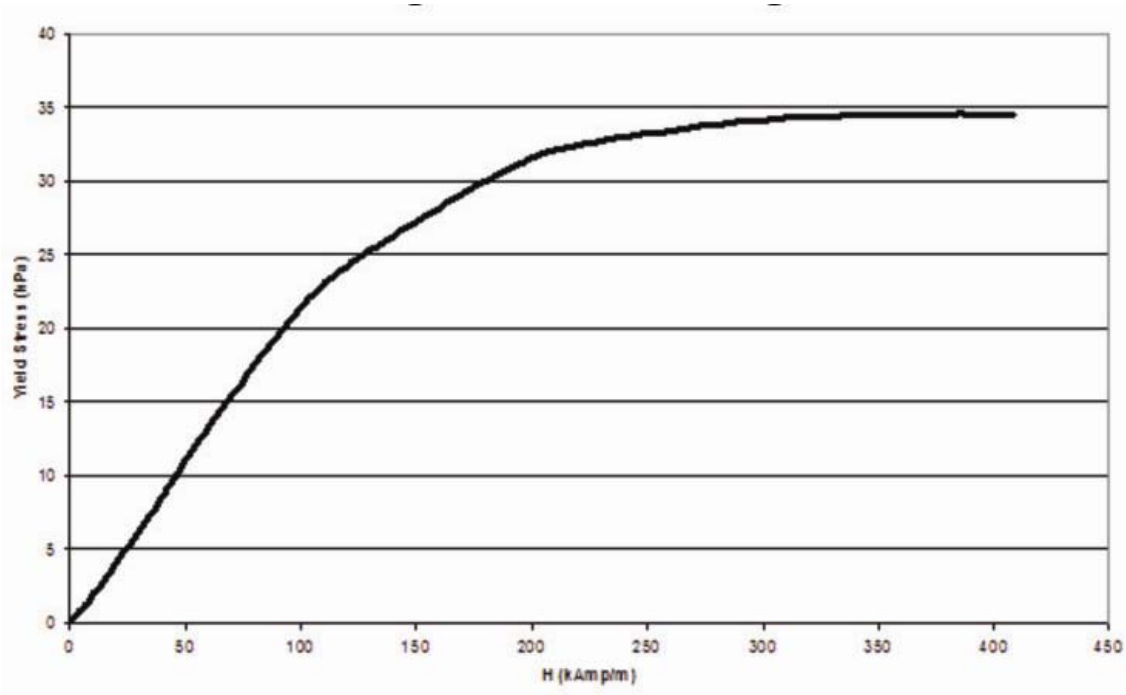

Figure A - 4. Yield stress characteristic curve for MRF-122EG [52]

Typical magnetic properties for MRF-132DG are shown in Figure A - 5. A plot of the MR fluid's yield stress versus the magnetic field intensity is shown in Figure A - 6.

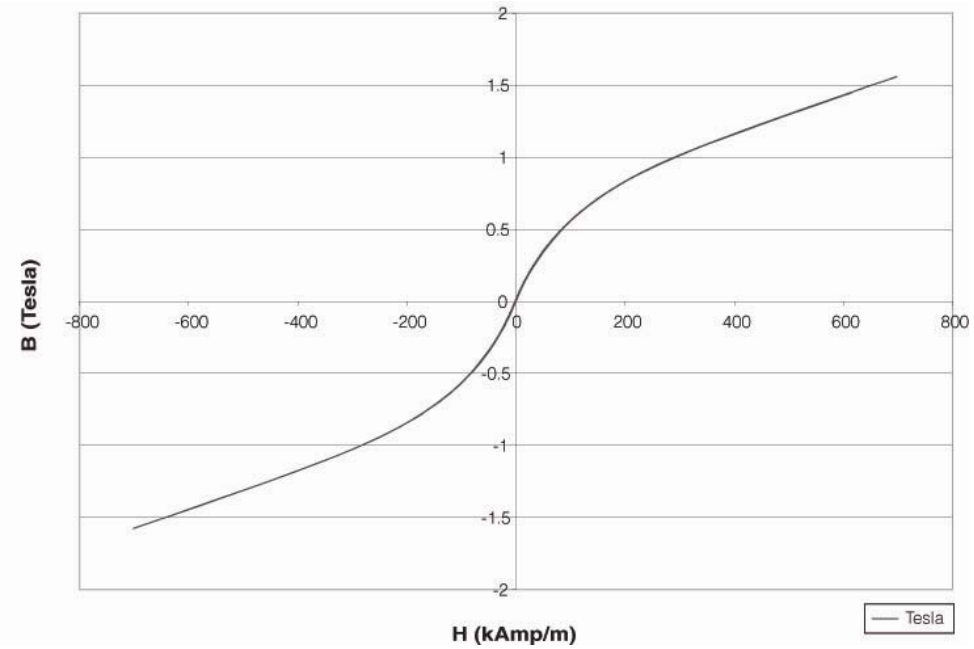

Figure A - 5. B-H curve for MRF-132DG [53]

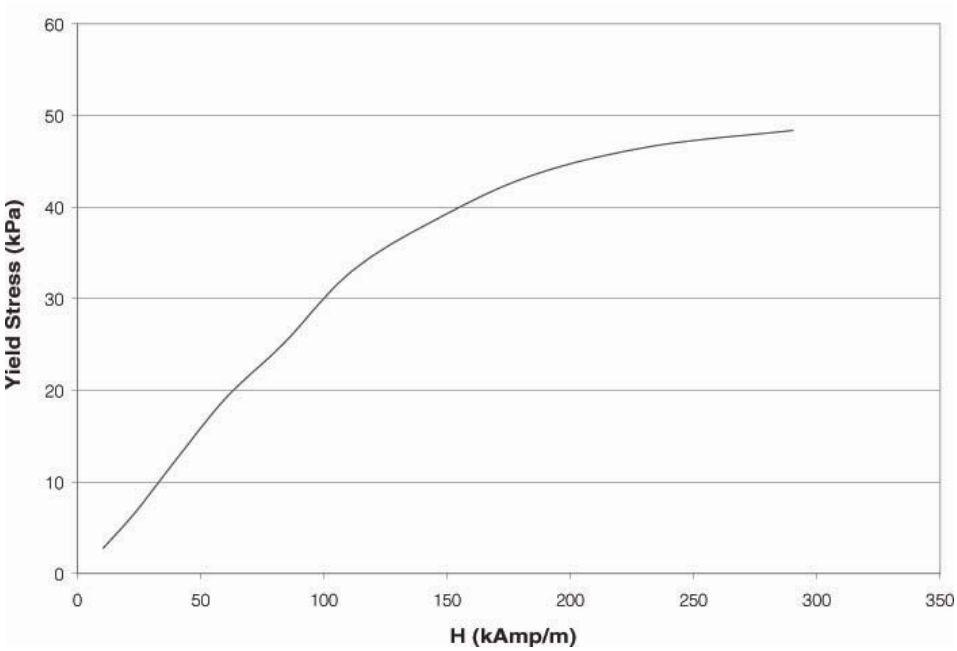

Figure A - 6. Yield stress characteristic curve for MRF-132DG [53]

The following pages in this appendix include detail drawings of the custom components found in the squeeze mode rheometer. The drawings are provided in order by part number as they correspond to Table A-2.

Table A-2. The list of custom components on the squeeze-mode rheometer

Bill of Materials – Custom Components		
Part Number	Description	Purchased/Custom
1	Top Strut	6061 Aluminum
2	Piston Mount	12L14 Steel
3	Piston	12L14 Steel
4	Piston Stud	Steel
5	Upper Plate	1018 Steel
6	Chamber Floor	12L14 Steel
7	Magnet Core	12L14 Steel
8	Outer Shell	1018 Steel
9	Inner Shell	6061 Aluminum
10	Bottom Plate	1018 Steel
11	Base Mount	6061 Aluminum
12	Gauss Probe Bracket	1018 Steel
13	Gauss Probe Clamp	6061 Aluminum
14	Multi-hole Piston Mount	12L14 Steel
15	Multi-hole Piston	12L14 Steel

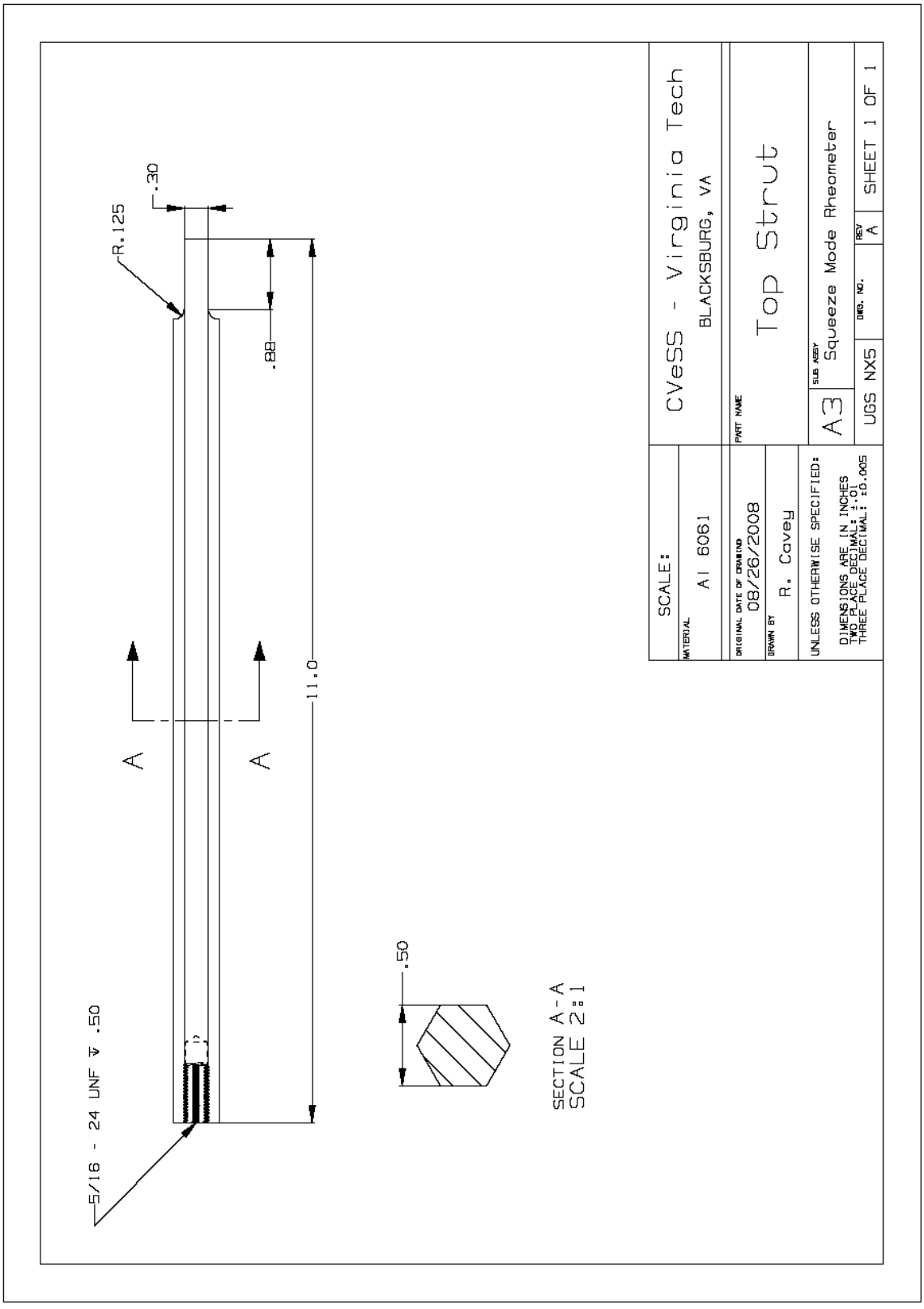

Figure A - 7. Detail drawing of the Top Strut

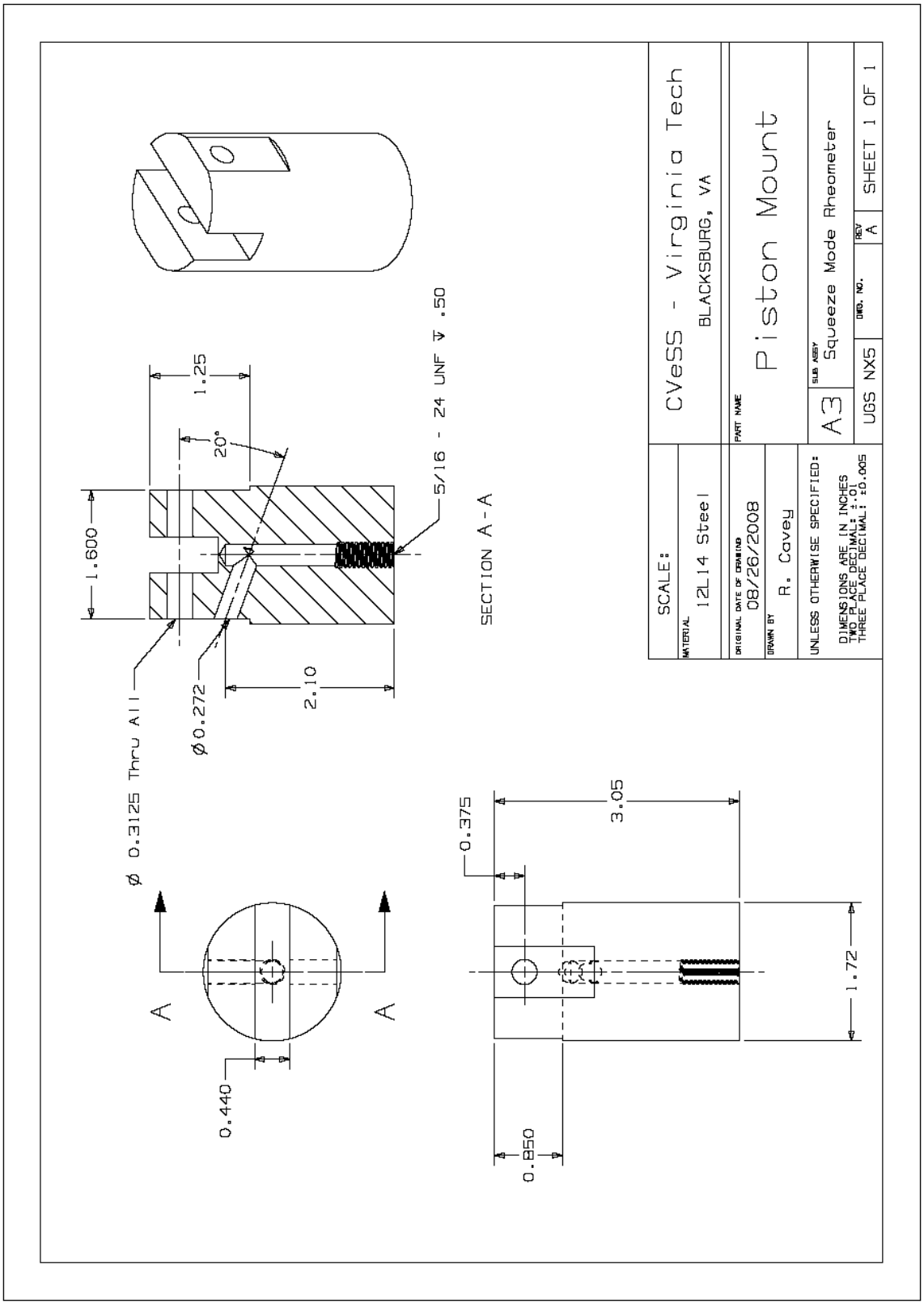

Figure A - 8. Detail drawing of the Piston Mount

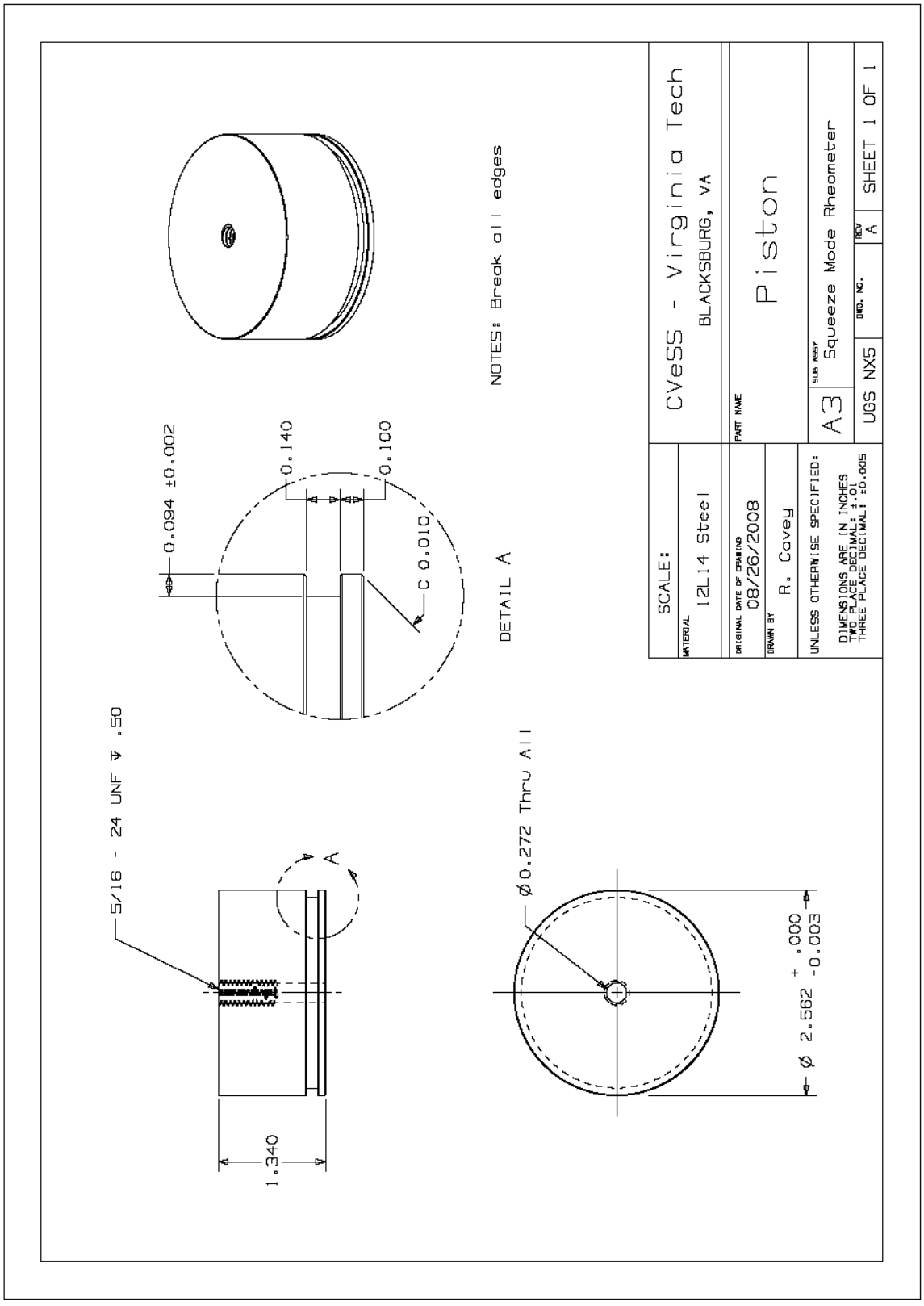

Figure A - 9. Detail drawing of the Piston

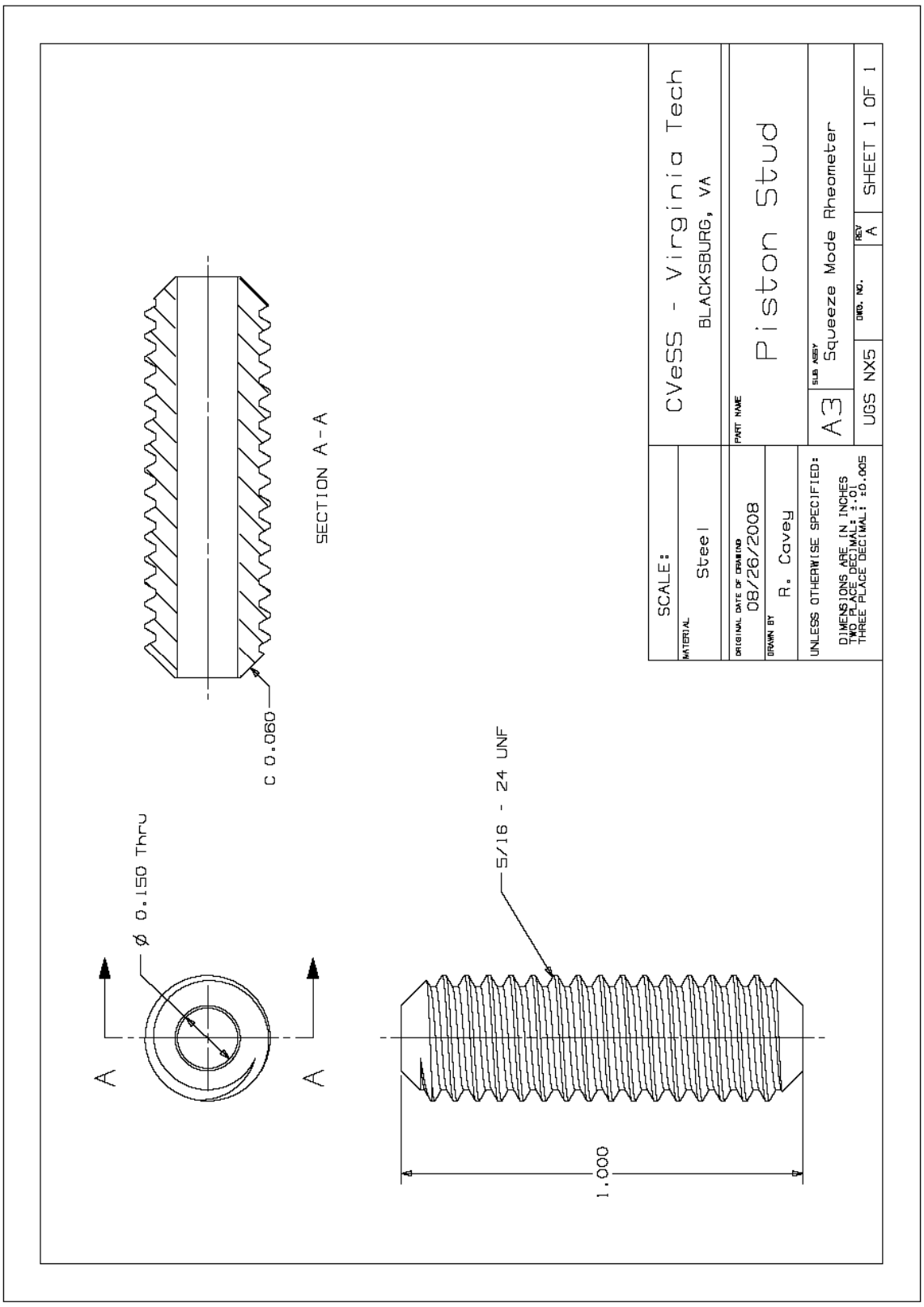

Figure A - 10. Detail drawing of the Piston Stud

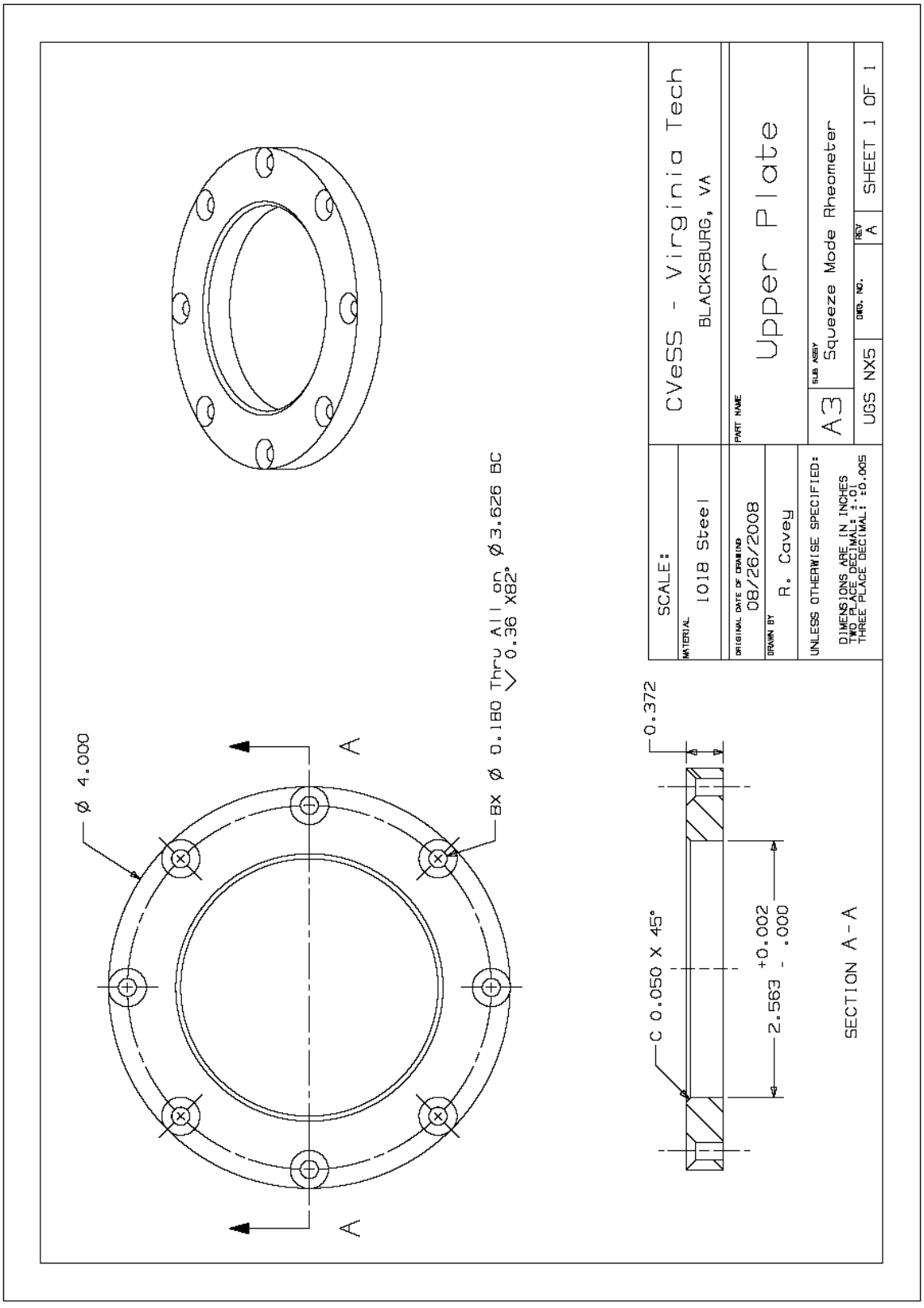

Figure A - 11. Detail drawing of the Top Plate

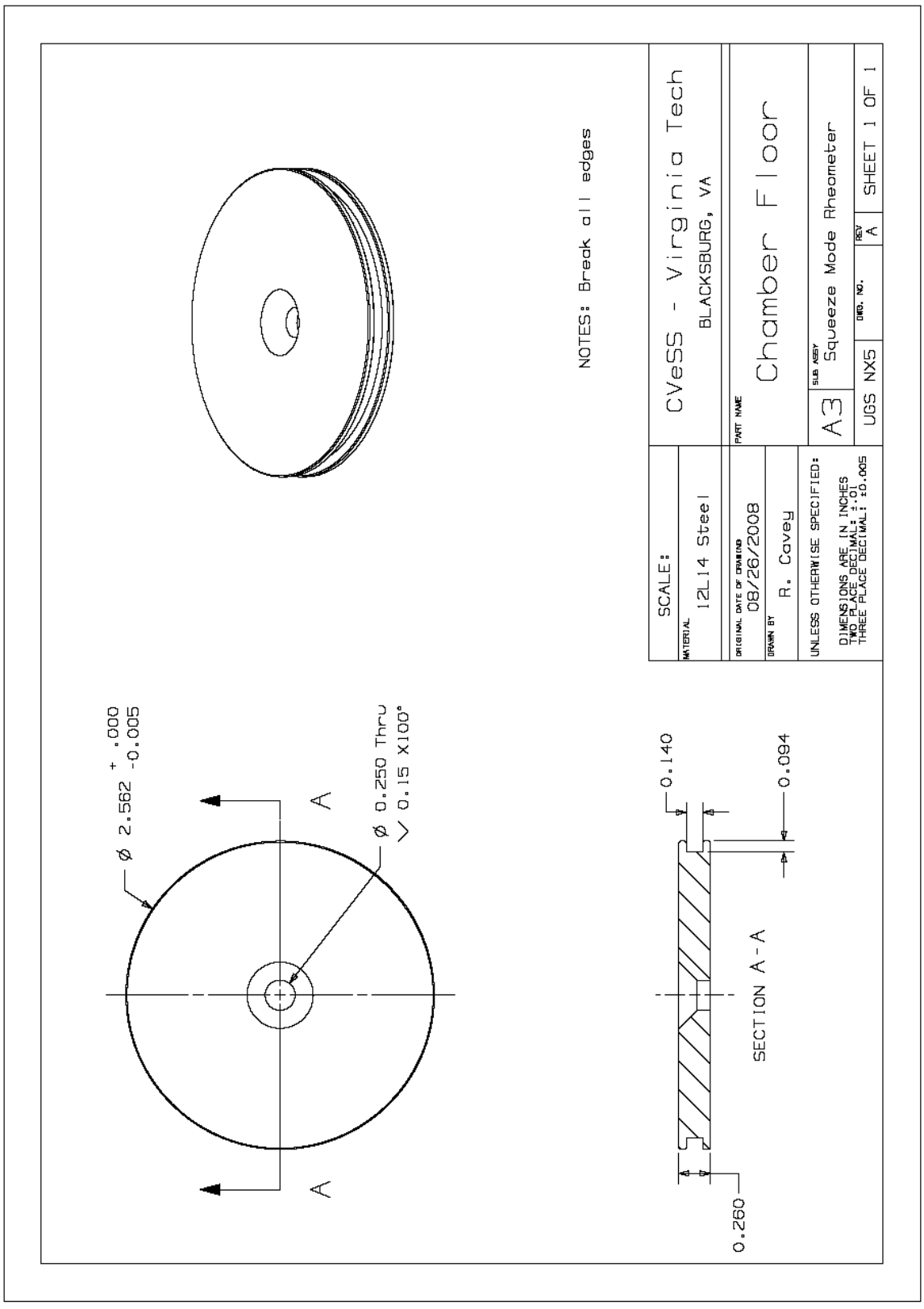

Figure A - 12. Detail drawing of the Chamber Floor

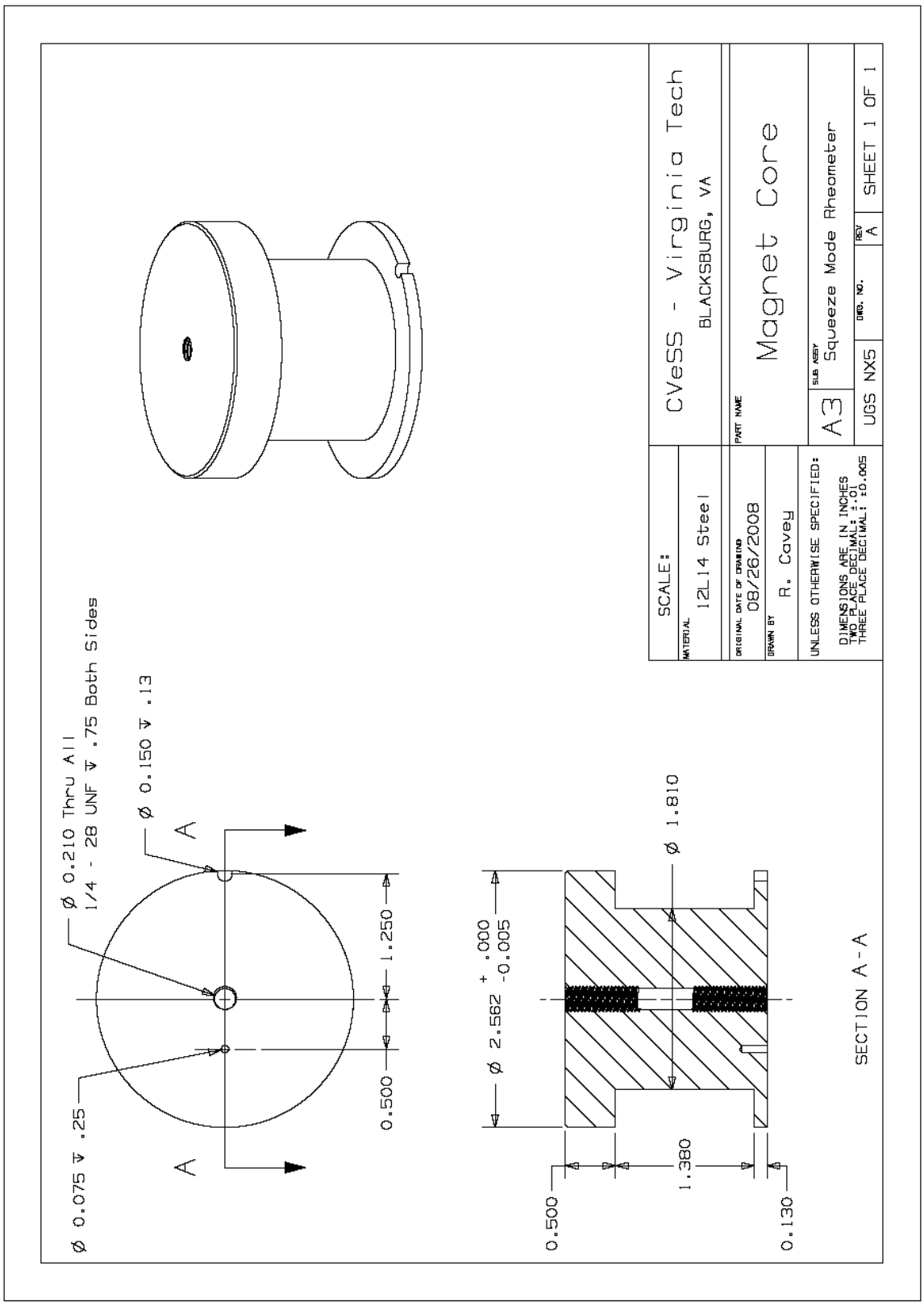

Figure A - 13. Detail drawing of the Magnet Core

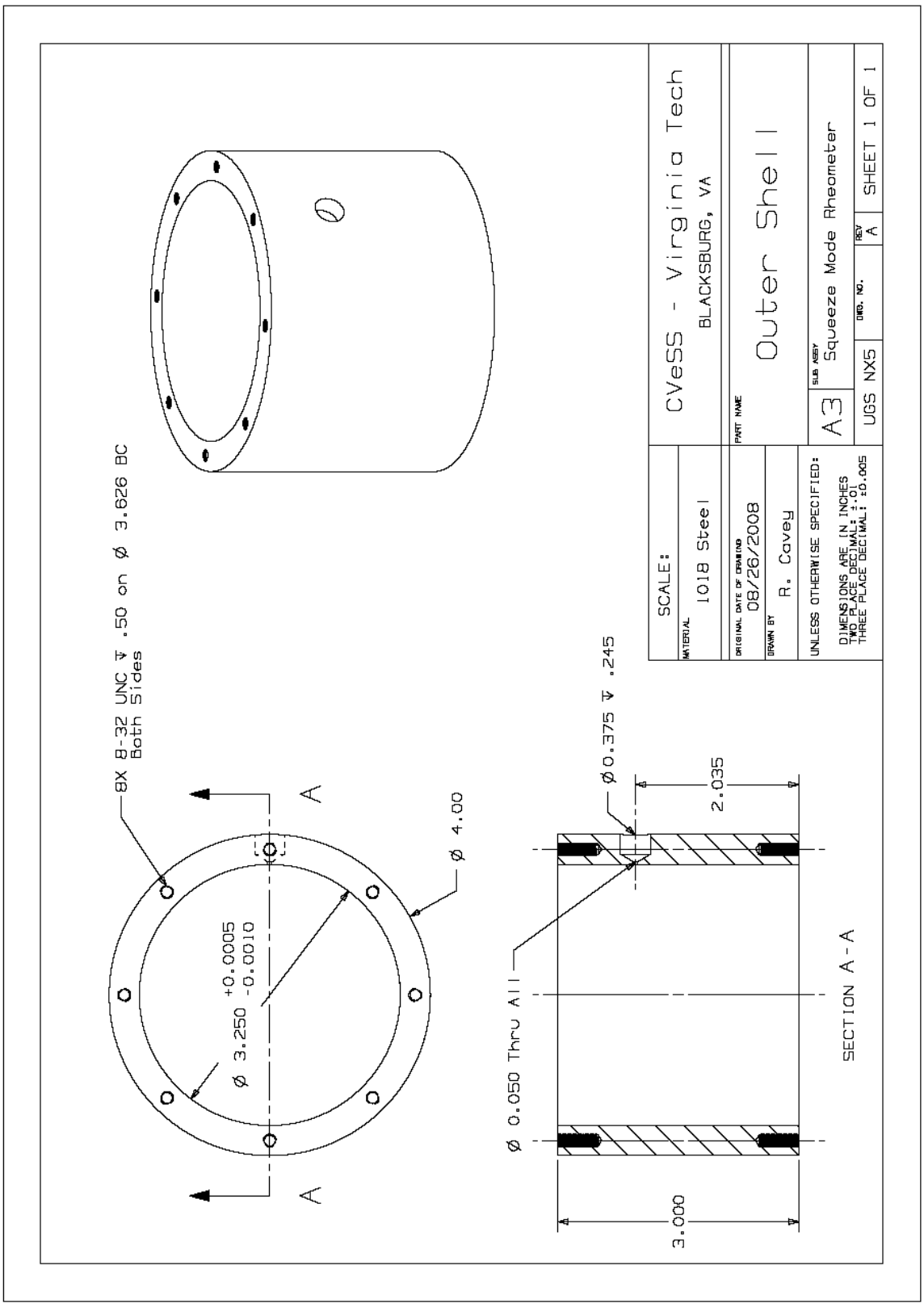

Figure A - 14. Detail drawing of the Outer Shell

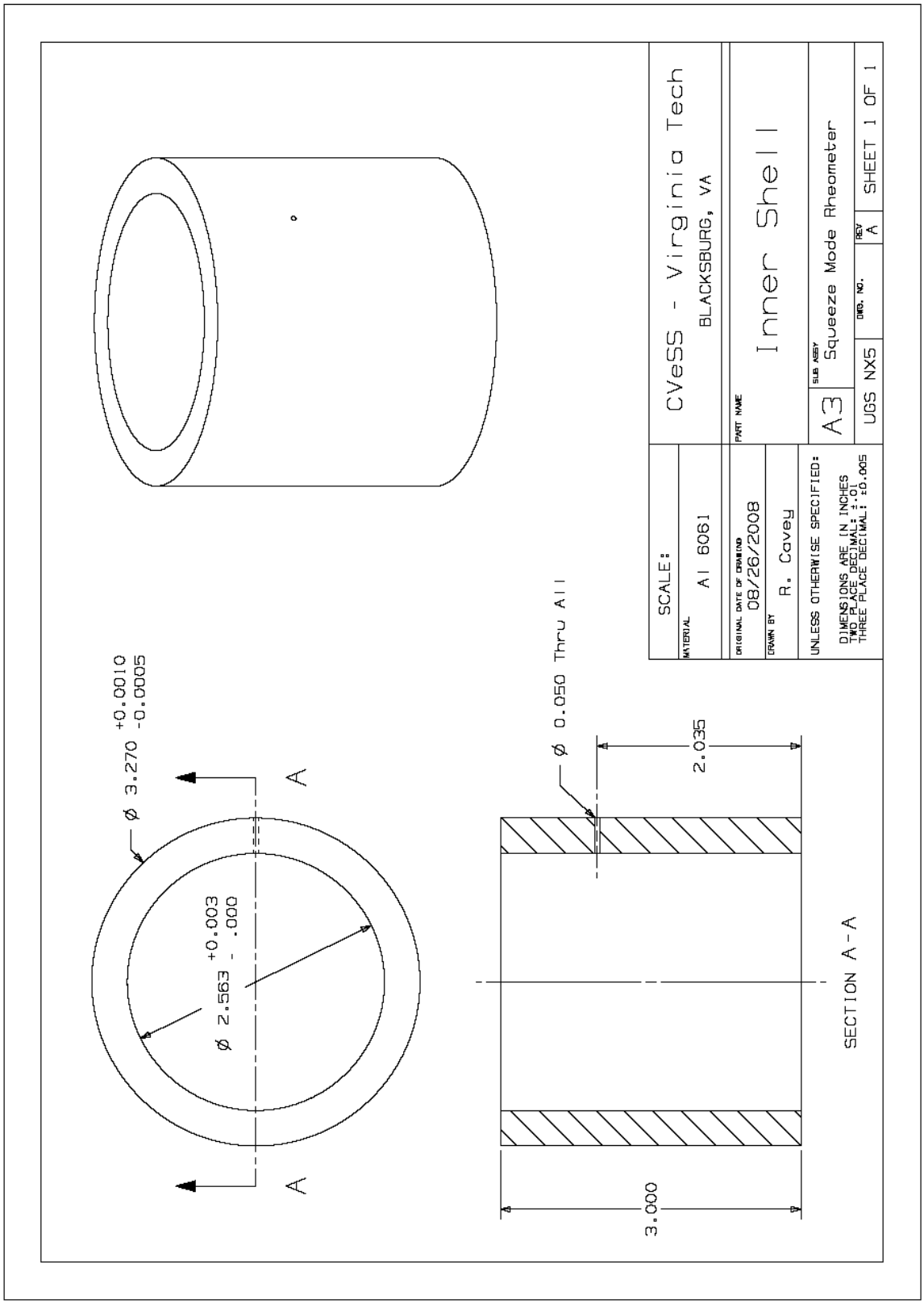

Figure A - 15. Detail drawing of the Inner Shell

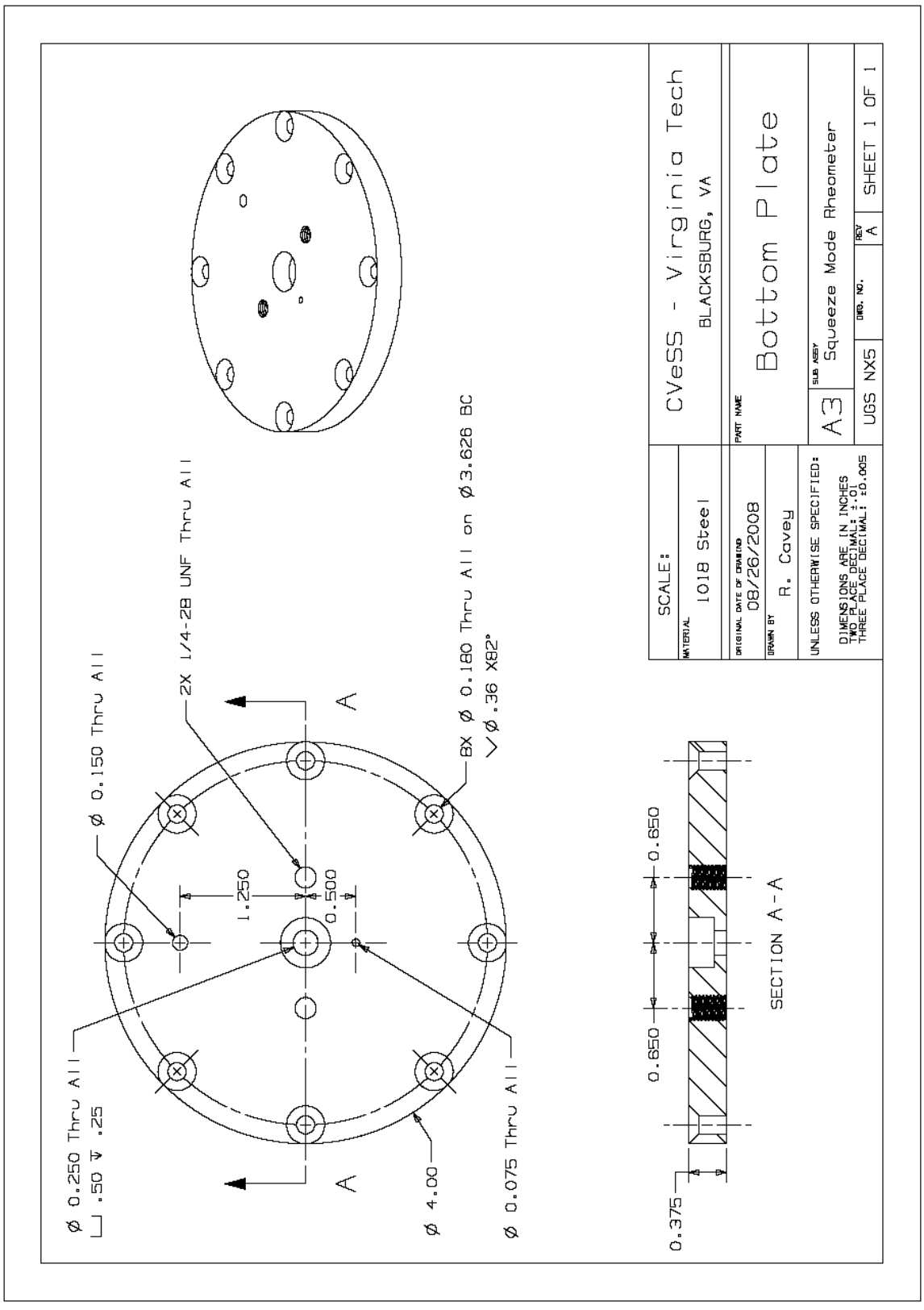

Figure A - 16. Detail drawing of the Bottom Plate

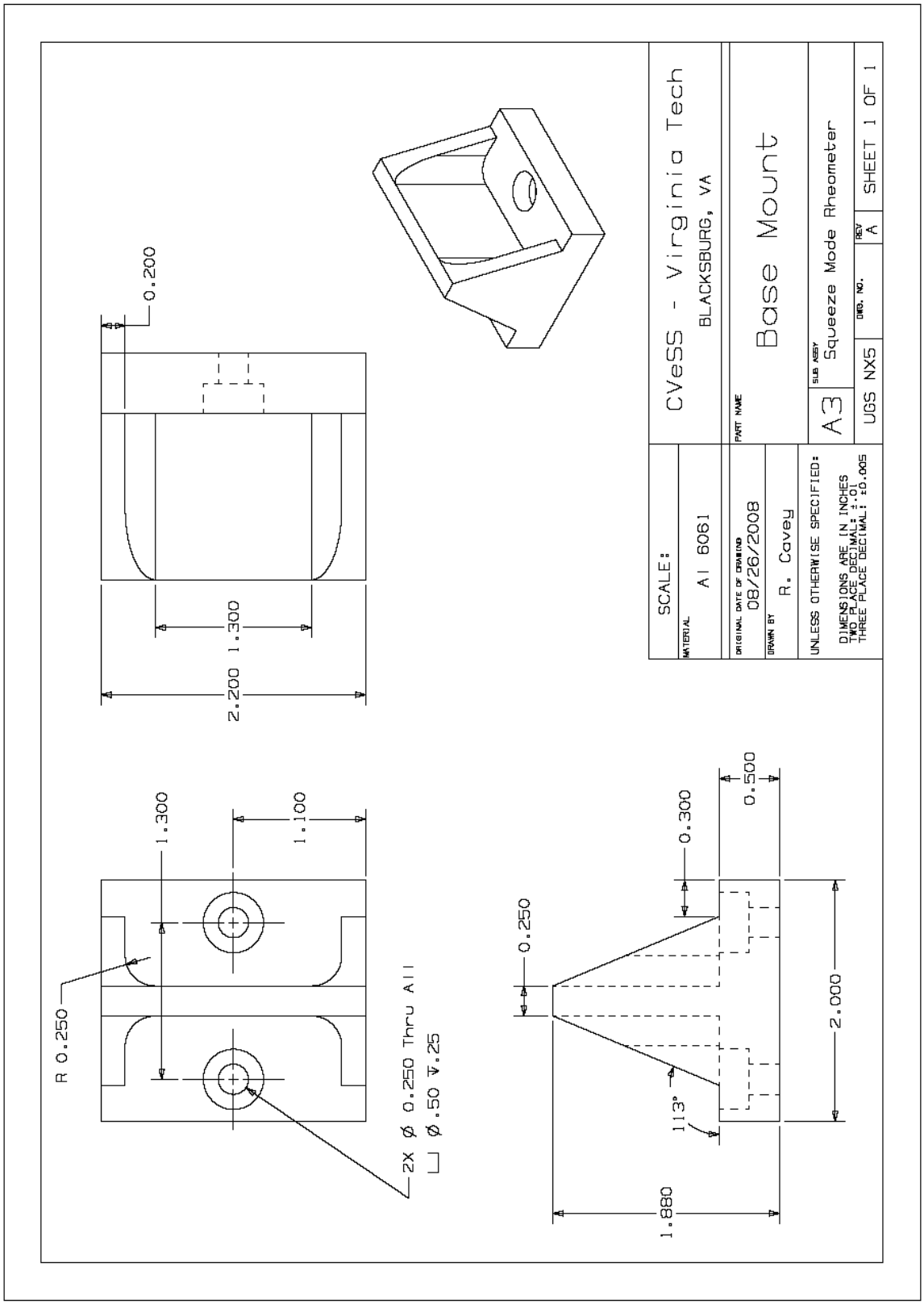

Figure A - 17. Detail drawing of the Base Mount

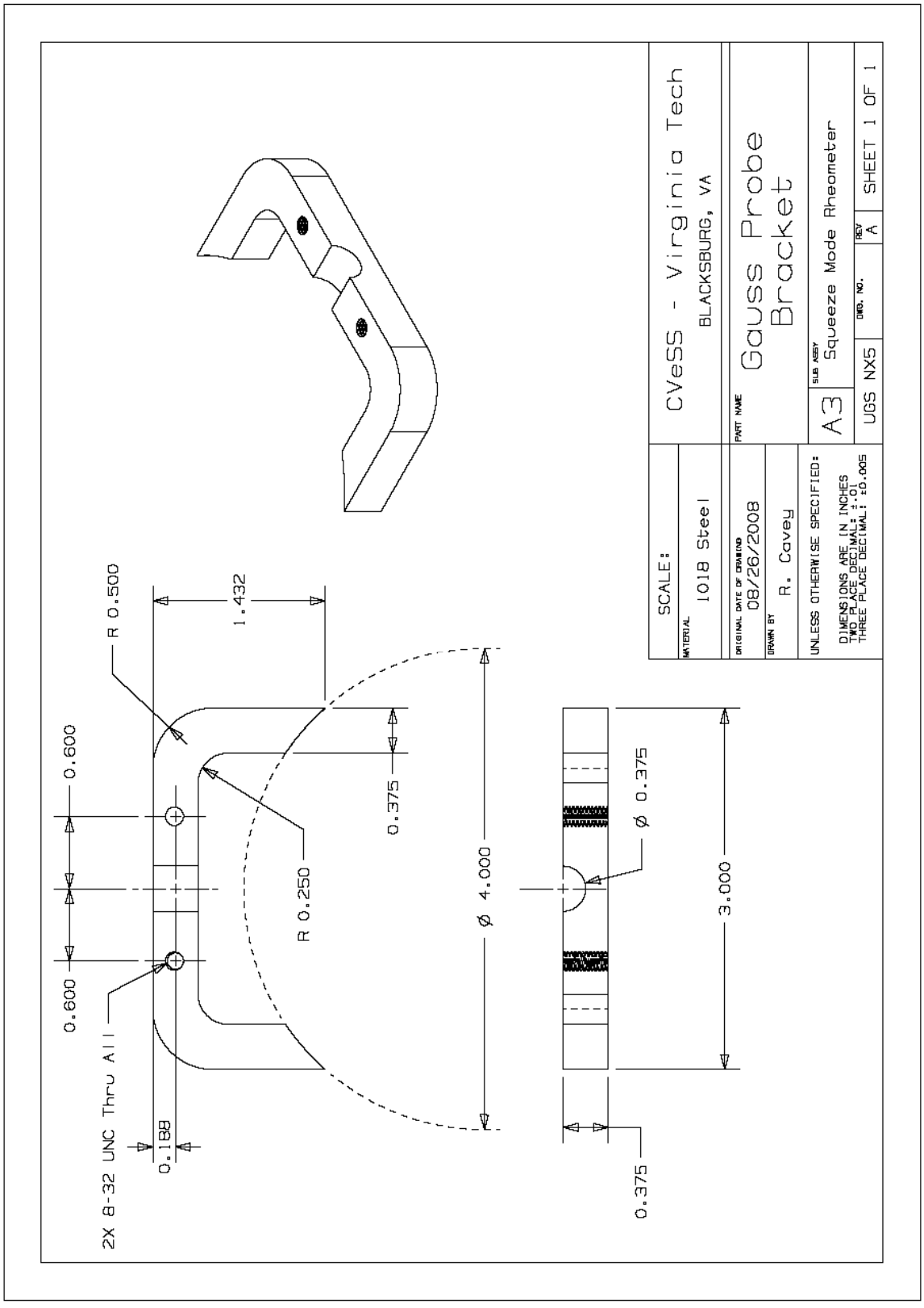

Figure A - 18. Detail drawing of the Gauss Probe Bracket

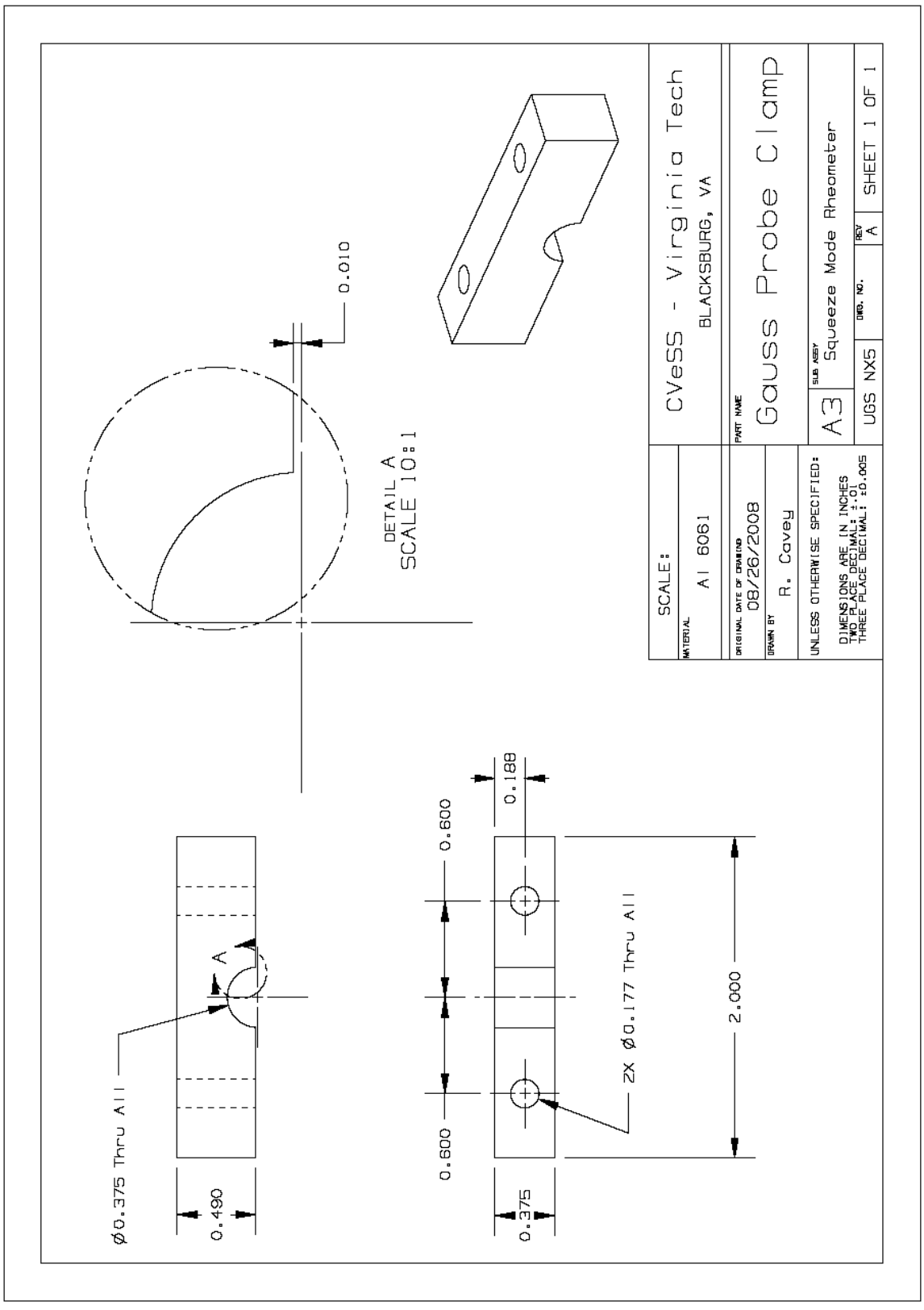

Figure A - 19. Detail drawing of the Gauss Probe Clamp

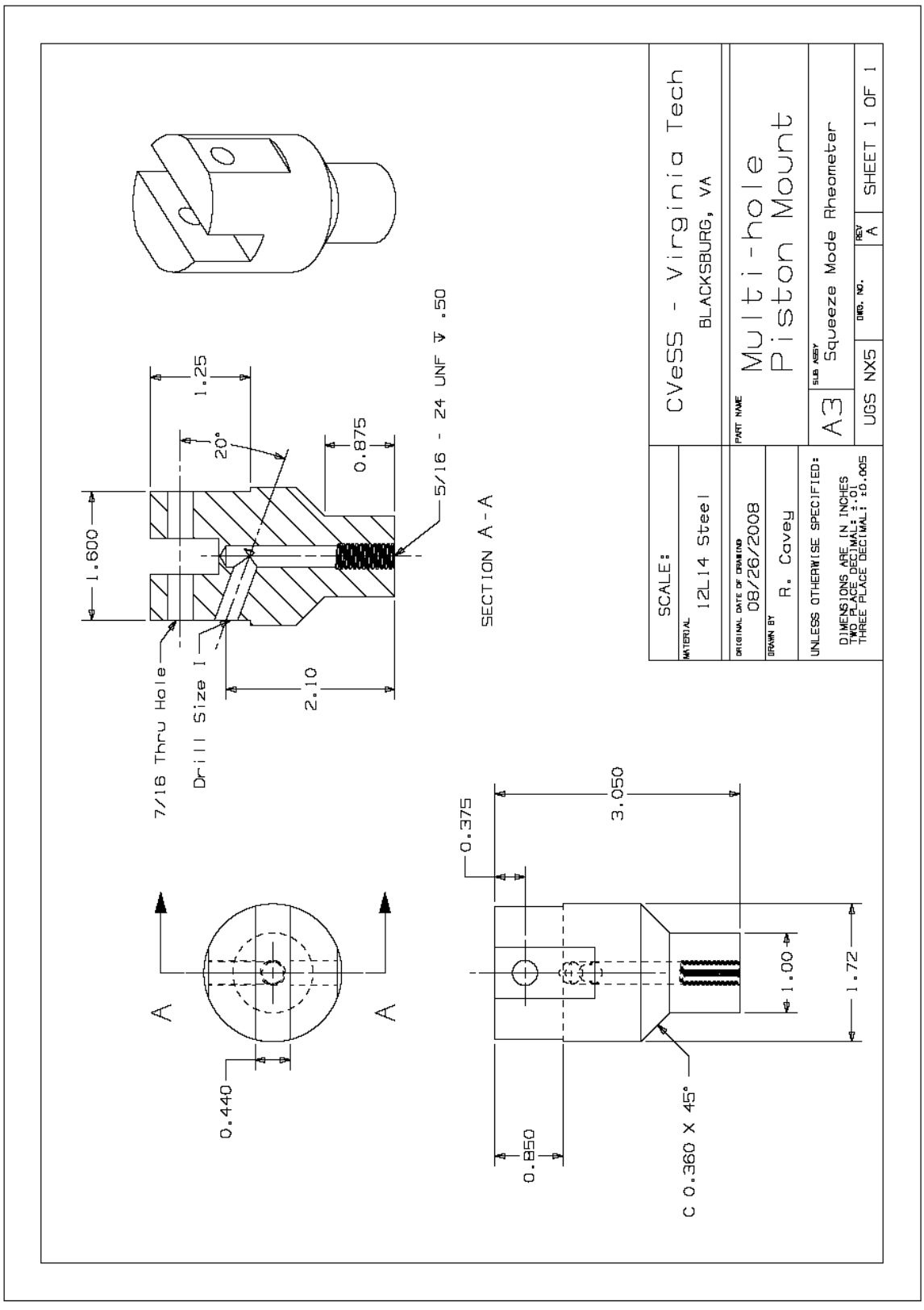

Figure A - 20. Detail drawing of the Multi-hole Piston Mount

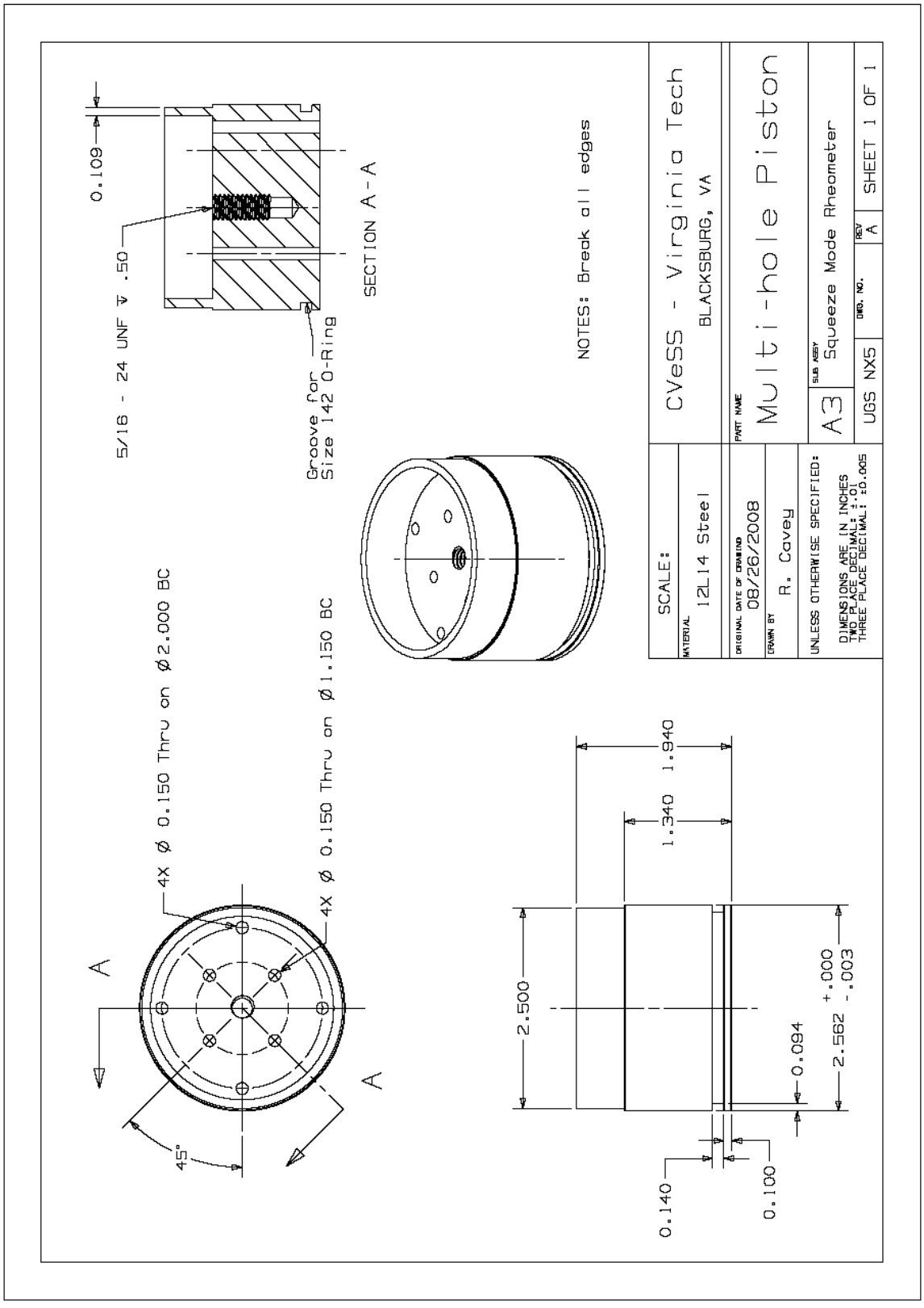

Figure A - 21. Detail drawing of the Multi-hole Piston